Coding of internal senses: vagal gut-to-brain circuits

A dissertation presented

by

Erika Kristen Williams

to

The Division of Medical Sciences

in partial fulfillment of the requirements

for the degree of

Doctor of Philosophy

in the subject of

Neurobiology

Harvard University

Cambridge, Massachusetts

April 2016

Dissertation Advisor: Dr. Stephen D. Liberles Erika Kristen Williams

Coding of internal senses: vagal gut-to-brain circuits

Abstract

Our ability to detect features of environments in and around us is fundamental. Organisms have developed highly specialized systems to allow for transduction of a broad variety of stimuli to convey sensory information to the nervous system. In addition to traditionally appreciated external sensory systems, such as sight, smell, taste and touch, organisms also posses internal sensory systems to detect changes in physiological state. One key body-to-brain connection is via cranial nerve X, the vagus nerve. The vagus nerve innervates most major organ systems, transmits information from peripheral organs to the brainstem, and plays a critical role in the regulation of diverse physiological processes. However, the organization of this sensory system, and direct links between response properties, terminal morphology, and signaling mechanisms is not currently available for many vagal neuron types.

To study the peripheral representation of autonomic inputs, we developed a vagal ganglion imaging preparation for large-scale parallel analysis of single neuron responses *in vivo*. Using this preparation, we can record responses evoked by a broad array of peripherally applied stimuli, including stretch in the lung, stomach, and intestine, responses to inhaled carbon dioxide, and to chemical cues perfused through the intestinal

lumen. This work allows for a careful description of response properties of vagal sensory neurons, and their organization within the ganglion.

Furthermore, to link response properties of vagal sensory neuron subsets to specific anatomical phenotypes and physiological roles, we developed a genetic strategy to molecularly define neuron subsets in the context of *in vivo* imaging. We identified one neuron subset marked by the gut hormone receptor *Glp1r* that responds to mechanical distension in the gastrointestinal tract, forms stereotyped mechano-sensitive terminals, and whose activation increases gastric pressure. A second neuron subset, marked by *Gpr65*, detects chemical cues in the intestine, projects into intestinal villi, and causes cessations of gastric contractions. These studies clarify the roles of vagal afferents in mediating particular gut hormone responses. Moreover, genetic control over gut-to-brain neurons provides a molecular framework for understanding neural control of gastrointestinal physiology.

Table of Contents

Chapter 1: Introduction 1
- 1.1 General Anatomy 2
- 1.2 The Cardiovascular System 4
- 1.3 The Respiratory System 7
- 1.4 The Gastrointestinal System 11
- 1.5 Conclusions 22

Chapter 2: *In vivo* imaging of vagal sensory neurons 23
- 2.1 Proof of principle 24
- 2.2 Respiratory stimuli 32
- 2.3 Gastrointestinal stimuli 38
- 2.4 Pharmacological stimuli 52
- 2.5 Failed stimuli 54
- 2.6 Salt and pepper organization of vagal ganglia 58
- 2.7 Voltage sensor imaging 61
- 2.8 Conclusions 64

Chapter 3: Molecularly defining gut sensory neurons 66
- 3.1 Defining vagal sensory neuron subsets 66
- 3.2 Imaging responses of molecularly defined subsets 79
- 3.3 Anatomical tracing of molecularly defined subsets 83
- 3.4 Optogenetic control of gut motility 92
- 3.5 Conclusions 94

Chapter 4: Future Directions 100
- 4.1 Vagal afferent information coding 100
- 4.2 Investigation of GLP1R and GPR65 neurons 101
- 4.3 Exploration of additional vagal sensory neuron subsets 106

Addendum: Response properties of other vagal sensory neuron subsets 108
- P2RY1 108
- NPY2R 112
- MC4R 113

Bibliography 115

Acknowledgements

Thank you first to my family. My mom and my dad who have been so generous with their time and themselves, I would not be here without your constant support and guidance. My brother never ceases to inspire and who will always be my best friend. My extended family, here in Boston, scattered across the States, and also in Sweden – it is a privilege to know you and to live through your adventures.

Thank you Liberles Lab, past members and present. David Ferrero (and honorary lab member, his wife Jenny Yang), some of the warmest and most solid of people. Wayne Korzan, whose humble demeanor and hunting tips will always be remembered. David Strochlic and his wife Allison – it has been fantastic to work with Dave in the lab, and an equally great treat to watch their family grow. Rui Chang, whose MacGuyver-like ingenuity is second to none. Qian Li, the lone olfaction post doc toughing it out and always with a smile. Rachael Brust, a most persistent and generous scientist. Ben Umans, provider of food and comics, only surface representatives of a much deeper and genuine care, support, and kindness. Yaw Tachie-Baffour –your curiosity and stubbornness will carry you far. Dheeraj Roy, whose tireless efforts were incredible to behold. Zecai Liang, Monica Cisneros and Maude Baldwin, though we overlapped less in our work it was always a pleasure to see your progress and excitement. Newer lab members Swathi and Nikhil – I hope this work serves as a useful foundation for you all moving forward. And of course, I'd like to thank Steve for his constant mentorship, support, and boundless scientific optimism and enthusiasm.

Thank you Program in Neuroscience, MD PhD Program, and HST Program for the fantastic communities you have built and continue to build. Thank you to my classmates for being the fantastically impressive people that you are.

Thank you to my dissertation advisory committee, Clifford Woolf, Mark Andermann, and David Ginty. Meeting with you was always a pleasure, and your advice was invaluable. And thank you also to my dissertation examiners, Clifford Saper, David Corey, and Charles Horn for making the time to offer your expert opinions.

Thank you mouse house, namely Chris Hallman, Abdel Zayoune, Brian Payne, Rigo, Tenzin and Emily. Without your dedication to your work none of this would be possible. We depend on you more than you may know. Thank you to our generous collaborators, Adam Cohen and Shan Lou, Ardem Patapoutian, and Bradford Lowell. Thank you to the resident Cell Biology Department Flanagan and vanVactor labs with whom we held regular and fruitful meetings. Thank you to so many people for technical help and expertise, Stan Pashkovski for his do-it-yourself mouse heating system, Joe Bell for his mouse respirator circuit, and Brendan Lehnert for excellent conversations over lunch.

Thank you Nikon Imaging Center at Harvard Medical Center for assistance with microscopy, and to the Boston Area Diabetes Endocrinology Research Center Transgenic Core for help with mouse generation. Support was from an F30CA177170 and NIH MSTP-T32GM007754.

Chapter 1: Introduction

Whatever I have accepted until now as most true has come to me through my senses.

- René Descartes

Organisms have developed exquisitely sensitive methods for detecting and responding to stimuli. Sensory stimuli such as light, sound, mechanical forces, and chemical odorants or tastants are transduced by specialized sensory systems into neural activity, and this activity propagates through discrete, organized downstream nervous system circuitry. In addition to traditionally appreciated external stimuli, many internal physiological states are also monitored by neural sensory systems. This information includes detection of food in the gastrointestinal tract, lung inflation and gas exchange, changes in blood pressure, and detection of toxins or infection. Communication of these internal states to the central nervous system is important for regulation of feeding behavior, respiration, cardiovascular function and sickness behaviors. These senses allow an organism to respond appropriately to vitally important and fluctuating internal states.

One of the major direct body-to-brain neural connections responsible for monitoring internal states is the tenth cranial nerve, the vagus nerve. In this chapter, we will review the anatomy, response properties, and physiological importance of the unique vagus system, with a focus on the sensory neurobiology of vagal afferents.

1.1 General Anatomy

While the majority of vagal fibers are sensory (~80%), the vagus nerve is a mixed nerve and contains fibers from both motor and sensory neurons (Figure 1.1, David Strochlic)[1]. The cell bodies of motor and sensory neurons of the vagus reside in distinct locations. All vagal sensory neuron cell bodies reside outside the central nervous system in ganglia at the base of the skull. The superior-most portion of these ganglia is derived from the embryological neural crest, while the inferior portion is derived from the cranial placodes[2,3]. In many organisms, including humans, these two components are often physically separated, and form visibly distinct cell clusters. However, in smaller rodents such as the laboratory mouse, the nodose and jugular ganglia are fused into a single structure. Furthermore, in the mouse the petrosal ganglion, or collection of neuronal cell bodies that give rise to cranial nerve IX, also fuse with the nodose and jugular ganglia early in development [4,5]. Therefore, the nodose/jugular/petrosal (NJP) complex provides a key major convergence point for interoceptive sensory neurons.

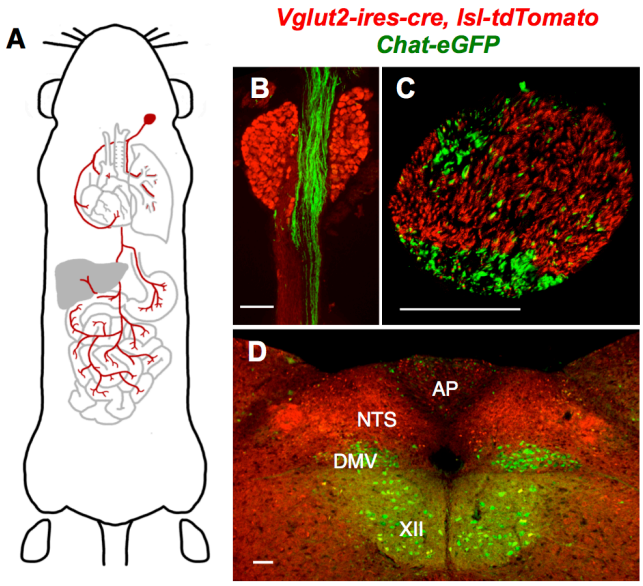

Figure 1.1 General anatomy of the vagus nerve. (A) Schematic of vagal innervation in the mouse. (B) Fluorescence image of a cross-section of a vagal ganglion. Scale bar: 100 μm. (C) Cross-section of cervical vagus nerve trunk. Scale bar: 100 μm. (D) Brainstem section depicting the nucleus of the solitary tract (NTS), area postrema (AP), Dorsal motor nucleus of the vagus (DMNV) and the motor nucleus of cranial nerve 12 (XII). Red marks sensory *Vglut2-ires-cre, lox-tdTomato* neurons, and green marks motor *Chat-eGFP neurons*.

The vagus nerve exhibits a wandering trajectory throughout the periphery, with projections to a broad

array of tissues via numerous nerve branches. Vagal targets include the skin of the outer ear (auricular branch, which carries ~75% of all fibers arising from the jugular ganglion[6]), dura of the posterior cranial fossa (meningeal branch), aortic arch (aortic depressor nerve), the heart (cardiac branches), the trachea, bronchi and lower airways (laryngeal and pulmonary braches), esophagus (esophageal branches), stomach, proximal small intestine, pancreas, the portal circulation and bile ducts in the liver (gastric and common hepatic branches), and the distal small intestine and proximal large intestine (celiac branch) [7] . In several of these sites, vagal sensory neurons display a diversity of terminal morphologies, to be discussed in detail subsequently.

Vagal sensory neurons relay information from the periphery to discrete central nervous system nuclei. The two primary targets are nucleus of the solitary tract (NTS) and the area postrema (AP), areas that regulate many physiological functions including feeding, respiration, heart rate, and nausea [8,9]. The brainstem serves as a major sensory and autonomic hub; the NTS also receives and integrates information from cranial nerves V, VII and IX[10-12]. In addition, a smaller set of vagal sensory neurons project via the spinal trigeminal tract to the spinal trigeminal nucleus in the cervical cord.

Information from the vagus propagates to other brain structures via three major pathways. Sensory information is transmitted to higher-order brain regions such as the insular cortex and limbic system either directly from the NTS[13], or via relays[14] such as the parabrachial nucleus[15]. NTS neurons also connect to local brainstem targets, and can engage motor circuits in the spinal cord or other cranial nerve nuclei[16]. Finally, information is transmitted to vagal motor neurons, either via the NTS, or in some cases, through direct vagal sensory-to-motor reflex arcs[17,18].

Vagal motor neurons regulate gastrointestinal motility, heart rate, respiratory rate and immune response. Most motor neuron cell bodies are located in the dorsal motor nucleus of the vagus (DMNV), a region immediately adjacent to the projection fields of vagal sensory neurons (Figure 1.1). These motor neurons in turn project to a diversity of peripheral targets, including smooth muscle in the airways and intestine, intestinal sphincters, and abdominal paraganglia. A smaller group of motor neurons are also located in the nucleus ambiguus (NA), and project to the heart. Therefore, the vagus nerve in considered one of the primary parasympathetic motor systems in the organism, despite the fact that motor neurons account for only 20% vagal trunk fibers.

Because the vagus nerve innervates and regulates a broad array of internal organs, subsequent sections will provide an overview of vagal sensory neuron anatomy, stimulus detection, and potential physiological roles within each organ system.

1.2 The Cardiovascular System

Anatomy

Vagal afferents innervate all four chambers of the heart, the aortic arch, and major branch arteries in the neck. Endings within the cardiac chambers consist of three primary types, 1) complex un-encapsulated end-nets found most densely near junctions of the great veins entering the atria, and 2) anastomosing nets of fine neurites distributed throughout atrial and ventricular endocardium, some of which closely contact cardiac myocytes and 3) terminals surrounding “small intensely fluorescent” (SIF) cells of unknown function in

cardiac ganglia[19-23]. Notably, the same neuron can give rise to multiple ending types within the heart, complicating interpretations of structure-function relationships[24].

Afferents also encircle the aortic arch, and provide scattered endings at the branch points and in walls of major blood vessels arising from the arch, including the coronary and carotid arteries[20]. Sensory terminals arise from both myelinated and un-myelinated afferents, and form complex ring and reticular structures embedded in the connective tissue of the vessel wall[25].

Response properties

Vagal afferents respond to both mechanical and chemical cues within the cardiovascular system.

Mechanosensitive afferents are sensitive to forces applied to the heart and vessel walls, and can be further classified based on the period of the cardiac cycle during which their activity peaks. Some afferents are maximally active during atrial contraction, and exhibit increases in firing rate with increases in heart rate, suggesting sensitivity to active changes in atrial wall stretch. Other receptors respond during atrial filling, and exhibit reduced activity with increases in heart rate. These receptors adapt slowly to changes in pressure, suggesting they act primarily as measures of overall wall strain. Both of these atria-sensitive fibers are exclusively fast-conducting A-fibers[19,26]. Whether entrainment to different parts of the cardiac cycle is caused by intrinsic differences in neuron types, or is driven by the heterogeneity of cardiac hemodynamics across different cardiac wall locations is debated[22].

Ventricular fibers, in contrast, are much less common than atrial fibers (of cardiac mechanosensors, 75% are found in the atria and 25% in the ventricles) and can be

classified further into two functionally distinct groups: one set responds primarily to ventricular contraction, and the other to gentle endocardial stroking [22,27]. Most ventricular fibers are C-fibers, and also respond to intracardiac administration of a broad array of chemical compounds. The functional significance of this chemical sensitivity remains unclear, but many endogenous compounds produced in the heart that activate these chemically-sensitive afferents are produced in response to cardiac stress or ischemia[28-32]. Furthermore, while many mechanically sensitive afferents are also activated by chemical stimuli, some afferents exhibit increases in firing rate only to chemical mediators and not to mechanical distension [22,29,33].

Vagal afferents also detect mechanical forces within several of the large vessels exiting the heart. Afferents can detect changes in coronary artery pressure, critical for adequate perfusion of the cardiac muscle[34]. In addition, vagal sensory fibers are exquisitely tuned to pressure changes within the great vessels exiting the heart to deliver blood to brain or the rest of the body[33,35-38]. Most mechanistic investigation of cardiac vagal afferent mechanosensation has been performed in aortic baroreceptors. While the specific molecular mechanism remains undefined, dissociated aortic baroreceptor neurons exhibit mechanically induced currents that can be blocked by gadolinium, suggesting the molecular mechanosensor may be a stretch-activated ion channel[39].

Physiology

Several cardiac reflexes are mediated by vagal afferents. Mechanical stretch of receptors in the atria, indicating high pressure in the circulatory system entering the heart, causes an vagus-dependent increase in heart rate and urine output to reduce pre-cardiac

fluid loads (Bainbridge reflex)[40]. Both mechanical stretch of the cardiac walls and intra-cardiac application of chemicals results in reflex bradycardia, hypotension, and coronary artery dilation; reflex effects similarly dependent on an intact vagus nerve (Bezold-Jarisch reflex)[22,34,41,42]. These effects are cardio-protective in situations of ischemia because they collectively decrease the work of the heart, and increase oxygen delivery to the cardiac muscle. Finally, increases in pressure within the large vessels from the heart, including the aortic arch, cause a reflex reduction in heart rate, the well-known vagal baroreceptor reflex[43]. Therefore, the vagus nerve plays a role in several well-described cardiovascular reflexes involved in regulation of organism volume status, cardiac ischemia, and blood pressure.

1.3 The Respiratory System

Anatomy

Vagal afferents travel along the major airways and provide terminals at all levels of the respiratory tree, from the trachea to the alveoli. Many studies describe neuron terminal morphologies in the upper airways, though not all use histological techniques or vagotomy controls to discriminate between fibers of vagal and non-vagal origin. Therefore, the vagal identity of some sensory terminals is inferred based on vagal response properties[44]. A brief summary of observed terminal types is included here, and those of confirmed vagal identity are noted.

Terminal types in upper airway structures include 1) free nerve endings adjacent to

the epithelial layer lining the inside of the airway (confirmed by vagotomy to be at least partially of vagal origin) [45,46], 2) taste-bud like endings concentrated around the epiglottis[47] 3) glomerular endings[45], and 4) rare spindles in the muscles controlling airway opening and closing[48]. Bronchopulmonary afferents, or terminals in the airways and lung parenchyma, form 1) ramified endings within the smooth muscle lining bronchi, particularly dense at bronchial branch points[49], 2) free endings within the alveolar tissue[50], and 3) candelabra-like innervation of neuroepithelial bodies, chemosensory cell clusters within the lung[50,51]. Alveolar and neuroepithelial body terminal morphologies have been identified with vagus-specific labeling methods, though not all terminals at these targets are necessarily vagal[52].

Response properties

Throughout the upper and lower airways, vagal afferents have been broadly classified into three categories based on mechanical versus chemical sensitivity, and adaptation properties[53-55]. Slowly-adapting stretch receptors (SARs) fire during inspiration in the respiratory cycle, and are activated by lung inflation or increases in transmural pressure, but not typically by chemical cues [56-59]. Probing for sites of mechanosensitivity within the respiratory tree allows for inferences regarding SAR terminal location and distribution. Many SARs receive inputs from multiple distributed endings, and are suspected to be located in the smooth muscle layer of conducting airways[60-62]. Intriguingly, inhaled carbon dioxide inhibits SAR stretch sensitivity[63]. This appears to be an effect mediated within the lung because CO_2 inhibits SAR sensitivity without changes in arterial carbon dioxide levels[64,65].

Rapidly-adapting stretch receptors (RARs), in contrast, are also activated by lung stretch, but as their name suggests, adapt within milliseconds to the stretch stimulus[59,66-68]. RARs generally exhibit a higher threshold for activation compared to SARs, though it should be noted that detailed recordings from mechanosensitive lung afferents reveals many fibers with properties intermediate between SARs and RARs[69,70]. RARs, in addition to their mechanosensitivity, are also sensitive to a number of irritating chemical mediators including pollutants such as ozone and smoke, a diversity of chemicals, and introduction of hypo-osmotic solutions within the airways, earning them the name 'irritant receptors'[44,71-74]. RARs are reportedly most dense in the large but not small airways, and their terminals are hypothesized to be either in, or adjacent to the airway epithelium[75,76].

The third type of pulmonary vagal neuron is the C fiber, or J receptor. This afferent type is the most common pulmonary vagal afferent, accounting for more than 75% of vagal innervation of the respiratory tree[55]. C fibers are almost entirely insensitive to mechanical perturbations in the lung, but respond robustly to chemical irritants introduced into pulmonary airways or vasculature, and to pulmonary edema; C-fibers are often activated by the same irritants as RARs[71,77-80]. These neurons exhibit a highly polymodal response repertoire, suggesting they act as broad detectors of chemical irritation[59,81].

In addition to these three pulmonary afferent classes, subsets of fibers specifically in the larynx exhibit additional unique response properties. One category are cold-sensitive fibers, concentrated in the epithelium of the vocal folds, that respond with increases in firing rate when the temperature within the larynx is lowered during an inspiratory breath[82,83]. A second category includes laryngeal receptors sensitive to contractions of musculature that controls the opening and closing of the upper airway[44]. A third set of

fibers exhibit responsiveness to 5-10% CO_2, though often this response can be mixed – some fibers are inhibited by CO_2, while others are stimulated[84], and some studies suggest these are not unique endings, confusing interpretations of the response properties and role of these fibers[85].

Physiology

The vagus nerve is implicated in several respiratory reflexes, each of which regulates normal respiratory physiology or protects the respiratory system from damage[43,86].

Inflation of the lung causes a reflex inhibition of inspiratory drive, termed the Hering-Breuer inspiratory reflex. The Hering-Breuer reflex provides protection against lung hyper-inflation, and depends on an intact vagus nerve[87]. Intriguingly, activation of A-fibers innervating neuroepithelia bodies can induce apnea, suggesting these neurons may mediate the Hering-Breuer reflex[50].

Elevated airway carbon dioxide evokes a reflexive hyperventilation termed the pulmonary-carbon dioxide ventilatory reflex. Transection of the vagus nerve eliminates this ventilatory response, and since vagal motor neurons do not impact breathing rhythm, a role for vagal sensory neurons in airway carbon dioxide detection is implied. Furthermore, because electrophysiological studies failed to observe carbon dioxide-induced increase in vagal afferent activity from extra-laryngeal sites, the impact of carbon dioxide on respiratory rate was thought to be mediated, at least in part, via the inhibitory impact of carbon dioxide on SARs[63,88,89].

Inhalation of chemical irritants evokes reflex pulmonary protective responses including apnea followed by delayed rapid-shallow breathing, mucous secretion, bronchoconstriction, and in some species cough [43,68,87,90-94]. This pulmonary chemo-reflex is though to contribute to airway protection against inhaled toxins, damaging agents or edema that develops secondary to damage.

Vagal afferents also play an important role in airway inflammation. Many C-fibers are responsive to inflammatory mediators[95]. In addition, many pulmonary afferents also express neuropeptides that can be released from afferent terminals in response to stimulation, essentially acting as sensory neuron effectors for neurogenic inflammation in the lung [46]. Selective ablation of TRPV1-expressing vagal afferents completely abolishes bronchoconstriction in a mouse model of asthma, suggesting these fibers are essential for airway hyper-reactivity in this inflammatory disease[96].

1.4 The Gastrointestinal System

Anatomy

While the cervical vagus nerve consists of 20% efferent fibers and 80% afferent fibers, as the nerve courses caudally the proportion of afferent fibers increases. At the diaphragm, only 10% of the fibers in the abdominal vagus trunks are efferent motor fibers. The remaining 90% are afferents, of which nearly all are un-myelinated [97]. At least six morphologically distinct vagal afferent ending types can be found in the gastrointestinal tract: two types of muscular wall endings, three types of mucosal endings, and terminals adjacent to hepatic portal vasculature and bile ducts[98,99]. Targets associated with

gastrointestinal function such as pancreatic islets may also receive sparse vagal afferent innervation[7,100,101]. This section will summarize muscular wall, mucosal, and hepatic terminal morphologies and distributions.

Muscular wall terminals

The gastrointestinal tract has two muscular layers with perpendicular fiber orientations (circular and longitudinal), important for the mechanical digestion and propulsion of food through the tract. Within the muscular layers of the gastrointestinal tract, vagal afferents form two distinct types of endings. The first terminal type, intra-muscular arrays (IMAs), are restricted to the stomach, to regions close to the esophageal and gastro-duodenal sphincters, and in the junction between the proximal and middle segments of the colon [102]. IMAs course between the longitudinal smooth muscle layers, forming long branching parallel tracts closely associated with intrinsically oscillatory, gastric contraction pace-making cells termed interstitial cells of Cajal[103,104].

The second muscular-layer terminal type, the intraganglionic laminar ending (IGLE), can be found throughout the gastrointestinal tract, from esophagus to cecum and large intestine[102,104,105]. IGLEs are characterized by complex branching patterns that span several millimeters and terminate in boutons intermingled with myenteric neuron ganglia resident in the gastrointestinal wall[106-108]. The greatest density of IGLEs is in the stomach, home by some estimates to well over 1000 individual IGLE terminals[105]. IGLEs are also relatively dense within the proximal 4 cm of the small intestine, though this density rapidly decreases along the intestinal length[102,105].

Mucosal terminals

Inside the gastrointestinal tract muscular layers lies a mucosal layer, which serves both as a barrier between the organism and the contents of the intestinal lumen, and functions to detect and absorb ingested nutrients. Vagal afferents form three terminal types within the gastrointestinal mucosa. In the stomach, vagal afferents project through the smooth muscle wall to form multiple bushy terminal arbors in between gastric glands, close to the gastric gland luminal surface[98]. In the small intestine, mucosal afferents form two morphologically distinct terminal types. To increase its absorptive surface area, the epithelium in the small intestine is folded to form projections into the intestinal lumen known as villi. One vagal afferent type encircles the base of villus finger-like projections in the intestinal crypts, or invaginations between villi. The second terminal type projects into the villi themselves, forming complex arborizations immediately adjacent to the intestinal epithelial barrier lining the intestinal lumen[98,109]. A systematic evaluation vagal mucosal afferent terminal density and distribution along the entirety of the intestinal length has yet to be completed.

Hepatic vascular terminals

Vagal afferents often travel in neurovascular bundles with mesenteric arteries en route to supply the intestine. However, despite passage along these mesenteric arteries, terminals in this vascular bed are supplied solely by spinal afferent neurons[99]. However, after supplying the capillary beds of the intestine, blood collects in the hepatic portal system. As its name suggests, these vessels travel from the intestine to the liver, allowing the liver to regulate delivery of nutrients absorbed from the intestine to the rest of the body, and also to metabolically convert potential toxins prior to systemic distribution.

Vagal afferents innervate the hepatic portal system, and form terminals in the vascular walls of blood vessels, bile ducts, and also around portal triads (a bundle of hepatic vein, artery, and bile duct) within the liver[110]. Vagal afferents do not penetrate the liver parenchyma, and terminals remain only around the portal triad critical vascular hubs[7,110].

Response properties and physiology

Vagal afferents are sensitive to a broad array of cues in the gastrointestinal tract. This section will discuss responses to mechanical forces, chemical cues, and gut hormones, as well as the physiological repercussions of these circuits, highlighting controversies present in the field.

Mechanical cues

The sensitivity of vagal afferents in the gastrointestinal tract to mechanical stimuli has been appreciated for nearly 70 years. Paintal, Iggo, and colleagues in the 1950s described the first electrophysiological recordings of afferents in response to distension of the stomach[111,112]. Furthermore, they characterized vagal mechanosensitive afferents as exclusively C-fiber, and functionally as "in-series" tension receptors, responsive both to external stretch the gastrointestinal wall, as well as to muscular contractions of the wall itself[113,114]. Intriguingly, the terminal type most likely involved in gastrointestinal mechanosensation is known and is not closely associated with muscle fibers themselves. Vagal afferent mechanosensitive hot-spots are enriched and highly localized around IGLE-type endings, which are closely intertwined with myenteric ganglia in the muscular wall [115,116]. The precise mechanotransduction mechanism of IGLE-type terminals remains unknown. The association between vagal afferents and enteric neurons suggests a key

functional relationship. However, two main lines of evidence point to the vagal afferent as the primary mechanosensory element. First, vagal afferent responses to mechanical perturbation of the gastrointestinal wall occur in less than 6 milliseconds following stimulus application, a rapid response for synaptic transmission. Second, extracellular calcium is considered a necessary component for vesicular transmitter release, and vagal afferents respond to stomach stretch both when extracellular calcium is removed, and in the presence of calcium-channel blocker Cd^{2+} [117].

Chemical cues

Gastrointestinal vagal afferents are sensitive to the chemical contents introduced into the gastrointestinal lumen. However, several different sites within the gastrointestinal tract may be responsible for chemical detection, and vagal sensory neurons innervating distinct parts of the alimentary canal may exhibit unique coding properties.

Whether the vagus nerve can detect chemical cues in the stomach has been the subject of extensive debate. Careful experiments to eliminate mechanical forces upon application of chemical stimuli have failed to reveal vagal afferents that respond only to the chemical identity of a stimulus, and not wall-distension evoked by stimulus administration[118]. These observations are in accord with behavioral experiments; artificially increasing stomach volume decreases food intake independently of the chemical identity of the distending stimulus[119,120]. However, original work by Iggo described gastric terminals insensitive to changes in wall tension, but highly sensitive to mucosal stroking and changes in pH [121]. These studies raise the possibility that gastric chemoreceptors exist, and that they may play a regulatory role independent of food intake control. In addition, other gastric or esophageal fibers are sensitive to the application of bile, or altered pH,

though reports in these studies suggest these responses are non-repeatable, raising doubts as to their physiological relevance[122].

In contrast, chemical cues in the intestine can clearly evoke vagal activity in the absence of changes in wall tension[123-126]. Whole-nerve and isolated fiber recordings indicate that vagal afferents can respond to carbohydrates, fatty acids, amino acids, hyperosmolar salt solutions, water and acidity[7,124,127,128]. While some studies report vagal afferents sensitive to specific nutrient classes[129-131], other studies report that individual vagal afferents are polymodal, or respond to cues belonging to a variety of chemical classes[132-134]. Therefore, whether vagal chemoreceptors are organized as labeled lines or broad polymodal receptors remains a subject of discussion.

Gastrointestinal chemosensation could occur at a variety of peripheral sites. Mucosal afferents that project into intestinal villi are one terminal type likely responsible for detection of intestinal chemical cues. Three lines of evidence support this conclusion. First, gentle mucosal stroking (but not increased wall tension) activates chemically sensitive afferents[135], second removal of the intestinal mucosa abolishes chemical sensitivity in the vagus[121], and third application of neuron inhibitors (capsaicin or lidocaine) to the mucosal surface can also prevent putative effects of chemical detection[136,137]. However, caveats to these methods abound: 1) removal of the mucosa would abolish not only vagal terminals, but would profoundly alter the absorptive capabilities of the intestine, and 2) the distribution and degree of effect of locally applied chemicals (e.g. lidocaine or capsaicin) to a highly absorptive epithelium is unclear.

Vagal terminals in the hepatic vasculature offer a second potential site of chemical detection because they are ideally located to monitor chemical changes in the blood

carrying absorbed nutrients or gastrointestinal hormones from the gastrointestinal tract. Administration of gut peptides to the hepatic portal system itself increases vagal firing, and nerve terminals, albeit of unclear origin, express gut-peptide receptors in the portal vein [138,139]. In addition, administration of metabolic inhibitors can also alter feeding behavior[140], and induce vagal afferent activity when injected into the hepatic portal system, suggesting vagal afferents may be sensitive to hepatic metabolic activity[141].

Gut Hormones

While uncertainty persists concerning the terminal locations involved in intestinal chemosensation, vagal afferents do not directly contact the intestinal lumen. Therefore, vagal chemosensors are largely thought to be second-order neurons, detecting gut hormones released by primary chemosensory cells resident in the intestinal epithelium.

Two different models concerning vagal nutrient detection persist. In the first model, different resident intestinal chemosensory cells detect different nutrients in the intestine. Chemosensory cells receptive to particular nutrients release specific second messengers, each of which acts on a dedicated vagal afferent type to convey nutrient-specific information to the brainstem. Gut peptide hormones are synthesized and released by resident chemosensory cells within the intestine. Evidence abounds both for and against this model as it relates to two key gut peptide hormones cholecystokinin (CCK) and glucagon-like peptide-1 (GLP1).

Though some studies present mixed evidence[142-144], peripheral injection of CCK reduces food intake, an anorectic effect that is sensitive to sub-diaphragmatic vagotomy[144-

[147]. Administration of CCK induces robust activity in the vagus nerve[148-151]. Furthermore, Cckar antagonists or receptor knock-outs block both the anorectic effects and vagal nerve activation induced by CCK administration[152,153]. Intestinal lipids act as a potent stimulus for CCK release from enteroendocrine cells resident in the intestinal epithelium, and can elicit CCK-receptor-A (Cckar) antagonist sensitive activity in vagal afferents[154,155]. From these lines of evidence, one might suspect that intestinal lipids induce CCK release, and that CCK exerts its anorectic effects by acting on Cckar on vagal terminals in the periphery. However, several problems and competing hypotheses confound this interpretation. First Cckar, itself is not detectable on vagal terminals in the intestinal wall, though it is easily visible on neighboring enteric neurons[156]. Second, vagal afferents responsive to CCK belong to the mechanical distension rather than chemosensitive intestinal afferent class, and CCK increases their mechanical sensitivity[149,153]. Therefore, CCK, and potentially other feeding-related hormones[157], may mediate their effects by modulating the sensitivity of vagal gastrointestinal mechanosensory circuits rather than via direct activation of a nutrient-sensitive afferent subtype.

A similar model exists to explain the anorectic effects of peripheral GLP-1 administration. GLP-1, and specific GLP1R agonists, reduce food intake, lower body weight and are currently in use for treatment of type-2 diabetes[158]. While the evidence is mixed[143,159], many groups report that the effects of GLP-1 are also vagotomy sensitive[160-163]. Intestinal carbohydrate perfusion, potentially via signaling through the taste receptor heterodimer T1R2-T1R3, induces GLP1R release from resident chemosensory cells[164]. GLP1R is expressed in vagal afferents, and GLP-1 administration induces activity in the vagus nerve, an effect that is sensitive to GLP1R antagonists[165]. From these lines of

evidence, one might suspect that intestinal carbohydrates reduce food intake via the effects of GLP-1 on vagal afferents expressing GLP1R. However, again several lines of evidence run counter to this theory. First, conditioned taste preference induced by administration of gut carbohydrates persists despite knock-out of T1R3[166], and despite abdominal vagotomy[167]. Most prominently, GLP1R agonists exert anorectic effects despite complete knock-out of GLP1R in vagal sensory neurons [168].

While intestinal chemosensory cells have traditionally been classified into discrete categories by the gut hormones they express (e.g. CCK chemosensory cells are different that GLP-1 chemosensory cells), recent work indicates that though gradients of specific peptides exist along the intestinal length, most enteroendocrine cells express several gut peptides and cannot be cleanly segregated into distinct populations based on gut peptide release [169-171]. Similarly, while evidence is scarce, some studies report vagal sensory neurons that co-express more than one gut peptide receptor, or that gut peptide receptor expression is dynamically regulated by the metabolic state of the animal[172-176]. These observations, in addition to the conflicting evidence presented above, already clouds interpretation of a gut-peptides labeled line model.

In an alternative model, resident chemosensory cells detect different nutrients or perturbations in the intestine, but these cues converge either at the level of the chemosensory cell, or at the level of vagal afferents. The most convincing evidence for this model arises from electrophysiological studies of polymodal intestinal vagal afferents that show that all intestinal responses are inhibited by a specific serotonin receptor 3 antagonist, suggesting that serotonin signaling drives all vagal afferent chemosensory

responses [132]. 85% of all serotonin in an organism is synthesized and released by a unique resident chemosensory cell population in the intestine, enterochromaffin cells (ECCs). ECCs express a variety of receptors thought to sample the internal environments, and are known to exhibit calcium transients and calcium-dependent serotonin release in response to multiple types of cues[177-179]. Historically, serotonin signaling through the vagus nerve has been most closely associated with development of nausea. Several lines of evidence support this connection. First, reductions in gastrointestinal serotonin synthesis inhibits nausea[180], and secondly serotonin receptor 3 (Htr3) antagonists and sub-diaphragmatic vagotomy both effectively block emesis or nausea-like behaviors in model organisms[181-186]. Furthermore, the amount of nausea experienced by human patients correlates to the amount of peripheral circulating serotonin[187], and Htr3 antagonists are a mainstay anti-nausea treatment for acute chemotherapy-induced nausea in human patients[188-190]. Vagal afferents express Htr3, and administration of serotonin induces robust vagal afferent activity[123,191,192]. However, in addition to a prominent association with nausea, serotonin signaling is also implicated in detection of physiologically encountered gastrointestinal cues[123,132,193]. Therefore, the distinction between nausea and satiety, and the role of serotonin signaling in each remains unclear.

Physiology: Nausea and Satiety

Gastrointestinal cues strongly drive behavior and gastrointestinal physiology. If food is artificially removed from the gastrointestinal tract as an animal feeds, the animal will consume more food to compensate[194]. Conversely if the stomach is stretched or if nutrients are introduced into the intestine, animals will eat less[119,120]. Introduction of

nutrients into the intestine or systemic toxins results in a reduction of feeding and of gastric contractions[147,195]. All of these behaviors depend on an intact vagus nerve[181,196-198], and though vagotomy often cannot distinguish between motor and sensory roles in these effects, subsequent research into vagal afferent neurobiology has suggested several putative gut hormone mechanisms, as outlined, by which afferents could contribute.

However, the difficulty discriminating between nausea and satiety is pervasive, and many interpretations of the physiological role of the vagus nerve are confounded by the fact that a reduction in feeding can be driven both by positive-valence satiety, and negative-valence illness. For example, while serotonin is often cited as the prime contributor to nausea, gut peptides can also induce nausea and illness behaviors[199,200]. Similarly, while gut nutrients can drive cessations in gastric contractions, so can nausea-inducing toxins, a physiological output that is alternatively interpreted as key for normal digestion, or for gastrointestinal pathological defense[147,201]. Even in human studies where subjects report on their experiences during gastrointestinal manipulations, the relative contributions of intestinal versus gastric, and chemical versus mechanical cues are mixed. For example, people do not experience nausea during duodenal perfusion, but they do following gastric balloon inflation, though the sensation is greatly modulated by prior duodenal nutrient exposure[202]. Peripheral cues may communicate satiety and illness via discrete pathways. However, it is also possible that different peripheral cues signal different gastrointestinal mechanical or chemical states, each of which may contribute to satiety at normal levels of activation, and to nausea when signaling is pathologically elevated.

In summary, the relevant vagal afferent terminals for detection gastrointestinal cues, how these cues are integrated, and what the physiological relevance of these cues

may be remains complex. The ability to selectively label and query specific vagal afferents with defined response properties in the intestine would help to shed light on the organization of this multi-faceted sensory system.

1.5 Conclusions

The vagus nerve is a key body-to-brain relay for the cardiovascular, respiratory, and gastrointestinal systems. Peripheral target organs receive dense and varied vagal afferent innervation, and vagal sensory neurons detect of a broad array of physiologically and pathologically relevant cues. Extensive work over the last 70-80 years has provided a fundamental catalog of vagal afferent anatomy, response properties, and physiological relevance. Basic questions remain concerning the coding of many peripheral stimuli. Furthermore, definitive links between neuron anatomy, response properties, and physiological relevance are still needed.

To address these questions I worked collaboratively with several members of the Liberles lab to investigate vagal sensory afferents. David Strochlic established viral tracing methods for vagal afferents in our lab, work that was followed up by Benjamin Umans and myself. Rui Chang developed optogenetic control of vagal afferents, performed some *in vitro* calcium imaging work, and generated the *Glp1r-ires-cre* mouse line. I worked entirely independently on the *in vivo* imaging, *Gpr65-ires-cre* mouse line, and much of the molecular characterization of vagal sensory neuron subsets. Specific notes are provided throughout to clarify contributions.

Chapter 2: *In vivo* imaging of vagal sensory neurons

The ability to determine the response properties of individual sensory neurons is fundamental to understanding the organization of any sensory system. Electrophysiological techniques have provided a wealth of knowledge concerning vagal afferents, but are limited by the fact that whole-nerve or bundle recordings lack single-neuron resolution, while single-neuron methods are difficult for large-scale analyses of neuron populations. Therefore we considered three features particularly important in advancing understanding of the vagal sensory subsystem. First, because the vagus nerve provides broad innervation to many internal targets with complex physiologies, response properties should be measureable in the intact, living organism. Second, because vagal sensory neurons are heterogeneous, the response properties of many neurons must be measured simultaneously and at single-neuron resolution to efficiently resolve the organization of this system. Third, measurement of response properties should interface with the ability to molecularly mark specific neuron subsets. The ability to relate response-property and molecular maps allows access to molecular/genetic tools to determine the peripheral and central anatomical projections, and the physiological roles of specific neuron subsets. To achieve these goals, we developed an *in vivo* imaging preparation of vagal ganglia that involves the well-characterized genetically encoded reporter of neural activity GCaMP3[203].

2.1 Proof of principle

Introduction

To collect robust data from all vagal sensory neurons using an imaging approach requires: 1) expression of a genetically-encoded calcium indicator in all vagal sensory neurons, 2) surgical access to vagal ganglia that preserves neuron viability and peripheral connections, 3) a stable imaging field to ensure the same neurons are imaged over the course of an experiment, and 4) evidence that fluorescence intensity correlates with the degree of neuronal activation. This section will detail achievement of these criteria.

Methods

Animals

All vagal sensory neurons are glutamatergic, and express the glutamate transporter Vglut2 (Chang, 2015). *lox-GCaMP3* mice were purchased (Jackson, Ai38), and crossed with either *Vglut2-ires-Cre* mice (generously provided by Bradford Lowell, Beth Israel Deaconess Medical Center) or *E2a-Cre* mice (Jackson), which drive germ line expression of Cre recombinase and therefore ubiquitous GCaMP3 expression (referred to as *GCaMP3**). Imaging was performed in heterozygous *Vglut2-ires-Cre; loxP-GCaMP3* mice and *GCaMP3** mice; both lines express GCaMP3 in all vagal sensory neurons, and were healthy with no obvious behavioral or physiological deficits. *Wnt1-Cre* animals were generously provided by Susan Dymecki, and were crossed with *lox-tdTomato* animals (Jackson Labs, Ai14).

Surgery

Mice were anesthetized with 4% isofluorane (Webster Veterinary, 14043-225-06) in 100% oxygen (Airgas). Following induction, level of anesthesia was maintained with 1.5% isofluorane in oxygen, delivered at 0.3-0.4L/min (Harvard Apparatus Limited) continuously throughout the surgery and imaging session. During surgery, body temperature was measured by rectal probe (Braintree Scientific, RET3) and maintained at 36-38^{0}C using a PID temperature controller (JLD 612, Amazon) connected to a SSR (Amico 250V 25A SSR-25DA Temperature Control Solid State Relay) and electric heating blanket (Robotshop, 12V heating pad 4"-2", RB-Spa-863). Mice were placed on a molded, thermally conductive ceramic (Aremco, Ceramacast 675n) to ensure even heating.

Once appropriate depth of anesthesia was reached, hair remover (Nair) was liberally applied to the ventral surface of the neck, and wiped clean along with the fur in the surgical site. A one-inch midline incision was made extending from just superior to the sternum to just inferior to the jawline. Blunt forceps were used to separate the submandibular and sublingual glands to expose the trachea. The left glands were carefully retracted, clamped with a hemostat, excised and cauterized. A hooked retractor and magnetic small animal retraction system (Fine Science Tools, 18200-20) was used to pull the sternocleidomastoid and associated soft tissue laterally, exposing the common carotid artery, internal jugular vein and vagal trunk. Gentle tension and blunt dissection separated the vagus nerve trunk from its close association with the carotid artery. A second magnetic retractor was then used to pull the carotid medially, and apply gentle tension to displace the trachea from the surgical site. Gentle dissection with custom curved fine (FST, Dumont 55) forceps separated the vagal trunk from surrounding soft tissue. Care was taken to avoid

grasping or damaging the nerve trunk as it was separated. The superior laryngeal branch, which separates from the main vagal trunk just a few millimeters below the ganglion, was preserved and similarly carefully isolated.

The vagus nerve enters the cranial cavity through the jugular foramen with the glossopharyngeal and accessory nerves and the internal jugular vein. The hypoglossal nerve loops over this site of entry before entering the skull through the hypoglossal canal. First, the hypoglossal nerve was grasped and transected to expose the superior-most portion of the vagus nerve. A final magnetic retractor was placed to apply tension superiorly on small carotid artery branches also located close to the jugular foramen. The auricular and meningeal branches of the vagus nerve, which exit the ganglion in the jugular foramen, were transected. The nodose ganglion, visible as a small bulge around the nerve trunk, was carefully isolated from the other jugular foramen structures. The proximal portion of the vagus was then grasped and transected to allow for elevation of the ganglion, with the intact vagus trunk attached, onto a stable imaging platform. Each of the magnetic retractors was then removed.

The imaging platform used was a small (5mm diameter, #0 thickness, untreated) glass coverslip (NeuVitro GG-5-0), glued to a custom metal arm. The arm extended horizontally from a vertical bar affixed to a micromanipulator (WPI, M3301L), and terminated in a 3mm-wide tip onto which the coverslip can be glued. KwikSil adhesive (WPI) was applied to this imaging platform and the nerve gently lifted such that the ganglion rested in the KwikSil. A drop of lactate ringers was applied to the ganglion, a second coverslip of equal size placed on top of the first, and held in place for 15min as the KwikSil adhesive set. The final position of the ganglion-glass complex within the surgical

field could therefore be controlled with high precision using the micromanipulator grasping the imaging arm.

The skin on the lateral edge of the surgical site was glued (Vetbond tissue glue, 1469SB) to the bottom surface of the metal imaging arm, and silicone layered around the edge of the surgical site to form a liquid-tight pool filled with lactate ringer's solution into which the microscope objective was lowered. The entire mouse preparation was completed on a metal plate that can be lifted and placed on the imaging table beneath the microscope.

Stimulus delivery

Electrical stimulation was delivered via a custom-made bipolar electrode. The exposed cervical portion of the vagus nerve was draped gently over the exposed metal electrode tips. A Grass S5 Stimulator was used to deliver 5Hz, 2msec duration stimuli for 10 seconds, at 1, 3, 5, 7, 10, 15, 30, 50 and 70V.

Imaging

Imaging was performed with an upright Leica confocal microscope with a Leica 20x, NA1.00 water-immersion objective. Imaging parameters were controlled using LAS-AF software. Excitation was provided by an Argon488 laser, and emission measured between 500 and 600nm. The confocal pinhole was reduced to allow collection of light from 5um of z-thickness to avoid overlapping cells in the z-plane. Laser power did not exceed 90uW, to prevent bleaching and tissue damage over the course of prolonged imaging experiments. Frames were collected at a rate of 2 Hz.

Analysis

Image files were exported to Fiji. A frame-average was generated for each imaging video, and used to align cells from all videos collected from each animal. Neurons were then identified by morphology, and a single region of interest selected such that one and only one neuron cell body was contained within it for the entirety of the experiment. Any neurons that shifted position during imaging and failed to reach these criteria were excluded from analysis. The average intensity within each ROI per frame was calculated using the Time Series Analyzer V 2.0 plug-in, and these data were exported to Matlab.

A baseline fluorescence intensity (fbase) was calculated for each ROI from a three-minute period at the beginning of each video, during which no stimuli were delivered. Raw intensity values for each ROI for each frame were converted to ΔF/F, where ΔF/F = (intensity – fbase)/ fbase. Neurons were categorized as responsive to electrical stimulation if they exhibited a ΔF/F during stimulation of seven standard deviations above a 30-second baseline mean prior to voltage step delivery.

Results

Imaging was performed by confocal microscopy of surgically exposed nodose ganglia in freely breathing, anesthetized mice (Figure 2.1 A, B). GCaMP3 fluorescence was readily visualized in individual sensory neurons by confocal microscopy (Figure 2.1 C). Almost all neurons exhibited nuclear exclusion of GCaMP3, which is indicative of neuron health. Typically, ~150 neurons were analyzed in parallel per imaging field, with neurons remaining viable and stably imaged for more than six hours.

Sensory neuron viability was determined after each experiment by electrical stimulation of the vagus nerve trunk, applied as a series of increasing voltage steps (Figure

2.1 D, E). Whole nerve electrical stimulation triggered robust calcium transients that were detectable in 65.9 ± 12.7% of vagal sensory neurons (12 animals, 2440 neurons).

We also observed that many vagal sensory neurons (~20-30%) displayed activity in the absence of experimental manipulations in the periphery (Figure 2.2). Transection of the nerve trunk below the electrical stimulator abolished this activity, but not electrical stimulation responsiveness, suggesting neurons remain electrically excitable following transection, and that transection-sensitive activity is derived from physiologically relevant peripheral inputs (Figure 2.2). Together, these findings indicate that *in vivo* calcium

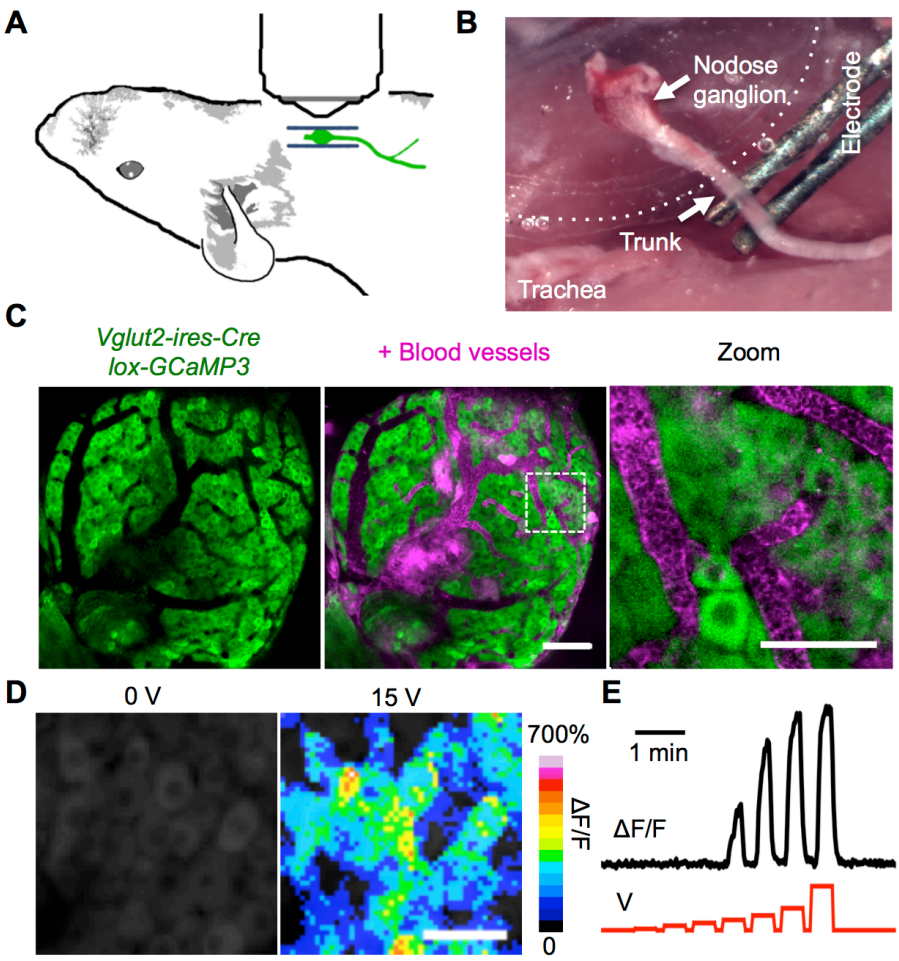

Figure 2.1 *In vivo* calcium imaging of vagal sensory neurons (A) Cartoon depiction of the vagal ganglion imaging technique. (B) Photograph of a vagal ganglion positioned on the imaging platform (dashed line) with electrodes placed on the peripheral nerve trunk. (C) Wholemount image of GCaMP3 fluorescence (green) in a vagal ganglion from a *Vglut2-ires-Cre; lox-GCaMP3* mouse following intravenous injection with Evans Blue, a vascular dye which enables blood vessel visualization (purple). Right figure is a higher magnification view of the boxed inset in the middle figure. Scale bars: middle 100 μm, right 50 μm. (D) GCaMP3 fluorescence changes presented as a ΔF/F color scale before (0 V) and during (15 V) whole nerve electrical stimulation. Scale bar: 50 μm. (E) Response (ΔF/F) of a single representative sensory neuron to a series of 20 second electrical stimulation steps (1, 3, 5, 7, 10, 15, 30 V).

imaging permits parallel analysis of over one hundred single sensory neuron responses within vagal ganglia.

Vagal ganglia in the mouse are composed of a fusion between neural crest-derived, superior jugular neurons, and placode-derived, inferior nodose neurons. We sought to determine in a typical imaging field the degree to which we were sampling from these different neuron populations. *Wnt1* is expressed specifically in neural crest, but not placode tissue derivatives. We observed very rare tdTomato-positive neurons in ganglia prepared from *Wnt1-Cre*; *lox-tdTomato* animals using the standard imaging surgery protocol. Therefore imaging experiments sample almost exclusively from a placode-derived neuron population.

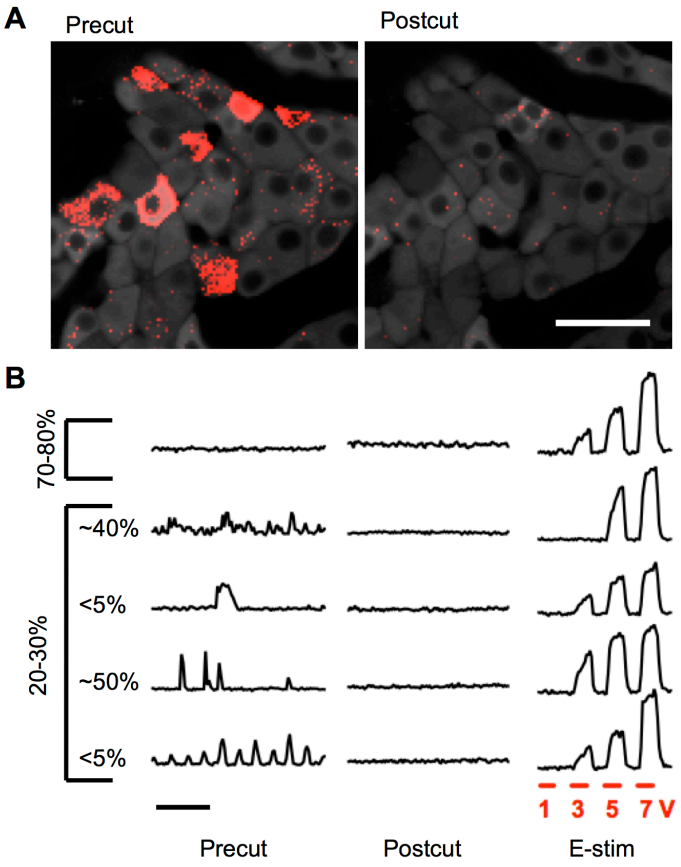

Figure 2.2 Vagal sensory neuron activity without exogenous stimulus application. (A) Neurons that exhibit activity before (precut) and after (postcut) cervical trunk transection are indicated in red. Ganglion morphology is in grey. Scale bar: 50 μm). (B) Representative traces of changes in neuron fluorescence intensity precut, postcut, and to electrical stimulation following the cut. (Left time bar 1 min, right electrical stimulation pulses each 20 sec).

Discussion

We developed an *in vivo* imaging preparation in vagal ganglia that permits real-time, stable measurement of calcium transients in ~150 individual, viable vagal sensory neurons per imaging field. These experiments provide a framework for studying peripherally

evoked responses in vagal sensory neurons. However, consideration of a few technical points is warranted.

Not all vagal sensory neurons exhibited fluorescence intensity increases in response to voltage steps applied to the nerve trunk in every preparation. This could be potentially attributed to three factors: 1) surgical damage to individual neurons or their axon proximal to stimulator placement, 2) incomplete contact between stimulator electrodes and the nerve trunk, 3) intrinsic neuron properties such that depolarization is not associated with calcium flux. Surgical damage is a likely contributor; two of the most proximal sensory branches (meningeal and auricular) were intentionally cut to allow for imaging access to the ganglion. In addition, non-responsive neurons were often located in a central ganglion zone, where physical compression of the ganglion between stabilizing glass coverslips was greatest. Incomplete electrode contact also is a likely contributor; the voltage required to elicit fluorescence intensity depended on the proximity of electrode placement and varied preparation-to-preparation. An intrinsic paucity of calcium influx in specific vagal sensory neuron subsets remains a theoretical possibility, and an important one to consider given this might result in invisibility of specific classes of sensory responses. However, if such a population exists, it is likely small given that electrical stimulation could activate over 90% of sensory neurons in some preparations.

In addition to electrically evoked activity, we observed several patterns of activity dependent on an intact connection with peripheral targets. These will be discussed in subsequent sections.

2.2 Respiratory stimuli

Introduction

Vagal sensory neurons respond to several classes of respiratory stimuli, including lung irritants and mechanical stretch. In this section, we establish the compatibility of imaging to record vagal sensory neuron detection of lung stretch. Furthermore, because imaging affords a unique opportunity to record in an unbiased fashion from hundreds of neurons simultaneously, we explore the response properties of rare respiratory-cue-sensitive vagal sensory neuron subsets.

Methods

Stimulus delivery

Respiratory stimuli were delivered via tracheal cannula. The musculature overlying the superior trachea was transected and reflected to expose the top 5 cartilaginous rings of the trachea. A 16G needle was used to punch a hole through the trachea wall between the first and second cartilaginous segments. PE-10 tubing (Braintree Scientific) was inserted through this hole, and advanced until the tubing end reached the carina. The tubing was tunneled externally under the skin in the neck, to a connector that would multiplex to several gas tanks. Flow rates out of each gas tank were controlled via tank-specific regulators set to 1L/min. Gases administered included 100% oxygen, 100% nitrogen, and various concentrations of carbon dioxide/ oxygen mixtures (5% CO_2/95% O_2, 10% CO_2/90% O_2, 100% CO_2/0% O_2). Acetazolamide (ACZ) was administered via intraperitoneal injection (40 mg/kg, as in Herson 2003).

EKG and respiratory rate recordings

Stripped needles (PrecisionGlide 23G3/4 Beckton Dickinson & Co) coated in conductive gel (Parker Laboratories Inc, Signa Creme, Ref 17-05) were inserted in the right forepaw and in the left hind paw, and were connected to a differential AC amplifier (AM Systems M1700) and DAC system (National Instruments) to record the mouse EKG. A piezoelectric sensor (Sparkfun, SEN-09196) was placed under the mouse thorax to measure respiratory events. All physiology data collection was performed using Matlab. A trigger box (generously loaned by Leica) was used in a subset of experiments to synchronize the EKG and respiratory recordings with the frames of videos from specific imaging sessions, allowing for accurate linking of the animal's respirations and imaged vagal sensory neuron fluorescence intensity changes.

Analysis

Neurons were categorized as responsive to introduction of gases in the lung if they exhibited increases in fluorescence intensity during the stimulus at least three standard deviations or greater above a 30-second baseline mean intensity. The fast-Fourier transform of a 3-min imaging period during which no exogenous stimuli were applied was determined, and oscillatory neurons were defined as neurons that exhibited a peak in the FFT between 0.1 and 0.75Hz greater than 5SD above the mean. To determine whether all oscillators were related to the animal respiratory rate, these FFT peaks were each compared to the animal respiratory rate. In addition, to determine how many neurons in total oscillate at the respiratory rate, the FFT trace from each neuron was queried at the

known respiratory rate of the animal: neurons exhibiting peaks at this frequency of 5 standard deviations above the FFT-plot mean or more were categorized as oscillatory at the respiratory rate.

Results

Lung inflation evoked rapid, robust, and reproducible calcium transients in 4.0 ± 0.9% (71/1711 neurons, 11 animals) of viable, imaging-accessible vagal sensory neurons (Figure 2.3 A). Infusion of ambient air, oxygen, and nitrogen activated the same neurons (Figure 2.3 B), suggesting (1) a mechanosensory response indifferent to gas composition, and (2) insensitivity to airway oxygen levels. Responses were typically sustained for the duration of inflation, and neurons returned to baseline abruptly when the stimulus was terminated.

Consistent with prior studies, lung-stretch responsive neurons were cyclically activated during tidal breathing, presumably detecting increases in lung volume during each inspiration (Figure 2.3, C). While many lung-stretch responsive neurons (52%; 37/71) displayed baseline oscillatory activity entrained to the respiratory cycle, few neurons unresponsive to lung stretch (1.3%; 23/1711) displayed such oscillatory behavior.

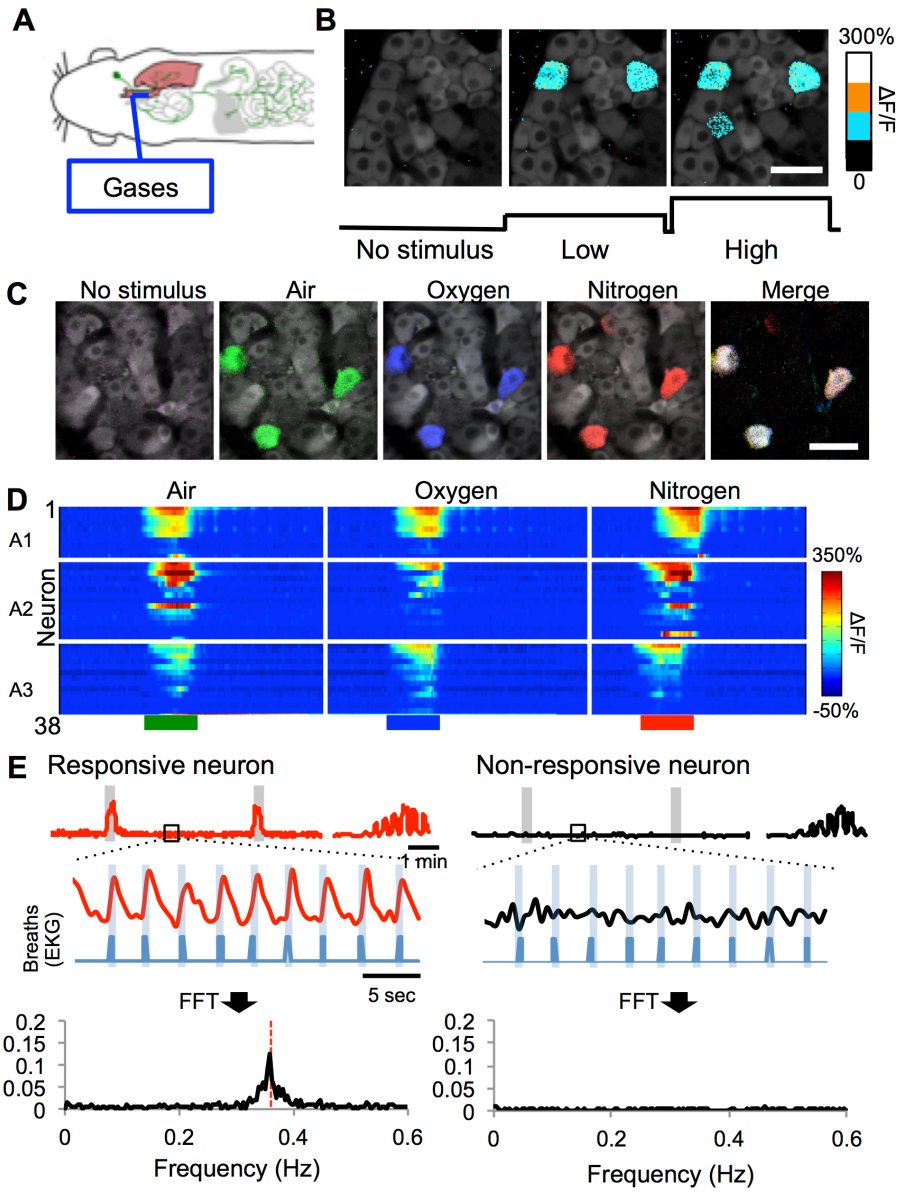

Figure 2.3 Sparse sensory neurons detect inflation of the lung. (A) Cartoon depicting introduction of respiratory stimuli via a tracheal cannula. (B) Air was infused into the respiratory system at low (0.5 liters/minute) or high (1.0 liters/minute) flow rates, and responses (ΔF/F, color scale) were observed in rare vagal sensory neurons by *in vivo* imaging. Scale bar: 50 μm (C) Single neuron responses before (no stimulus) and during lung inflation with ambient air (green), oxygen (blue), and nitrogen (red) visualized by confocal microscopy of vagal ganglia. Scale bar: 50 μm (D) Time-resolved responses (ΔF/F, color scale) of 38 neurons (3 mice) to lung inflation (30 seconds, colored bars) by stimuli indicated. (E) Representative responses during tidal breathing of single neurons that detect (responsive neuron) or do not detect (non-responsive neuron) lung stretch (grey bars). Neuron viability was verified by electrical stimulation (right). Breaths observed by electrocardiogram recordings (blue bars) are aligned with activity traces (black, red) in figure inset. Fast Fourier Transform (FFT) revealed a peak in the power spectrum at the frequency of the respiratory rate in stretch-responsive neurons.

While nitrogen, oxygen, and ambient air infusion activated the same neuron cohort, a more complicated response was observed with the introduction of carbon dioxide. We observed that carbon dioxide simultaneously 1) inhibited the majority of lung mechanoreceptors, and 2) activated a discrete neuron cohort comprising 5.9% (36/611, 4 animals) of vagal sensory neurons (Figure 2.4 A-D). Carbon dioxide-responsive neurons were not cyclically entrained to respiration, suggesting that these neurons detect only elevated carbon dioxide levels. Responses were rapid (<1 sec after stimulus introduction), faster than responses to lung stretch, and transient. Furthermore, responses to carbon dioxide were sensitive to the carbonic anhydrase inhibitor, acetazolamide (Figure 2.4 E-F).

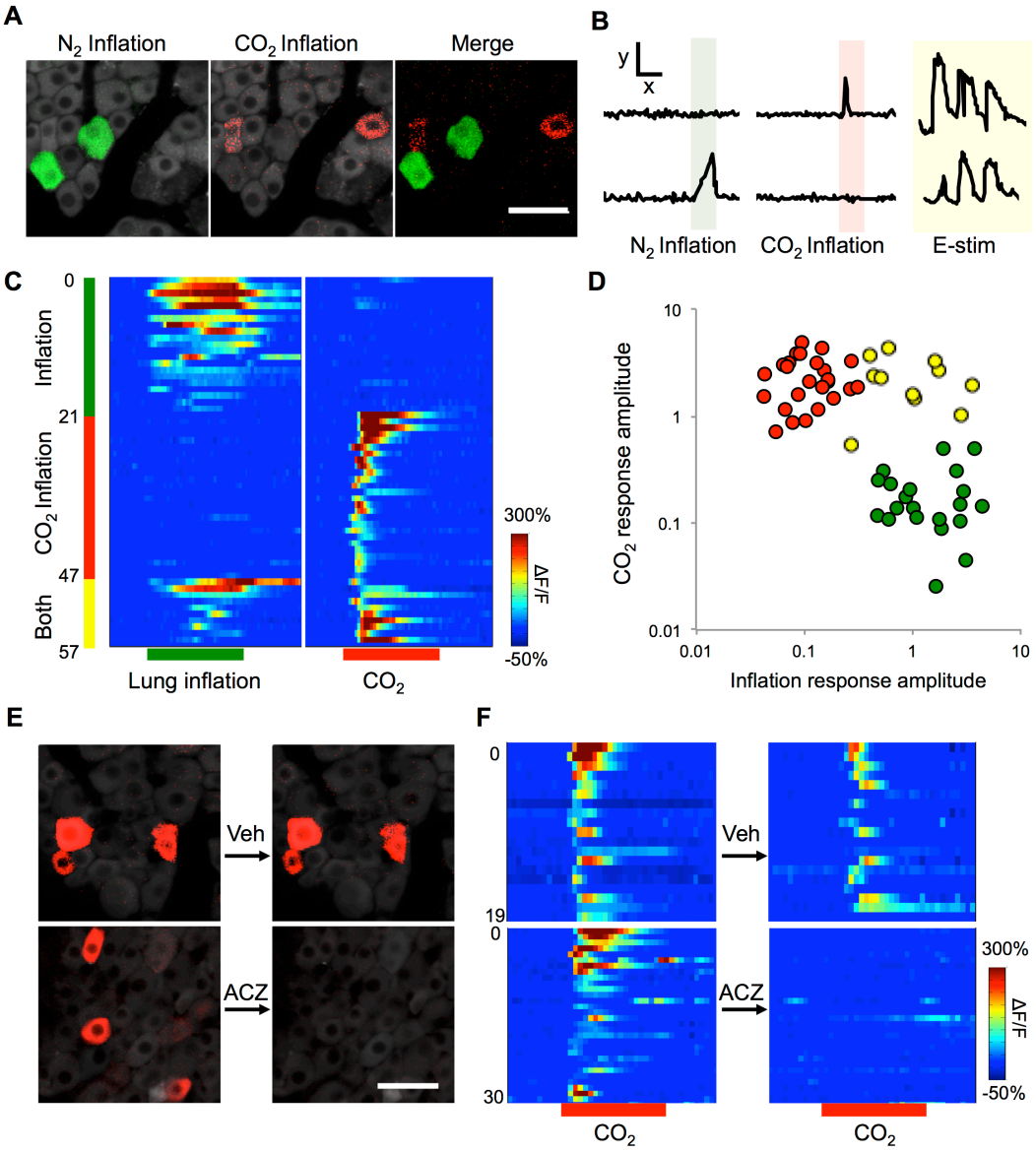

Figure 2.4 Carbon dioxide evokes a complex vagal response. (A) Single neuron responses in vagal ganglia following infusion of oxygen (green) or carbon dioxide (red) in the lung. (B) Representative single neuron responses (ΔF/F) to oxygen-induced lung inflation (green), carbon dioxide-induced lung inflation (pink) and electrical stimulation (E-stim, yellow). x = 30 seconds; y = 100% ΔF/F. (C) Time-resolved responses (ΔF/F, color scale) of 57 neurons responsive to lung inflation by air/oxygen/nitrogen (green, 15 seconds), by carbon dioxide (red, 15 seconds), or both (yellow). (D) Graph depicting the magnitude (maximal ΔF/F increase) of single neuron responses to lung inflation induced by ambient air and carbon dioxide. (E) Single neuron responses and (F) time-resolved responses to carbon dioxide before and after injection of vehicle control or acetazolamide (ACZ, intraperitoneal, 40 mg/kg). Scale bar: 50 μm.

Discussion

Together, these findings indicate that *in vivo* calcium imaging in vagal ganglia can reliably report on physiological stimuli introduced in the periphery, and can do so over a time scale as rapid as tidal breathing.

Lung-stretch responsive vagal sensory neurons cyclically entrained to the respiratory cycle and inhibited by carbon dioxide are likely previously described slowly-adapting receptors (SARs).

Intriguingly, carbon-dioxide-responsive cells may represent the rare laryngeal carbon dioxide receptors. However, because the nodose and petrosal ganglia are fused in the mouse, carbon-dioxide-sensitive afferents observed here may be 'petrosal' neurons physically intermingled with nodose populations. To date, no molecular marks have been identified to reliably distinguish petrosal and nodose sensory neurons, so this is a difficult hypothesis to validate. The sensitivity of the CO2-evoked response to the carbonic anhydrase inhibitor acetazolamide is consistent with the mechanism of carbon dioxide detection by carotid-body innervating neurons. However, it does not exclude the possibility that this neuron subset is responsive to another carbonic anhydrase –dependent process.

2.3 Gastrointestinal stimuli

Introduction

The vagus nerve provides dense innervation to various targets within the gastrointestinal tract. Response properties of vagal sensory neurons to a variety of

gastrointestinal stimuli have been studied for over 90 years. In this section, we establish the compatibility of *in vivo* imaging with recording of gastrointestinal stimuli. Furthermore, because imaging affords the ability to record from many neurons simultaneously, it is a uniquely powerful tool to resolve basic debates about gastrointestinal stimulus coding.

Methods

Stimulus delivery

Mice were fasted overnight for gastrointestinal experiments. To introduce liquid diet into stomach and intestine separately, the gastro-duodenal sphincter was tied off by surgical thread looped circumferentially around the sphincter. Liquid diet (100-200 μl, TestDiet 0054451, 37°C) was then introduced into the stomach or the small intestine with a 26G needle. Liquid diet was injected into distal intestinal regions by injection into a surgically exposed intestinal segment. Following imaging, the distance of food migration from the injection site was measured.

Gastric distension was achieved by either of two methods: 1) inflation of a surgically implanted latex balloon (Braintree Scientific, 73-3478) affixed to a small rodent feeding needle (FST, 18061-20) and syringe, or 2) inflation of the stomach with nitrogen gas (flow rate 3-6 mL/min, 7-15 sec of inflation).

Intestinal stretch involved introducing a duodenal entry cannula through the pyloric sphincter, and an exit port located ~11 centimeters distally in the small intestine. Prior to stretch, intestinal contents were flushed with saline, and stretch was introduced by introducing fixed liquid volumes in the presence of an exit port clamp.

To introduce intestinal chemical stimuli, a small rodent feeding needle was inserted through an incision in the stomach, pushed past the gastroduodenal sphincter, and placed in the proximal duodenum, within 0.5 centimeters of the sphincter. The intestine was transected ~11 centimeters distally to create an exit port, and saline (PBS, Gibco 14040) was continuously perfused (125 μl/minute) using a peristaltic pump, with stimuli (500 μl) periodically introduced. Use of a perfusion system allowed for delivery of unique chemical stimuli without alterations in the mechanical forces on the intestinal wall. Stimuli (glucose, sodium glutamate, sodium chloride, sodium oleate, sodium dodecanoate, polyethylene glycol, mannitol, unconjugated bile salts) were dissolved in saline. The fatty acids dodecanoate and oleate are not water-soluble, so were suspended in bile collected from mouse gallbladders before dilution in saline. Solution osmolarity and pH was measured using a standard osmometer and pH meter respectively. The stimulus pH was corrected to pH = 7.0 unless otherwise specified.

Experiments were excluded if surgical complications prevented stimulus delivery or imaging.

Analysis

Neurons were coded as responsive to liquid diet injection if both of two criteria were met: 1) peak GCaMP3 fluorescence was two standard deviations above the baseline mean within 250 seconds of stimulus introduction and 2) the mean GCaMP3 fluorescence over a 20 second window around the peak response was >50% above baseline. Neurons were coded as responsive to mechanical stimuli (stomach, intestine) if either of two criteria were met: 1) maximal GCaMP3 fluorescence was > seven standard deviations above the baseline mean during the stimulus (for rapidly adapting responses) or 2) if mean GCaMP3

fluorescence was > three standard deviations above baseline mean during the entire stimulus (for slowly adapting responses). Response amplitudes to perfused intestinal stimuli were calculated as the difference between the mean intensity at the peak of the response, and the baseline fluorescence mean. Correlation coefficients to compare the similarity of response amplitudes to different stimuli were calculated for all cells encoded as responsive to any one or more perfused stimuli.

Results

Introduction of 200uL liquid diet into the stomach, a volume of food consumed by a mouse during a meal, activates 18.9% (156/829, n = 7 mice) of all nodose sensory neurons. A food bolus in the proximal duodenum activates 17.8% of nodose sensory neurons (139/780, n = 6 mice). The majority of neurons sensitive to introduction of food into the stomach do not respond to food in the intestine (86%, 105/122, n = 4 mice), and similarly the majority of intestinally responsive neurons are insensitive to food in the stomach (84%, 88/105, n = 4 mice), indicating discrete nodose populations responsible for each of these cues (Figure 2.5 A).

A liquid food bolus both mechanically distends the gastrointestinal tract, as well as alters the chemical composition of the intestinal lumen. Therefore, we further sought to determine which of these stimulus features (chemical vs mechanical) to which vagal neurons are sensitive. Neurons in the small intestine responsive to a liquid diet are not activated by distension of the same volume as a saline bolus (Figure 2.5 B, right). Furthermore, while neurons can be activated by larger distensions of the intestine, the majority of distension-responsive neurons are different neurons than those activated by

intestinal food (93%, 59/64, n = 2 mice). A small subset of liquid-diet-responsive neurons did respond to saline distension (24%, 5/21, n = 2 mice). This suggests that vagal afferents in the intestine are comprised of a mechincally sensitive cohort, and a distinct chemically sensitive cohort.

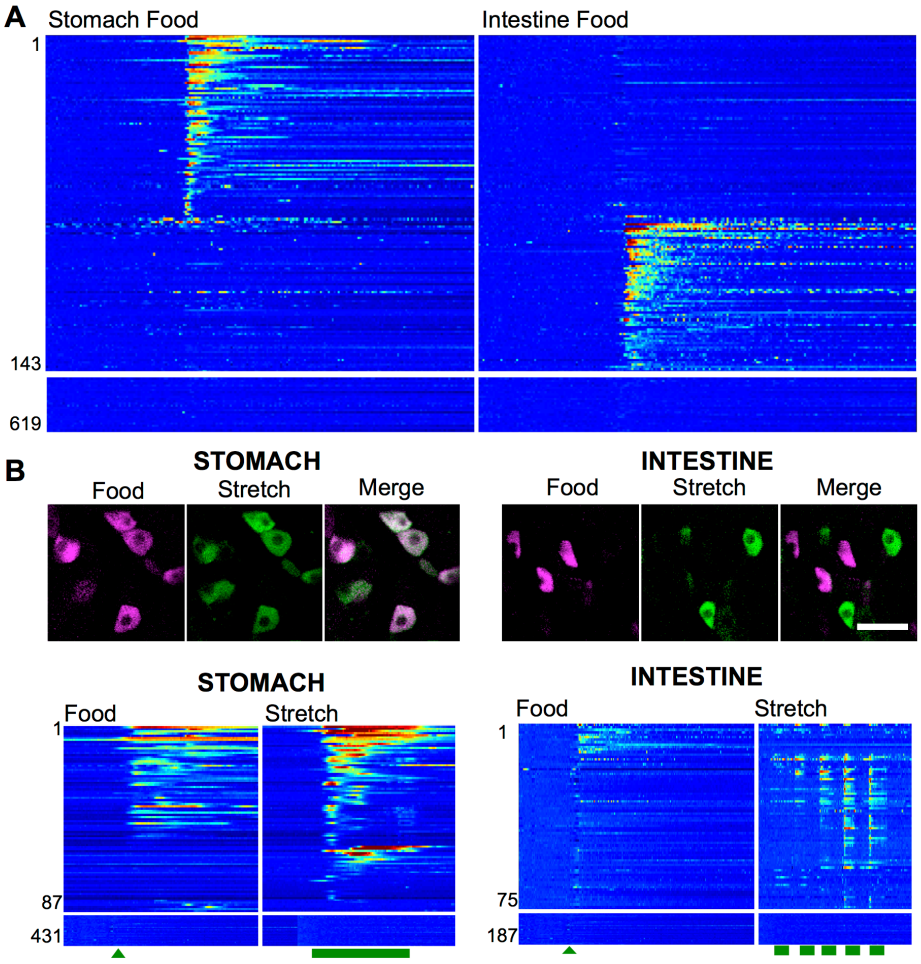

Figure 2.5 Vagal sensory neurons responsive to chemical and mechanical cues in the gastrointestinal tract. (A) Time-resolved responses (10min per panel, ΔF/F, color scale) of 143 neurons to injection of liquid diet (200 μL) into the stomach and small intestine activated discrete cohorts of neurons. Each panel represents 10 minutes of imaging data. (B) Single neuron and time resolved responses to stomach food versus stomach stretch (30 seconds, green bar), and intestine food versus serial intestine stretches (each 30 seconds, green bars). Scale bar 50 μm.

In contrast, the majority of neurons responsive to a gastric food bolus are sensitive to mechanical distension via non-nutritive nitrogen gas inflation of the stomach (90%, 56/62, n = 4 mice), suggesting that vagal afferents activated by food in the stomach are

sensitive to the mechanical (but not chemical) component of food injection. Non-nutritive distension, whether by balloon or nitrogen inflation consistently activated a slightly larger neuron cohort than liquid diet injection; only 70% (56/81, n= 4 mice) of nitrogen-inflation-responsive neurons responded to a subsequent liquid diet injection (Figure 2.5 B, left). This may be due to differences in mechanical forces applied during each type of stimulus administration. Acute distension of the stomach with a surgically implanted gastric balloon activated a sparse subset of vagal sensory neurons. Responses to gastric distension typically occurred in the same neurons across stimulus strengths, and increasing distension volume recruited additional neurons. Low (300 μl), medium (600 μl), and high (900 μl) volume distensions activated 7.9%, 12.7%, and 17.3% of viable, imaging-accessible vagal sensory neurons respectively (Figure 2.6 A-D).

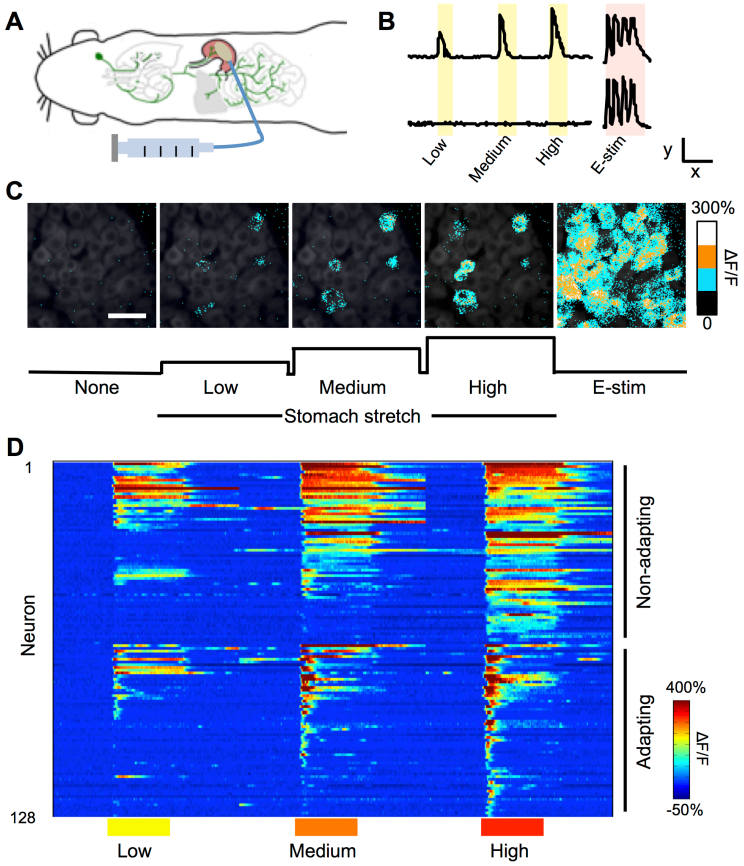

Figure 2.6 Visualizing stomach mechanoreceptors. (A) Cartoon depicting method for inducing gastric distension. (B) Representative traces (ΔF/F) of single neurons responding or not responding to low (300 μl), medium (600 μl), and high (900 μl) volume gastric distension (yellow bars) and electrical stimulation (E-stim, pink bars). x = 1 minute, y = 200% ΔF/F. (C) Representative images of GCaMP3 fluorescence (ΔF/F, color scale) obtained by confocal microscopy of vagal ganglia when stomach volume was in the resting state (none), during low, medium, and high volume gastric distension, and during whole nerve electrical stimulation (E-stim). Scale bar: 50 μm (D) Time-resolved responses (ΔF/F, color scale) of 128 neurons responsive to low (yellow bar, 30 seconds), medium (orange), or high (red) volume gastric distention. Cells are sorted based on whether they adapt to the high volume distension.

These findings support

three conclusions: 1) different cohorts of vagal sensory neurons innervate the stomach and small intestine, 2) stomach vagal sensory neurons are activated by mechanical cues, 3) there are two populations of intestinal vagal afferents, sensitive to mechanical distension versus intra-luminal contents.

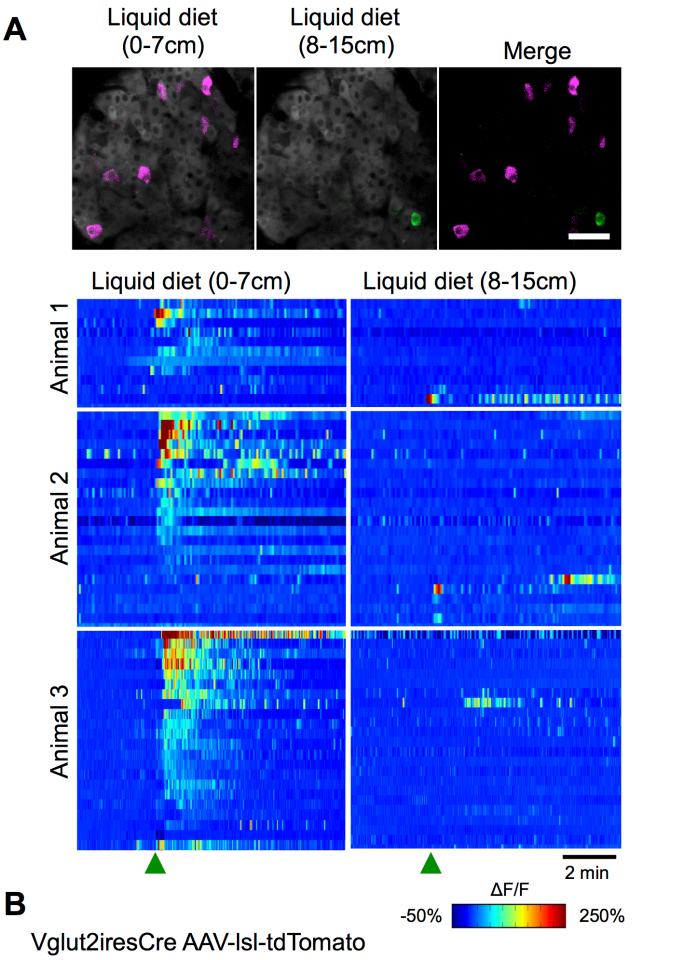

Figure 2.7 The duodenal bulb is a critical site for detection of intestine lumen contents. (A) Single neuron representatives and Time-resolved responses (ΔF/F, color scale) of 94 neurons responsive to injections of liquid diet (green arrows) in a proximal and distal small intestine segment. (B) Whole mount image (upper), and zoomed in representatives (lower) of a flattened small-intestine segment from a *Vglut2-ires-cre* mouse after nodose injection of cre-dependent AAV-lsl-tdTomato. Scale bar 100 um.

We sought to characterize distension-independent small intestine responses more thoroughly. First, we began by examining where in the small intestine vagal afferent intra-luminal detection occurs by injecting liquid diet into the proximal 0-7 cm vs. the subsequent 8-15 cm of intestinal length. In this set of experiments, liquid diet injection within the first 0-7 cm of the duodenum resulted in activation of ~15% of vagal sensory neurons (n = 3 mice). In contrast, injection further down the intestine in the same animals resulted in very limited acute

afferent activation (<3%, n = 3 mice) (Figure 2.7 A). These response properties map directly onto the density of vagal innervation of intestinal villi. Vagal afferents form dense net-like arborizations within intestinal villi; these terminals are present in nearly every villus in the proximal 0-2 cm of the duodenum. However, these terminal types are almost entirely absent from villi located 4 cm or further from the pyloric sphincter (Figure 2.7 B, see Chapter 3.3 for description of the anatomical tracing technique used). Vagal afferents that detect intra-luminal intestinal cues are concentrated within the duodenal bulb, so are exquisitely poised to detect gastric contents emptied into the intestine.

The sensory specificity of vagal sensory neurons responsible for detection of changes in intestinal luminal contents remains highly controversial. In vivo imaging affords an advantage over past electrophysiology techniques in addressing this question because of its unique ability to track neuron responses in many neurons simultaneously, therefore providing large population-level analyses for each stimulus delivered. Therefore, we sought (1) to characterize nutrient responses in the vagus nerve, (2) to determine whether such nutrient responses evoked activity in nutrient-specific vagal labeled lines.

We observed by in vivo imaging that vagal afferents respond dose-dependently to a variety of chemical stimuli: a carbohydrate (glucose), amino acid (glutamate), fatty acid (sodium dodecanoate), and salt (sodium chloride) (Figure 2.8).

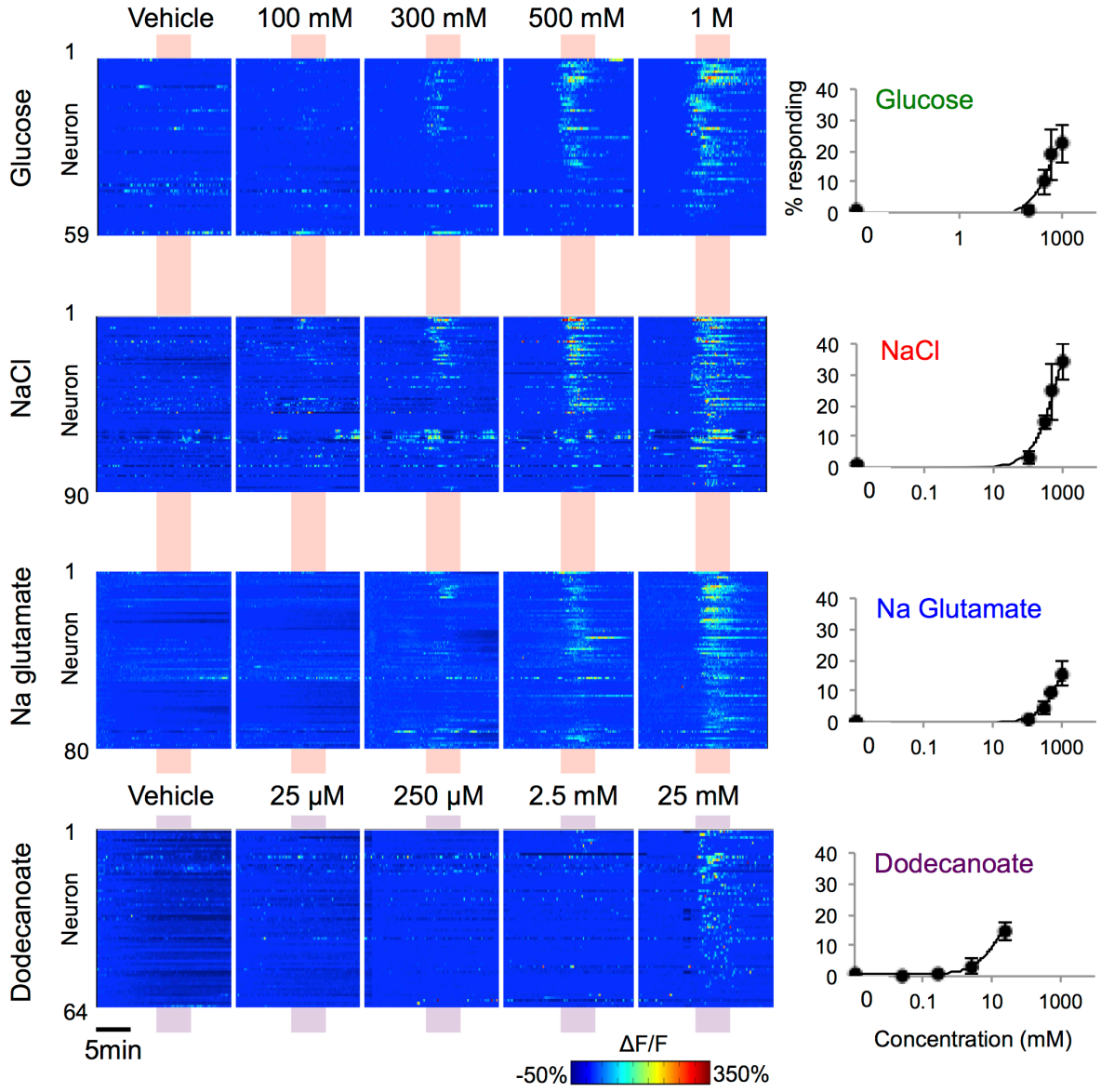

Figure 2.8 Intestinal perfusion of nutrients dose-dependently recruits vagal afferents. Left: Time resolved responses of neurons during administration of glucose, sodium chloride, glutamate and dodecanoate emulsified in mouse bile. Red/ purple boxes indicate stimulus administration times (5 min). Right: Percent of nodose neurons responsive to each cue (mean ± sem, n = 3 mice per cue).

We first examined whether the same or different neurons detect a nutritive versus non-nutritive stimulus by alternately perfusing glucose and sodium chloride stimuli. Alternate administrations of sodium chloride and glucose revealed that the great majority of neurons responded to both these stimuli without distinction. Of 88 neurons responsive to two or more of these stimuli, 77 (87.5%) responded to both glucose and sodium chloride, while 9 (10.2%) responded only to glucose and 3 (3.4%) only to sodium chloride stimuli, lower numbers of neurons than those responsive to any single stimulus administration (10-20 neurons) (Figure 2.9 A, C). We reasoned that perhaps both these stimuli might recruit the same neurons, but that neurons could still encode stimulus identity by exhibiting a preferred response to one stimulus over the other. Therefore, we performed correlation analyses between the response amplitudes to each of these stimuli. Each of the six comparisons yielded significant correlations, whether comparisons were made between like stimuli (e.g. glucose vs. glucose and NaCl vs. NaCl) or between different stimuli (e.g. glucose vs. NaCl) (Figure 2.9 A,C). These experiments suggest that a subset of vagal intestinal chemoreceptors is activated by each stimulus, but that the vagus sensory system cannot discriminate salt and sugar stimuli.

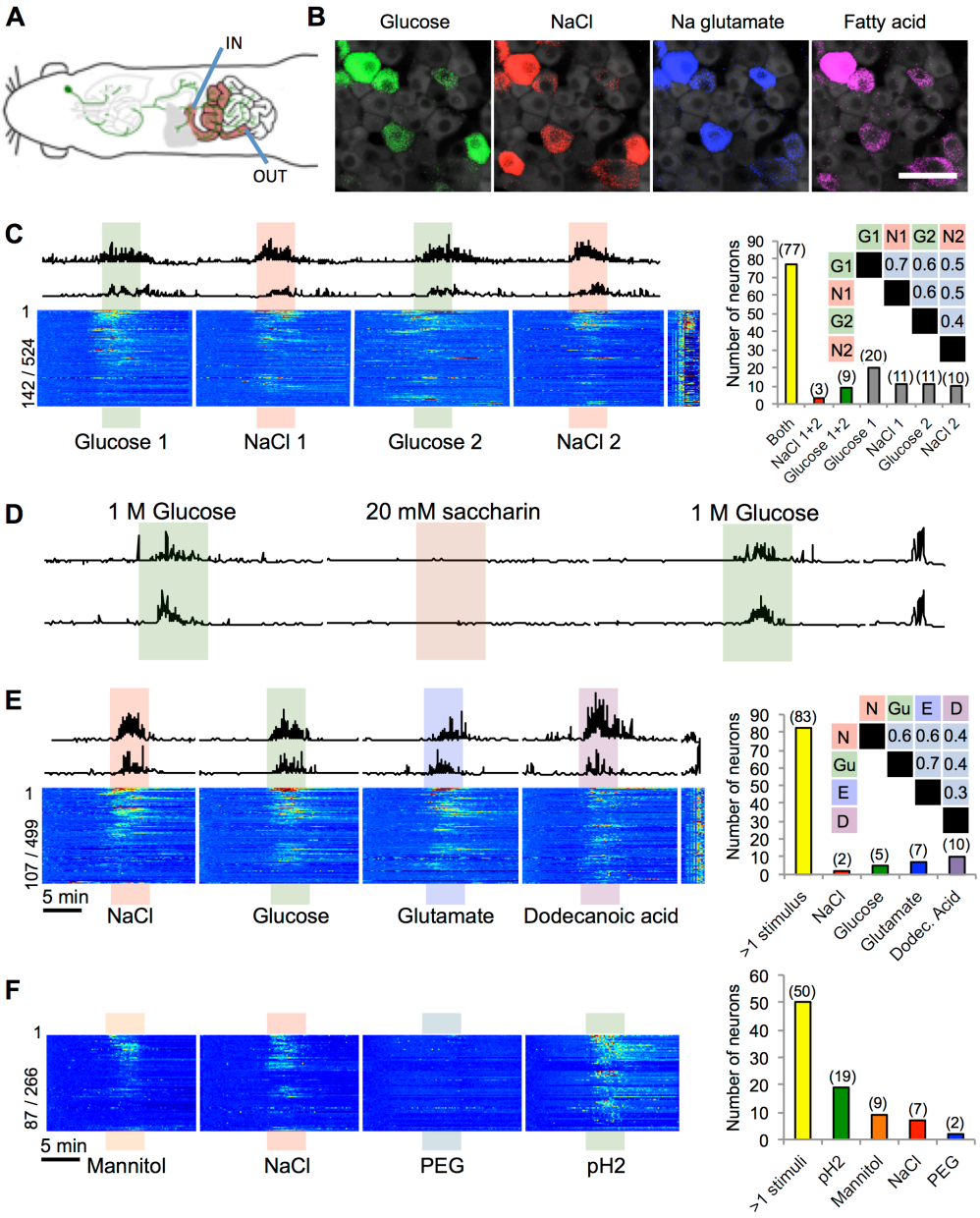

Figure 2.9 Vagal afferent intestinal chemosensors are polymodal. (A) Cartoon depicting method for introducing stimuli in the lumen of the proximal intestine. (B) Representative images of GCaMP3 fluorescence signal obtained by confocal microscopy of vagal ganglia following intestinal perfusion of glucose (1 M, saline, green), sodium chloride (500 mM, saline, red), sodium glutamate (500 mM, saline, blue) and dodecanoic acid (25 mM, saline and conjugated mouse bile, purple). Scale bar: 50 μm (C) Time-resolved responses (top: ΔF/F of two representative neurons, bottom: ΔF/F color scale of 142 responsive neurons out of 524 imaged neurons) following alternating perfusions of glucose (1 M in saline, green, 240 seconds) and sodium chloride (500 mM in saline, pink, 240 seconds). Right: The number of neurons responsive to both glucose and sodium chloride (yellow), or either stimulus alone. Correlation coefficients of response patterns across the neuron repertoire were calculated for each stimulus pair (G1- glucose 1; N1- sodium chloride 1; G2- glucose 2; N2- sodium chloride 2). (D) Representative ΔF/F traces of two neurons responsive to glucose, but not the artificial sweetener, saccharin (stimulus administration indicated by colored bars, 5 min). (E) Time-resolved responses (top: ΔF/F of two representative neurons, bottom: ΔF/F color scale of 107 out of 499 responsive neurons) following perfusion of stimuli indicated, Right: graphs as in panel B. (N- sodium chloride 1; Gu- glucose; Ga- glutamate; D- dodecanoic acid) (F) Time-resolved responses (ΔF/F color scale of 87 out of 499 imaged neurons) following perfusion of stimuli indicated.

The T1R2-T1R3 receptor heterodimer is responsible for the specific detection of carbohydrates in the gustatory system, and has been proposed to function to detect carbohydrates in the gastrointestinal system[204], and of irritants in the upper airways[205]. However, we found that vagal responses to intestinally perfused artificial sweeteners at concentrations sufficient to evoke T1R2-T1R3 activation failed to activate vagal sensory neurons (Figure 2.9 D). While it is possible that responses to artificial sweeteners fall below the sensitivity of calcium imaging, this may also suggest that metabolic responses mediated by intestinal sweet receptors may involve alternative pathways[164].

Furthermore, many of the same neurons that responded to each of these stimuli also responded to the intestinal perfusion of an amino acid, monosodium glutamate (500mM), and a fatty acid, sodium dodecanoate (25mM) (Figure 2.9 B, E). 97% (67/69) of sodium-chloride responsive neurons exhibited responses to at least one other stimulus. Similarly, 92% (60/65) of glucose-responders, 90% (63/70) of monosodium glutamate responders, and 85.7% (60/70) of sodium-dodecanoate responders also responded to a stimulus of a different type (Figure 2.9 B, E). Furthermore, comparisons of the response amplitudes between the neurons responsive to any one of these stimuli revealed their response amplitudes to be correlated (Figure 2.9 E). These findings support the hypothesis that vagal sensory neurons do not detect specific nutrients.

Polymodal detection could arise in a number of different ways. One possibility is that vagal sensory neurons are sensitive to a coarse stimulus property, such as osmolarity. While responses to fatty acids occurred at iso-osmolar concentrations of this stimulus, responses to glucose and glutamate required hyper-osmolar solutions of these compounds. Therefore, we tested whether other osmolites can activate vagal sensory neurons. While

vagal sensory neurons respond to the small-molecule osmolite mannitol, we could not detect responses to the large-molecule osmolite polyethylene glycol (PEG) (Figure 2.9 F). In addition, we tested an additional iso-osmolar, low-pH stimulus, which elicited robust activation in vagal sensory neurons. These data suggest that hyper-osmolarity alone is neither necessary nor sufficient to activate vagal sensory neurons.

A second possibility is that because constant perfusion of liquids through the intestine is not physiological, this means of stimulus delivery could cause intestinal damage, resulting in non-specific vagal responses. Therefore, we administered the same stimulus set using serial injections of 100uL of each stimulus into the duodenal bulb at the pyloric sphincter. Despite altering the stimulus delivery paradigm to better mimic physiological gastric emptying, the same vagal sensory neurons responded to a diversity of intraluminal cues (Figure 2.10). Distension-sensitive neurons were not recruited using this stimulus delivery paradigm because responses were not observed to saline injections both preceding and following stimulus set administration. Intriguingly, while stimuli induced responses in the same neuron cohort, the kinetics of the responses varied per stimulus. Sodium chloride and low pH induced rapid and rapidly terminating calcium transients, while the response

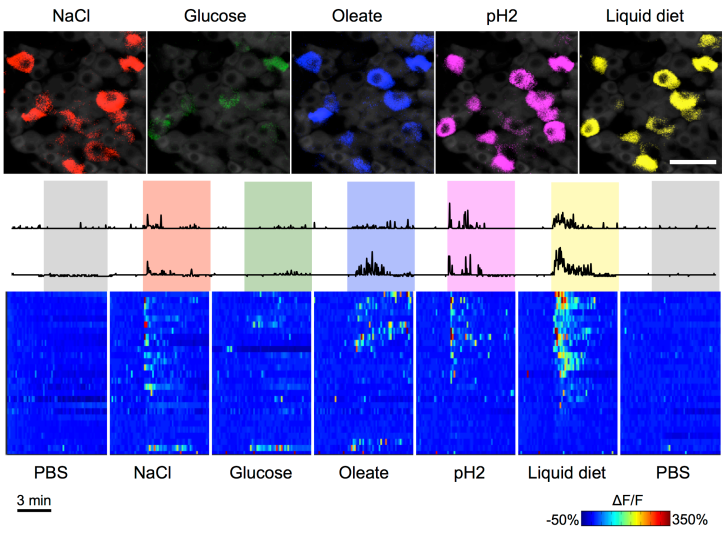

Figure 2.10 Vagal afferents are polymodal sensors of luminal contents. Representative images, traces, and time-resolved responses of 26 neurons responsive to sodium chloride (red, 7 minutes), glucose (green), sodium oleate emulsified in mouse bile (blue), low pH (magneta), liquid diet (yellow) or saline (grey). Scale bar 50 μm.

to the fatty acid oleate exhibited a delayed and more gradual onset.

Discussion

The stomach and the intestine receive innervation from two distinct vagal sensory neuron populations. Consistent with prior work, we did not uncover evidence for nutrient-specific vagal sensory neurons in the stomach.

In contrast, vagal afferents exhibited both mechanical and chemical sensitivity in the intestine. Results from *in vivo* imaging strongly support the conclusion that the vagus nerve does not contain labeled lines each dedicated for a specific class of nutrients, but rather that the majority of vagal intestine chemosensory neurons are broadly tuned polymodal sensors. Furthermore, because iso-osmotic stimuli such as fatty acid emulsions and low-pH solutions can activate vagal afferents, and hyperosmotic stimuli such as PEG cannot, these experiments suggest that osmolarity is not sufficient to explain intestinal chemosensitivity. Intriguingly, stimuli that activated vagal sensory neurons only in hyper-osmotic concentrations (e.g. NaCl, glucose, mannitol) are small molecules to which the intestinal epithelium is permeable. Therefore, one possibility is that any transit across the intestinal epithelium, in addition to cue-specific mechanisms such as for detection of low pH or fatty acid emulsions, activates release of a common signal (likely serotonin) onto vagal afferents.

2.4 Pharmacological stimuli

Introduction

Injection of pharmacological stimuli can induce a broad array of physiological changes. However, in the intact living organism, these effects are often pleiotropic, and the ability to discriminate vagal sensory neuron responses to primary, secondary or tertiary effects of pharmacological compound administration is difficult. This section describes a brief catalog of vagal sensory neuron responses to various pharmacological agents. However, because of the lack of physiological specificity of these stimuli, they will not be explored in depth.

Methods

Different pharmacological agents were dissolved in PBS for intra-peritoneal injection, or Lactated Ringers for intravenous injection. 300uL of 100uM serotonin, 100nM-100mM mCPB (an HTR3A agonist), or 10nM-100uM CCK was injected IP. 200uL of 100nM to 100uM epinephrine was injected IV via femoral vein catheter.

Results

IP injection of serotonin caused robust and prolonged activation of 50-60% of vagal sensory neurons. This stimulus was rapidly adapting – subsequent serotonin injections would fail to initiate another response. IP injection of CCK would cause dose-dependent, robust activity. CCK injection could recruit up to 50% of vagal sensory neurons. IV injection of epinephrine resulted in activation of ~20% of vagal sensory neurons. Serial injections of

several agonists revealed a high degree of overlap between the vagal sensory neurons activated (Figure 2.11).

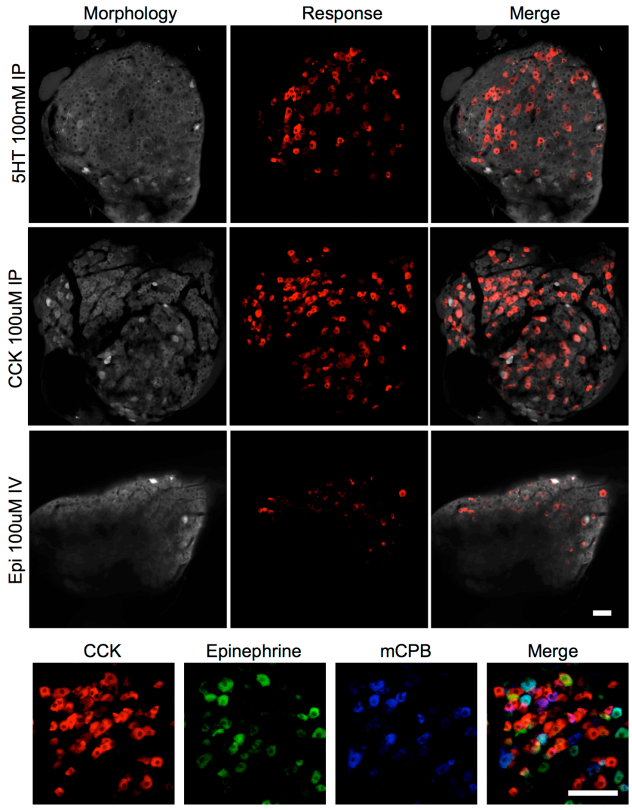

Figure 2.11 Activation of vagal sensory neurons by pharmacological stimuli. Top: Representative images of neurons activated by serotonin, CCK and epinephrine I the whole ganglion. Bottom: Representative images of neurons activated by sequential administration of three pharmacological agents shows many neurons respond to multiple different pharmacological cues. Scale bars: 100 μm.

Discussion

The agonists used here activated large cohorts of vagal sensory neurons, consistent with their known roles in a diversity of physiological processes. Serotonin, for example, impacts gastrointestinal motility, elevates the heart rate, and causes vasoconstriction, which could alter the status of many organ systems. Epinephrine, in addition to causing vasoconstriction, elevated heart rate and cardiac contractility, also acts as a bronchodilator, and impacts adrenergic receptors throughout the sympathetic nervous system. CCK increases gallbladder contractility, pancreatic secretion, hepatic bile production, and alters gastrointestinal motility. Perhaps with future studies the vagal afferent responses to each of these compounds can be deconstructed, and correlated to specific physiological changes induced by each of these compounds.

2.5 Failed stimuli

Introduction

Several stimuli reported or hypothesized to activate vagal afferents failed to elicit changes in calcium transients in the *in vivo* imaging preparation. This section will detail experimental attempts with these stimuli, and discuss implications. Because results were negative, the results section will be omitted.

We attempted blood pressure manipulations because while many cardiac changes detected by the vagus nerve would occur on time-scales too rapid for *in vivo* imaging using our equipment, tonic changes in blood pressure do alter vagus nerve activity, and are thought to play a critical role in the vagal baroreceptor reflex[37,38].

In addition, the vagus nerve is heavily implicated in the development of chemotherapy-induced nausea, and mainstay anti-emetics are thought to act via inhibition of vagus nerve activity[182,206]. We attempted cisplatin administration, to try to identify the afferents relevant for detection of this cue.

The vagus nerve is also implicated in the detection of other toxin and inflammation-related cues [207]. Therefore, we attempted to administer pathogenic bacteria (*S. typhimurium*), bacterial wall components (LPS), and intestinal inflammation-inducing toxins (DSS). Vagal sensory neurons are reported to respond to LPS and inflammatory cytokines.[208-211] Furthermore, a series of elegant studies have identified the efferent vagus nerve as the motor arm of a critical anti-inflammatory reflex. Vagal efferents synapse onto abdominal ganglia, which in turn send projections via the splenic nerve to release epinephrine in the spleen. A subset of choline-acetyl-transferase expressing T-cells in the

spleen release acetylcholine in response, signaling a reduction in cytokine release from splenic macrophages via nicotinic acetylcholine receptor 7[212-215]. Vagus nerve stimulation improves outcomes in animal models of sepsis and is currently under investigation in clinical trials for several autoimmune disorders such as rheumatoid arthritis.[216,217] However, the endogenous afferent arm of the cholinergic anti-inflammatory reflex is undetermined.

In addition, the normal microbiota is increasingly appreciated as an important regulator of gastrointestinal function. Butyrate, a bacterial metabolite present in micromolar concentrations in the intestinal lumen, is thought to increase host serotonin biosynthesis in enterochromaffin cells[218]. The vagus nerve could serve as a microbiome-to-brain link.

Methods

Gross blood pressure manipulations were performed by rapidly injecting 1-3mL of lactated ringers into the mouse vascular supply via femoral vein catheter (4 mice). Cisplatin (10mg/kg) was administered either by IP and IV injection. Imaging times after injection ranged from 30 minutes to several hours (7 mice). Administration of *S. typhimurium* was performed using well-established models; mice were pretreated with an oral gavage of streptomycin (20mg) 24 hrs. prior to experiments, and were given 10^8 cfu of *S. typhimurium* by oral gavage 2 hrs. prior to imaging (2 mice)[219,220]. Signs of *S. typhimurium* infection occur within 4-8 hours of infection, so mice were imaged over this time period. LPS (10 mg/kg) from *E. coli* or *S. typhimurium* was injected IP (6 mice), or was perfused through the intestinal lumen (1 mouse). A standard mouse model for

inflammatory colitis was also established by administration of dextran sodium sulfate (DSS, 3% w/v) via the drinking water; within three days animals exhibited weight loss, diarrhea and blood stool, and were collected for *in vivo* nodose imaging (3 mice). The bacterial metabolite butyrate was perfused through the intestinal lumen as previously described (1 mouse).

Discussion

General technical reasons may contribute to the absence of responses in any of these preparations. Perhaps the physiological quality of the mouse in the *in vivo* imaging preparation was insufficient to elicit or observe responses. For example, mice under anesthesia lose the ability to thermo-regulate, and therefore become profoundly hypothermic without external heating. Robust immune system activation, and therefore subsequent inflammation or intestinal damage may depend upon normothermia. While mice were artificially heated during imaging preparation, heating during imaging causes regular z-shifts of the ganglion, precluding collection of analysis-quality data. Therefore, mice were alternatively heated and imaged, a solution that allows for data collection but would expose the mouse to periods of hypothermia that might impact mouse physiology. Alternatively, while bleeding was typically minimal in the imaging preparation, bleeding and hypotension could worsen mouse quality and reduce the likelihood of observation of normal responses.

Several considerations to specific stimuli also may contribute to the lack of a measureable response.

Cisplatin causes increases in activity in the common hepatic branch of the vagus nerve within ~11 minutes after IV injection. This activity is dependent upon intact vagal connections to the proximal small intestine, and can be reduced by administration of an Htr3a antagonist[221]. Notably, electrophysiological recordings of cisplatin-responsive neurons were performed in the gastroduodenal branch, and not all recorded units within this branch are sensitive to cisplatin administration. A sparse afferent population that only exhibits increases in activity 10 minutes or more after stimulus delivery may be difficult to identify and clearly attribute to cisplatin administration in the whole-ganglion context, particularly because 20-30% of vagal afferents already exhibit variable stimulus-independent activity.

Blood pressure responses are particularly sensitive to nodose ganglion exposure surgery. Increases in blood pressure are communicated from the periphery to the brainstem via the aortic depressor branch of the vagus nerve and the carotid sinus nerve, fine nerve branches located within the neck. The difficulty in identifying and protecting these branches from surgically induced trauma raises the possibility that they were inadvertently damaged during imaging preparations.

DSS colitis experiments depend upon the ability to detect differences in basal activity between DSS treated and untreated animals. The variability preparation-to-preparation with *in vivo* imaging, and the fact that vagal innervation of the distal intestine (the site of greatest DSS damage) is sparse, likely reduces the ability to detect any statistically significant differences between groups.

In summary, while it is possible that the vagus nerve does not mediate responses to many of these stimuli, a negative result is difficult to interpret and may just as well be caused by any one of many potential technical failures.

2.6 Salt and pepper organization of vagal ganglia

Introduction

In vivo imaging provides a robust analytical tool for monitoring single neuron responses of the vagus nerve to stomach stretch, intestinal nutrients, intestinal distension, inhaled carbon dioxide, and lung inflation. Each of these stimuli activated a sparse population of sensory neurons, between 4% and 26% depending on the stimulus. This section describes the spatial organization of respiratory and gastrointestinal inputs in vagal ganglia.

Methods

Stimulus administrations were as described previously. The spatial organization of neurons within vagal ganglia was examined by computing the distances between all stomach stretch-sensitive neurons, all lung-inflation sensitive neurons, all intestinal glucose sensitive neurons, and all the pairwise comparisons between these three groups. To combine information from four animals, the ganglion location in the imaging field was standardized by taking the minimum x and y coordinates of any responsive cell, and calculating the positions of every other responsive neuron in relation to these coordinates. All analyses were also performed on an individual animal basis, and yielded the same

results as the 4-animal pooled dataset. To formally test whether the spatial organization was random, we randomly re-assigned neuron functional identity and computed the same distance comparisons.

Results

We sequentially imaged single neuron responses in vagal ganglia following tandem administration of sensory stimuli in the stomach, intestine, and lung in the same mouse. We observed that gastric distension, intestinal nutrients, and lung inflation activated non-overlapping cohorts of sensory neurons. Responses of 617 neurons were imaged in 4 mice, with 154 neurons responding to stomach stretch, 77 neurons responding to intestinal glucose, and 17 neurons responsive to lung inflation. The vast majority of stomach stretch-responsive neurons (150/154) were insensitive to intestinal glucose, and vice versa (73/77). Furthermore, none of the lung mechanoreceptors responded to either gastrointestinal stimulus (Figure 2.12 A, B). Thus, individual vagal sensory neurons have highly specific response properties.

Next, we asked if neurons responsive to particular cues were spatially arranged within vagal ganglia. *In vivo* imaging provides positional information about responsive neurons, and we calculated the average distance between neurons with different response characteristics. We observed that stomach mechanoreceptors, lung mechanoreceptors, and sensors of intestinal osmolarity were not spatially clustered within the imaging field. The mean distance between neurons was independent of their response properties. Furthermore, to test if neurons with different response characteristics are randomly organized within the ganglion, we randomly shuffled neuron functional identity, and repeated the same distance comparison on this shuffled data set. Random assignment of

neuron functional identity yielded mean neuron-neuron distances that were the same as those acquired in the un-shuffled data set. (Figure 2.12 C, D) These findings indicate that neurons responsive to respiratory and gastrointestinal inputs are organized in a salt-and pepper distribution within vagal ganglia.

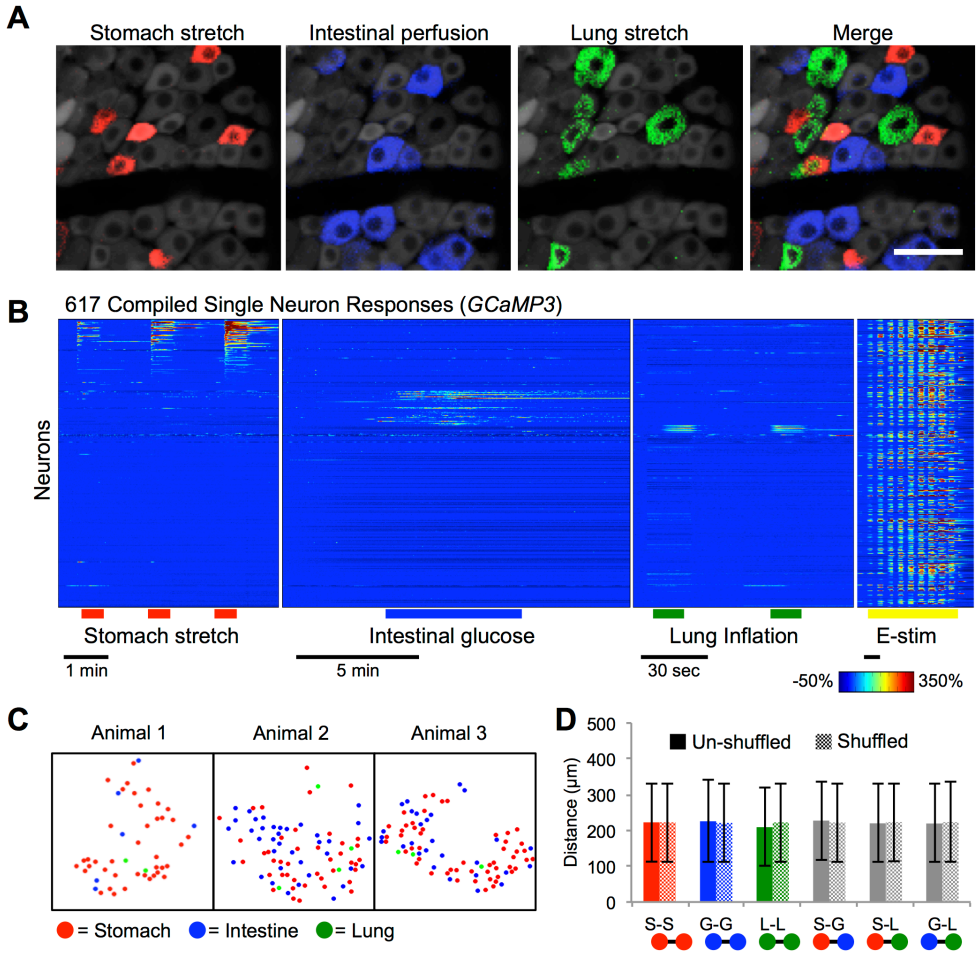

Figure 2.12 A 'salt and pepper' organization of vagal inputs
(A) Representative images of GCaMP3 fluorescence signal in a vagal ganglion following tandem application of stomach stretch (red), intestinal glucose (blue), and lung inflation (green). Scale bar: 50 μm (B) Time-resolved responses (ΔF/F, color scale) of 617 neurons to stimuli indicated. (C) Position in the imaging field of neurons responsive to stomach stretch (red), intestinal glucose (blue) and lung inflation (green). (D) Average distance between two neurons responsive to stimuli indicated (S- stomach stretch; G- intestinal glucose; L- lung inflation). Calculations were repeated with the same data set in which neuron response properties were randomly assigned ('shuffled') and no differences were observed. (n= 245 neurons from 4 mice, ± sd).

Discussion

Salt-and-pepper organization of cell bodies in vagal ganglia is consistent with several observations. First, in vagal ganglia, retrograde labeling of neuronal cell bodies from various peripheral tissues failed to reveal any spatial organization to vagal sensory neurons based on peripheral target innervation. Second, other peripheral sensory ganglia, such as the geniculate ganglion housing the sensory neurons responsible for transmission of gustatory information, exhibit a salt-and-pepper organization as well[222].

We do, however, note that more neurons responded to gastrointestinal inputs than respiratory inputs in imaging-accessible vagal sensory neurons. Perhaps gastrointestinal inputs are simply represented by a larger cohort of vagal sensory neurons; alternatively, it is possible that organ system patterning occurs on an axis perpendicular to the imaging field. Distal regions of the jugular ganglion were not accessible for *in vivo* imaging, and pulmonary inputs may be enriched in these regions.

2.7 Voltage sensor imaging

Introduction

Genetically encoded calcium indicators such as GCaMP3 have two key technical shortcomings. First, GCaMP3 kinetics are slower than the voltage changes that underlie neural activity. Second, though uncommon, some neuron subsets have strongly buffered calcium dynamics, and can exhibit activity to which sensors like GCaMP3 would be blind. Calcium imaging provides a low-pass-filtered, integrated surrogate to measure neuronal

firing. While improvements in calcium indicators, such as the development of newer generations of GCaMP (e.g. GCaMP6), have ameliorated many of these shortcomings, the need to optically record changes in membrane voltage directly remains. Adam Cohen's group here at Harvard has developed an optical electrophysiology tool set comprising channelrhodopsin (ChR2) and an Archaerhodopsin-based genetically-encoded voltage sensor (Quasar2) named "Optopatch". We collaborated with the post doc, Shan Lou, leading development of this tool and their new Cre-dependent optopatch mouse line.

Methods

The Cohen lab performed all voltage sensor and mouse development, and customized microscope construction to enable voltage sensor imaging. Briefly, the optopatch mouse consists of insertion of the Quasar2 allele and a GFP-tagged Cheriff allele into the Rosa26 locus (*Rosa26-pCAG-LSL- QuasAr2-mOrange2(Y71A)-P2A-CheRiff-eGFP-WPRE-bGHpA*). This line was crossed with *Nav1.8-Cre* (provided by Rohini Kuner via Qiufu Ma) to allow for optopatch expression in ~80% of all vagal sensory neurons. This construct allows for Cheriff-mediated excitation upon exposure to blue light, while simultaneously recording the membrane voltage using red light illumination of QuasAr2. The surgical preparation for imaging in the nodose was performed as described (Section 2.1).

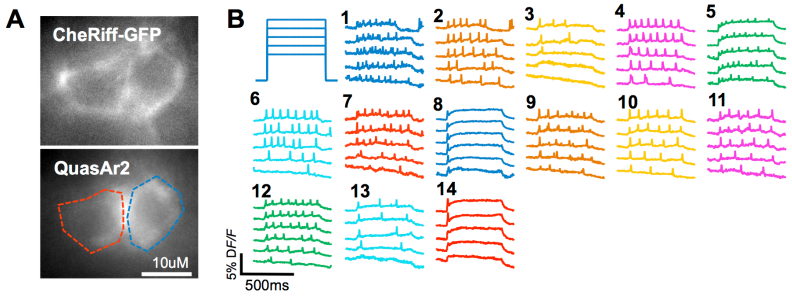

Figure 2.13 Voltage sensor imaging in nodose ganglia. (A) Reresentative field of view containing two CheRiff-GFP, QuasAr2 expressing neurons, outlined in red and blue (low). (B) Representative QuasAr2 fluorescence intensity traces from 14 individual neurons to increasing intensities of blue light.

Results

Green Cheriff-eGFP and red QuasAr2 fluorescence could be visualized in 2-3 neurons per imaging field (Figure 2.13 A). We imaged sequentially from 14 different neurons and observed a variety of optically induced spiking patterns. Some neurons exhibited tonic firing, while others fired only a single action potential at the initiation of depolarization (Figure 2.13 B). The heterogeneity of neuron responses observed is consistent with the known heterogeneity of vagal sensory neuron types. Optopatch, therefore, can discriminate electrophysiologically diverse subsets in this unique sensory neuron population *in vivo*.

Discussion

Voltage sensor imaging overcomes several of the caveats inherent to calcium imaging. First, voltage sensor imaging captures events on a millisecond time-scale, allowing for resolution not only of single action potentials, but also of action potential waveforms. Therefore, voltage sensors offer greater information content concerning action potential properties that could play an important role in sensory information coding. Furthermore, because voltage sensor imaging directly measures neuron membrane potential, it can detect activity in all neuron types. Calcium imaging can only detect activity in neurons that undergo changes in intracellular calcium concentrations. Finally, using the optopatch system, voltage sensor imaging has been successfully paired with optogenetic activation, allowing for electrophysiological characterization of neurons solely with the use of light. These benefits may be particularly useful for gaining insights into mechanisms underlying activity in specific sensory systems. For example, one might ask if desensitization to a

peripheral stimulus is related to intrinsic membrane properties, or whether desensitization is more likely due to features of the sensory terminal and the tissue it innervates.

Voltage sensor imaging is improving rapidly, but is still plagued by several shortcomings. Frame rates required to capture action potentials are extremely rapid, and the fluorescence intensity of voltage sensor signals is dim, limiting the size of the field-of-view from which light can be collected. Therefore, analysis is currently restricted to at most 2-3 neurons per field. Optimization of voltage sensors like QuasAr2, both of their inherent optical properties and also of their expression and trafficking in biological systems, should improve their signal-to-noise and applicability.

2.8 Conclusions

In conclusion, we developed an *in vivo* imaging preparation in vagal ganglia that permits real-time measurement of calcium transients in ~150 individual vagal sensory neurons per imaging field. Using this approach, we found small cohorts of sensory neurons that detect stomach stretch, intestinal distension and luminal contents, lung inflation, and inhaled carbon dioxide. These five inputs account for ~70% of viable imaging-accessible sensory neurons, with other sensory neuron populations likely devoted to cardiovascular inputs, such as aortic baroreceptors and cardiac mechanoreceptors. *In vivo* imaging also provides information about the frequency, identity, and spatial organization of responding neurons. We find that the vagus nerve is populated by discrete sensory neurons with highly specific response properties (labeled lines), and that these neurons are intermingled within vagal ganglia. Findings reported here will help provide a comprehensive description of

vagal sensory systems that relay vital information to the brain about the state of internal organs.

Chapter 3: Molecularly defining gut sensory neurons

3.1 Defining vagal sensory neuron subsets

Introduction

We previously used a genome-based strategy to identify G Protein-Coupled Receptors (GPCRs) expressed in vagal sensory neurons. In this section, we characterize two vagal sensory neuron populations, one marked by the gut hormone receptor *Glp1r* and another by the putative acid sensor *Gpr65*. *Glp1r* is an intriguing nodose neuron marker because of the putative role of these neurons in detection of intestinal chemical cues[160-163]. *Gpr65* is also an intriguing nodose neuron marker, largely because of the data presented within this section. We examine receptor co-expression data for these populations using both *in situ* hybridization and *in vitro* calcium imaging. In addition, we detail the generation of mouse tools to further investigate these neuron subsets.

Methods

In situ hybridization

In situ hybridization studies were performed on 10-20 μm cryosections of vagal ganglia as described. Digoxigenin or Fluorescein-labeled cRNA riboprobes were prepared for several targets.

Table 3.1 *In situ* probe information

Target	Probe length (bp)	Primers
Gpr65	1014	Full coding sequence
Glp1r	1392	ATGGCCAGCACCCCAAGC TCAGCTGTAGGAACTCTGG
Htr3a	845	CAACGGCCATCGGTACCCCC ATGAGCAGTTCCAGGGGCCG
Cckar	994	AGGAGGAAGATGGAAGGACC GCTACTTATTAAGTGAGTCCC

Rolling-ball background subtraction (ImageJ) was performed on in situ images in Figure 3.1 A to normalize background intensities.

In vitro calcium imaging

Fura-2 based calcium imaging in acutely dissociated vagal sensory neurons was performed using *Glp1r-ires-Cre; lox-L10-GFP* and $Gpr65^{GFP/+}$ mice. Left and right nodose/jugular ganglia were harvested and digested with enzyme mix (collagenase I (1 mg/ml, Roche), Dispase II (3 mg/ml, Roche)) at 37°C for 40-45 min, washed with L-15 medium (Invitrogen), and gently triturated with three glass aspiration pipettes of decreasing diameters. Isolated single cells were filtered with a 40 μm cell strainer (BD Falcon), re-suspended in culture medium (10% FBS in L-15 medium), placed onto laminin-coated cover glass and incubated ~2 hr at 37°C until most cells were attached to the glass surface. Cells were loaded with Fura-2 AM (Invitrogen) for 30 min and imaged with excitation wavelength at 340 and 380 nm. Test chemicals were dissolved in Hank's balanced salt solution and included CCKAR agonist A71623 (100 nM, Tocris), CCK-8 (10 nM, Sigma), Exendin-4 (100 nM, Tocris), serotonin (10 μM, Sigma), *m*-chlorophenylbiguanide (100 μM, Sigma), and capsaicin (1-2 μM, Sigma). Only cells that

responded to KCl (50 mM) were counted. GCaMP3 imaging involved *Vglut2-ires-Cre; lox-GCamp3* mice, and were imaged with excitation-emission filters for GFP.

Mouse generation

Gpr65-ires-Cre and *Glp1R-ires-Cre* mouse constructs were prepared using standard BAC recombineering approaches. I synthesized *Gpr65-ires-Cre* and Rui Chang made *Glp1R-ires-Cre*. A vector was designed to contain the *ires-Cre* cassette, an excisable neomycin resistance gene, and homology arms for cassette insertion 3 base pairs downstream of the receptor stop codon. Vectors were electroporated into W4/129S6 ES cells and selected for neomycin resistance. Appropriately targeted cells were identified by Southern Blot and PCR analysis, and injected into C57/BL6 blastocysts to generate chimeric animals. The neomycin resistance gene was subsequently removed by crossing with *Act-Flpe* (Jackson, 003800).

Glp1r and *Gpr65* Southern blots to confirm appropriate vector targeting involved standard protocols. 5′ and 3′ probes (500 bp, amplified by PCR from mouse genomic DNA using primers described below) were radioactively labeled with dCTP [α-^{33}P] (PerkinElmer) using a DNA labeling system (GE Healthcare) and purified with NickTM columns (GE Healthcare).

Table 3.2 PCR primers for Southern Blot probe synthesis

Probe Name	Primer Sequences
Gpr65	CAGTTTGCATGTGAACCTGC CTCACTTTCTGCTTTATCCC
Glp1r	GGGTGTGGAGAGGACCTGGTCACTGTG AATACATGGCCACTCACAGAGCCACCC

10 µg ES cell genomic DNA was digested (overnight, 37°C) with restriction enzymes (BamHI for *Gpr65-ires-cre*, expected sizes: WT 6.8 kb, 3′ TG 5.7 kb).

Mice were genotyped using standard PCR; both lines could be bred to homozygosity, confirming appropriate targeting of the inserted allele.

Table 3.3 Genotyping primers for *Gpr65-ires-Cre* and *Glp1r-ires-Cre* mice

Mouse line	Primer Sequences
Gpr65-ires-Cre	F (WT): GGAGAGCTGATATGTGGAAC R (WT): CCAGTACATGGAGTGGCTTC F (KI): CCTGTTTCGGACGTGCATGG R (KI): GGAGGGAGAGGGGCGGAATT
Glp1r-ires-Cre	F: GTTTCTTCCTCTCTTCCTGCC R (WT): TCATCAAGCCCATCTCTCTCC R (KI): ACCGCTTCCTCGTGCTTTAC

P2ry1-ires-Cre, *Vglut2-ires-Cre*, *lox-L10-GFP,* and *Advillin-Cre* mice were described previously. *lox-GCaMP3* (014538), *lox-tdTomato* (007908), and *Gpr65*$^{GFP/+}$ (008577) lines were purchased (Jackson).

Optogenetic measurements of conduction velocity

All optogenetic experiments were performed by Rui Chang. Neuron activity was evoked in anesthetized mice by focal illumination of the vagus nerve trunk, and robust light-induced action potentials were observed in the *Glp1r-ChR2*, *Gpr65-ChR2*, and *Vglut2-ChR2* mice. Neuron conduction velocities were measured by whole nerve electrophysiology at fixed intervals from the illumination site, as published.

Results

Two GPCRs - GLP1R and GPR65 - mark small neuronal subsets in vagal ganglia, as revealed by colorimetric and fluorescence *in situ* hybridization (FISH). GPR65 and GLP1R

expression was observed in nodose ganglia, with little or no expression in adjacent jugular ganglia, trigeminal ganglia, or any dorsal root ganglia along the entire rostral-caudal axis (Figure 3.1 A, 3.2, 3.3). By two-color FISH analysis each receptor to be expressed in largely non-overlapping sensory neurons (Figure 3.1 B). Nearly all GPR65 neurons lacked GLP1R (99.5%, 220/221) and nearly all GLP1R neurons lacked GPR65 (99.5%, 198/199); similarly orthogonal results were obtained in pairwise analyses involving P2RY1, the marker for a neuron subset that innervates the lung and is critical for the control of breathing.

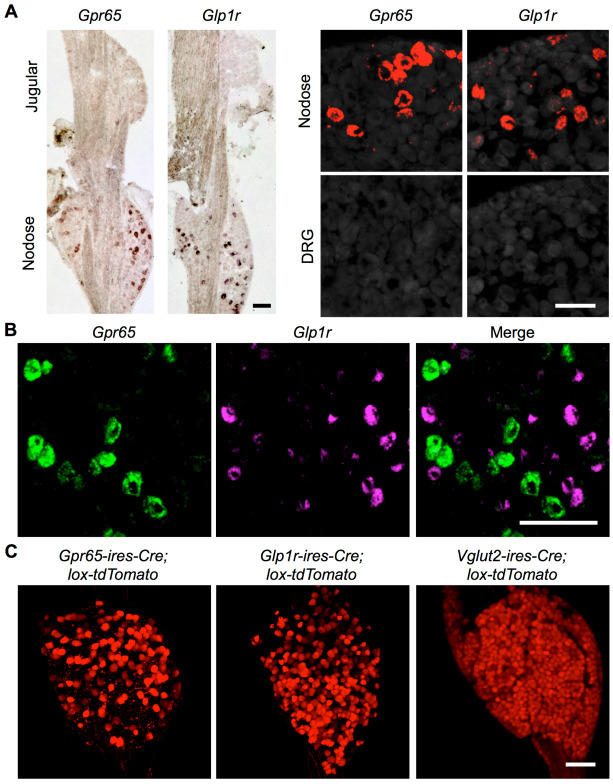

Figure 3.1 Genetic control of vagal sensory neuron subtypes. (A) RNA *in situ* hybridization reveals expression of *Gpr65* and *Glp1r* in sparse sensory neurons of nodose but not jugular or dorsal root ganglia, scale bar left: 100 μm, right: 50 μm. (B) Two-color FISH in nodose ganglia reveals expression of *Gpr65* and *Glp1r* in different sensory neurons, scale bar 100 μm. (C) Wholemount tdTomato fluorescence in vagal ganglia from knock-in mice, scale bar 100 μm.

For genetic access to each neuron type, we made knock-in mice in which Cre recombinase is expressed from endogenous *Gpcr* loci using an internal ribosome entry site (IRES) sequence. In crosses with reporter mice containing a Cre-dependent *tdTomato* allele (*lox-tdTomato*), sensory neuron fluorescence was visualized by whole mount analysis of vagal ganglia (Figure 3.1 C).

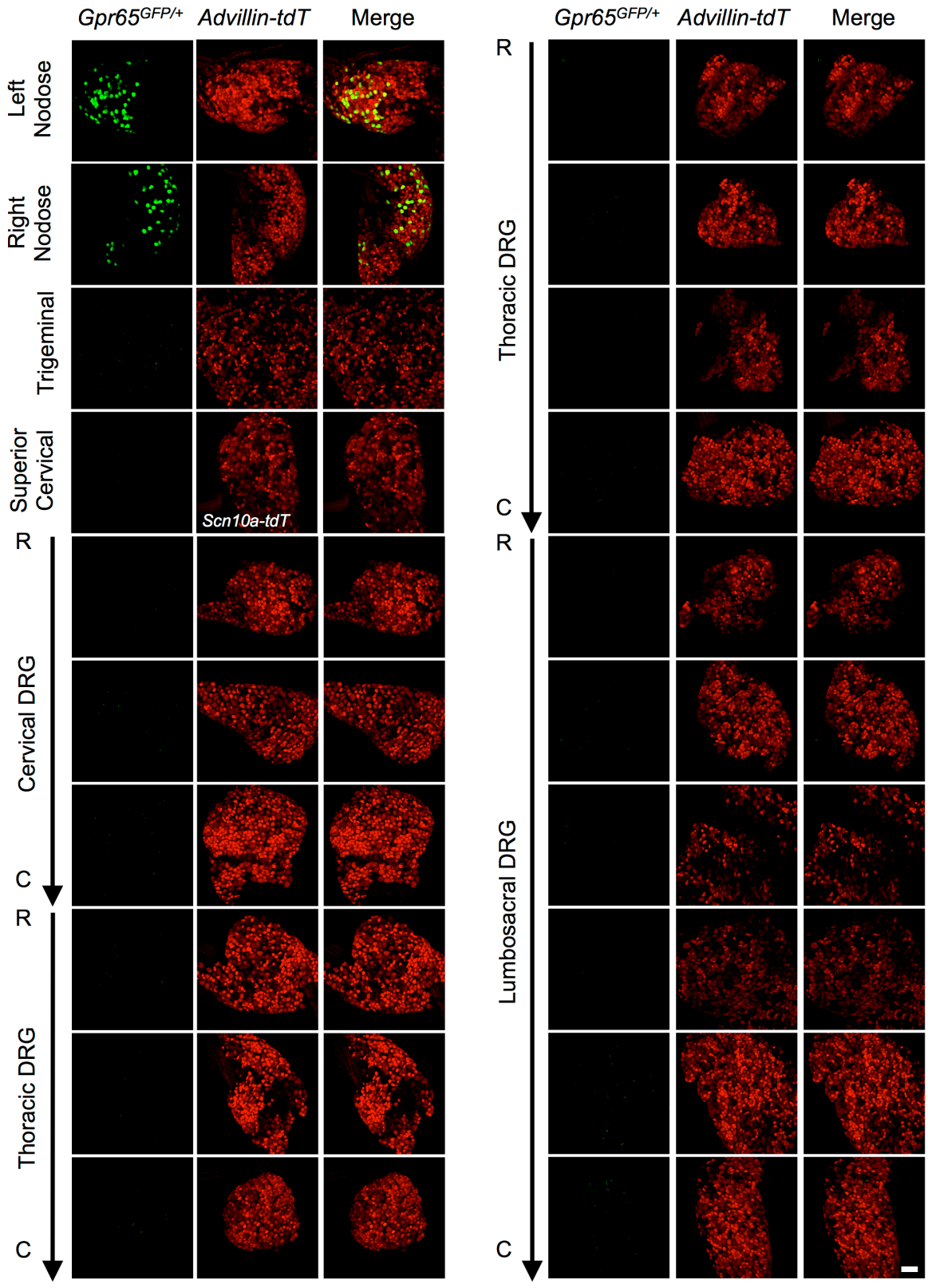

Figure 3.2 *Gpr65* is not expressed in other peripheral ganglia. Scale bar: 100 μm.

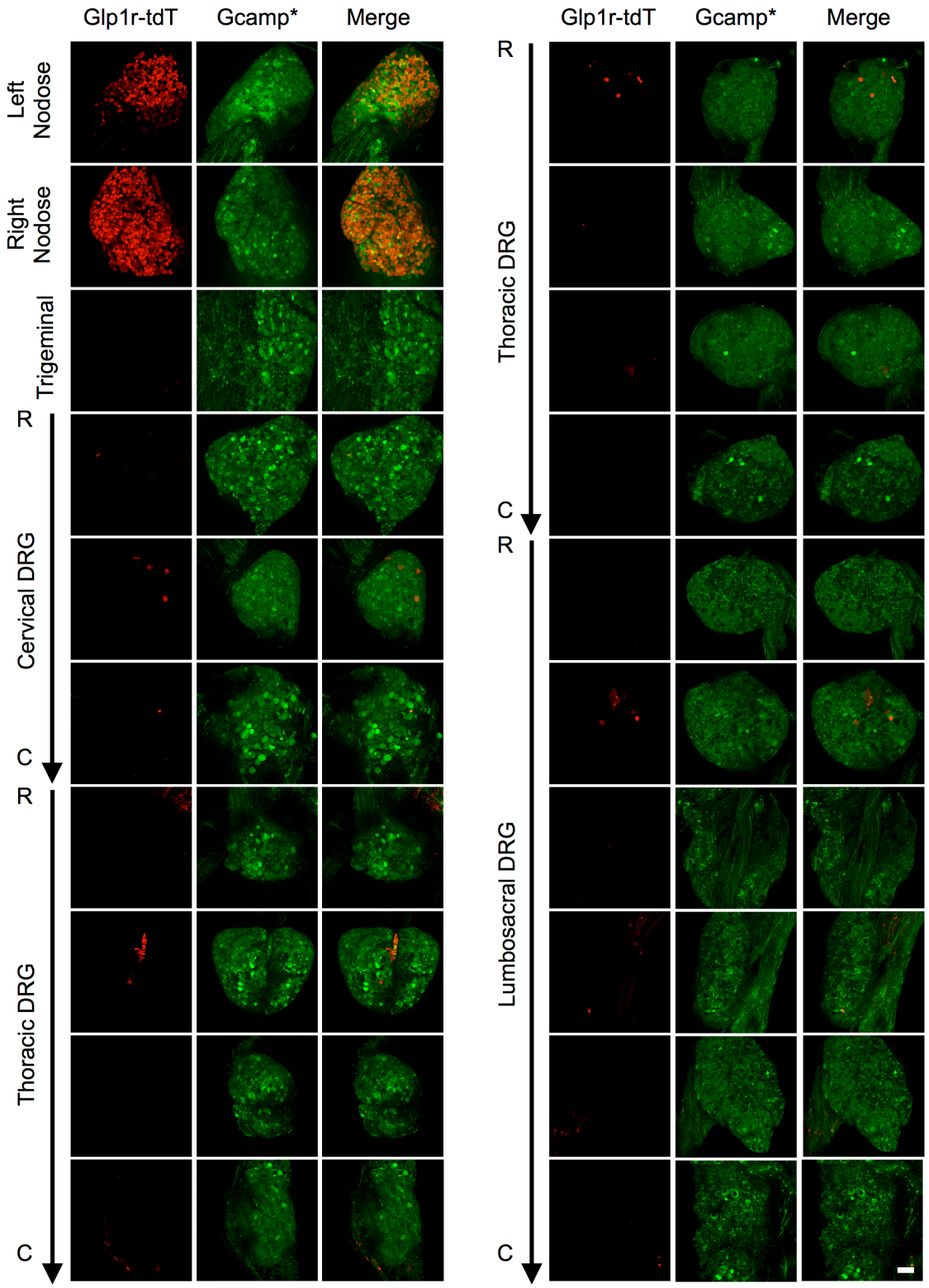

Figure 3.3 *Glp1r* is not expressed in other peripheral ganglia. Scale bar: 100 μm.

Furthermore, comparison to *Vglut2-ires-Cre, lox-tdTomato* nodose ganglia in which all vagal sensory neurons are labeled highlights that tdTomato fluorescence was restricted to neuron subsets in *Glp1r-ires-Cre* and *Gpr65-ires-Cre* mice. Expression of Cre-dependent reporters in *Glp1r-ires-Cre* and *Gpr65-ires-Cre* mice was observed in many cell types known to contain these receptors, and two-color analysis validated that appropriate cells were targeted in the nodose ganglion (Figure 3.4).

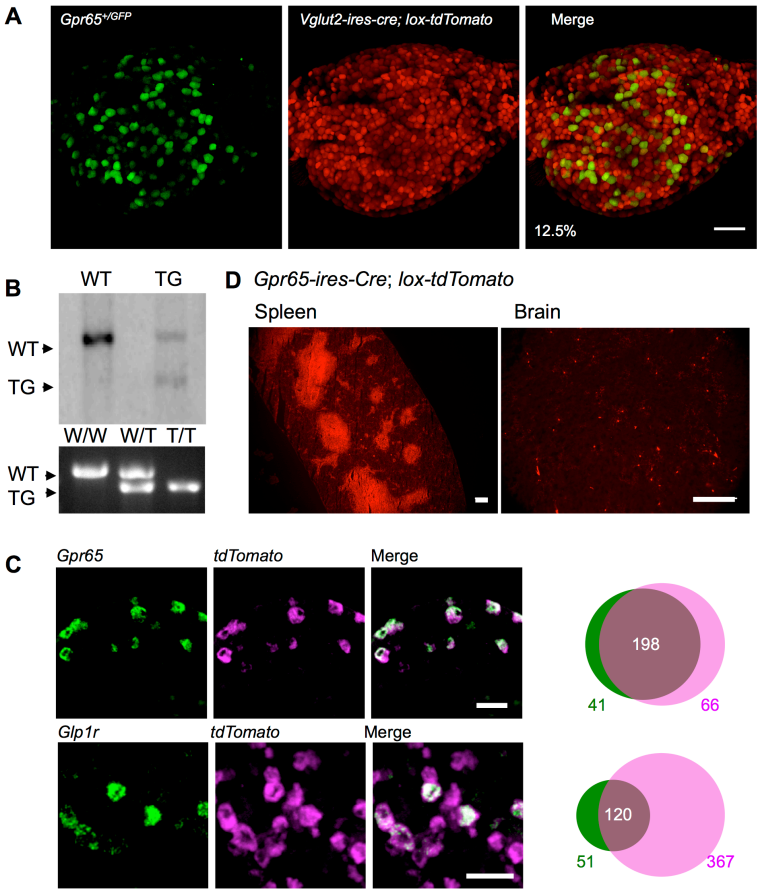

Figure 3.4 Validation of *Gpr65-ires-cre* and *Glp1r-ires-cre* knockin mice. (A) Gpr65 is expressed in a small nodose subset by whole-ganglion imaging. Scale bar 100 μm. (B) Southern Blot (top)and genotyping (bottom) confirmed appropriate targeting of the Cre insertion in the *Gpr65-ires-cre* mouse. (C) Two-color *FISH* for *Gpr65* or *Glp1r* (green) and *tdTomato* in the respective *Gpr65-ires-cre; lox-tdTomato* nad *Glp1r-ires-cre; lox-tdtomato* mouse lines, confirming high degree of overlap between gene and reporter expression in both lines. Scale bar: 50 μm. Cell counts from two-color *FISH* are depicted in Venn diagrams (right, n = 3-4 sections from 2 or more mice). (D) Expression of *tdTomato* in *Gpr65-res-cre; lox-td-Tomato* animals in expected immune cells in the spleen. Gpr65 is expressed by glia, but not neurons in the brain.

We noted an increase in fluorescent cells visualized in nodose ganglia of *Glp1r-ires-Cre*; *lox-tdTomato* mice (Figure 3.5), likely due to inefficient detection of low-level *Glp1r* transcript by FISH, or due to transient expression of *Glp1r* during development. Therefore, while *in situ* labeling of *Glp1r* revealed no overlap with *Gpr65*, *in situ* labeling of *tdTomato*

in *Glp1r-ires-Cre*; *lox-tdTomato* mice revealed partial overlap with *Gpr65*. Similarly, partial overlap was observed between *tdTomato* positive neurons and *eGFP* positive neurons in nodose ganglia from *Glp1r-ires-Cre*; *lox-tdTomato; Gpr65*$^{GFP/+}$ mice (Figure 3.5).

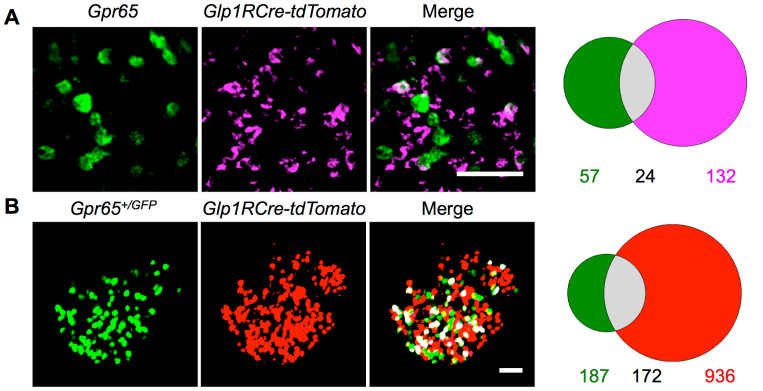

Figure 3.5 *Glp1r-ires-cre lox-tdTomato* expression partially overlaps GPR65 neurons. (A) Two color *FISH* for *Gpr65* (green) and *tdTomato* in the nodose ganglion of a *glp1r-ires-cre; lox-tdTomato* mouse. (B) Whole-mount image of a ganglion from a *Gpr65*$^{+/GFP}$*; Glp1r-ires-cre; lox-tdTomato* mouse. Cell counts from two-color *FISH* are depicted in Venn diagrams (right, n = 3-4 sections from 2 mice). Scale bars 100 μm.

Vagal GLP1R and GPR65 neurons can be distinguished by their responses to gut hormones and expression of gut hormone receptors. Serotonin and CCK are two key signaling molecules released in the gut. The majority of vagal sensory neurons that express transcripts for the serotonin receptor *Htr3a* are distinct from neurons that express the CCK receptor *Cckar* (70/79 neurons, 89%, 2 sections), and the majority of *Cckar*-expressing sensory neurons do not express *Htr3a* (16/25, 64%, 2 sections) (Figure 3.6 C). Furthermore, by *in vitro* calcium imaging most CCK-responsive neurons are distinct from serotonin responsive neurons (57/87 CCK-neurons, 66%, 8 dishes), and most serotonin-responsive neurons are distinct from CCK-responsive neurons (116/146 neurons, 79%, 8 dishes) (Figure 3.6 A, B). Nearly all serotonin responsive neurons also responded to the HTR3A-sepcific agonist mCPB (106/129 neurons, 89%, 8 dishes), and nearly all mCPB responsive neurons were serotonin responsive (106/133, 86%, 8 dishes), suggesting that serotonin responses *in vitro* are mediated by HTR3A.

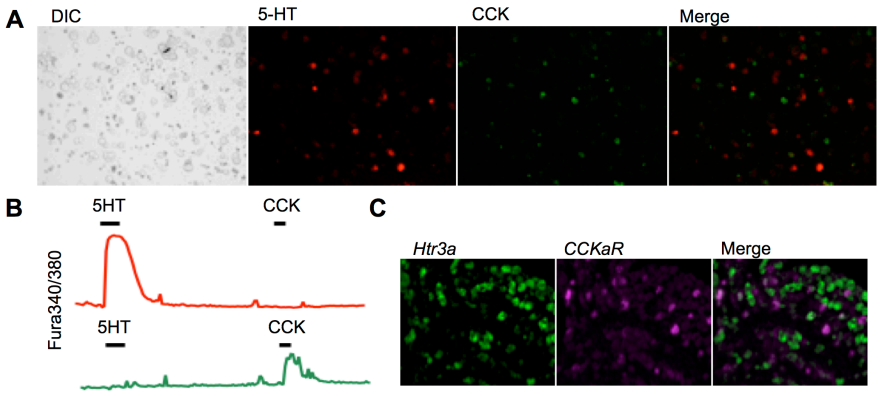

Figure 3.6 Htr3a and Cckar are expressed in distinct nodos sensory neurons. (A) Neurons responsive by *in vitro* calcium imaging to serotonin (red) and CCK (green). (B) Representative trace of Fura 340/380 ratio in a serotonin (red) and CCK (green) responsive neuron. Stimulus administration times 10 sec. (C) Two-color *FISH* for *Htr3a* and *Cckar* in the nodose ganglion.

In vitro calcium imaging and in situ hybridization was performed to determine to which category of vagal sensory neurons GLP1R and GPR65 neurons belong. Responses of single, genetically defined sensory neurons were imaged using the calcium indicator Fura-2 in acutely dissociated vagal sensory neurons from *Glp1r-ires-Cre*; *lox-L10-GFP* mice and heterozygous knock-in/knock-out mice containing a *GFP* allele inserted into the endogenous *Gpr65* locus (*Gpr65*$^{GFP/+}$). The gut hormone cholecystokinin (or an agonist for the cholecystokinin receptor CCKAR) activated the majority of vagal GLP1R neurons (62%, 53/85), but not vagal GPR65 neurons (2%, 1/41) (Figure 3.7). Consistently, two-color FISH studies revealed frequent co-expression of the cholecystokinin receptor CCKAR with GLP1R but not GPR65 (Figure 3.7). The TRPV1 agonist capsaicin also activated most GLP1R neurons (68%, 58/85) but only rare GPR65 neurons (9%, 3/34), consistent with expression patterns observed in the ganglia (Figure 3.7 A, B). In contrast, serotonin (or a specific agonist for the serotonin receptor HTR3A) activated most GPR65 neurons (58%, 15/26), but not most GLP1R neurons (19%, 16/85) (Figure 3.7); by two-color FISH, GPR65 neurons predominantly represent a subset of HTR3A-containing neurons (Figure 3.7 C).

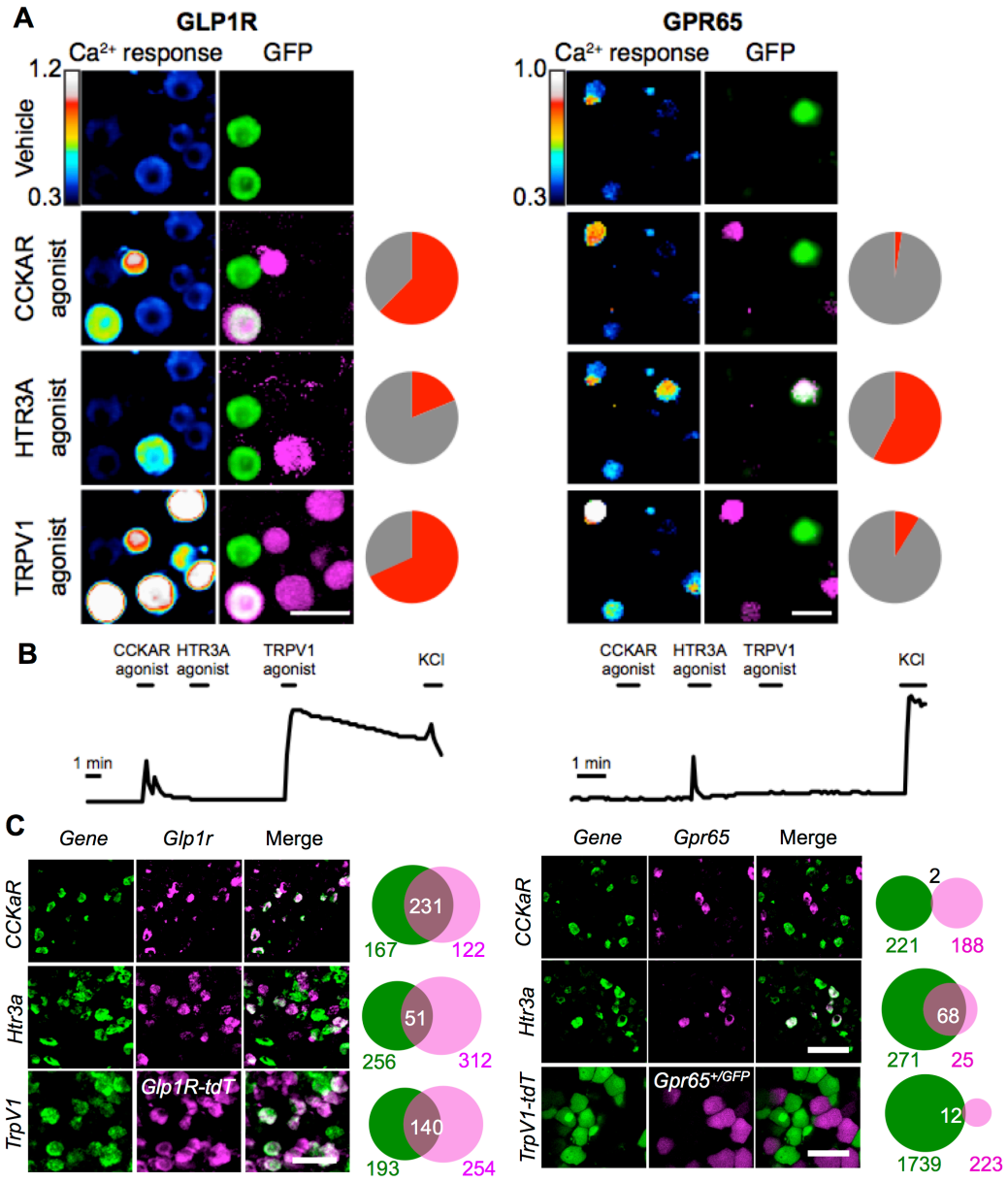

Figure 3.7 Characterizing vagal sensory neuron types. (A) Calcium responses of dissociated vagal sensory neurons from *Glp1r-ires-Cre; lox-L10-GFP* and *Gpr65*$^{GFP/+}$ mice. Left: Fura-2 excitation; middle: GFP fluorescence (green) and calcium responses (magenta); right: GFP+ neurons activated (red) or not activated (grey). CCKAR agonists: A71623 (left, 100 nM), CCK-8 (right, 10 nM); HTR3A agonists: serotonin (left, 10 μM), *m*-chlorophenylbiguanide (right, 100 μM); TRPV1 agonist: capsaicin (1-2 μM). scale bar: 40 μm. (B) Representative single neuron responses. (C) Two-color *FISH* or mouse crosses confirming gene expression patterns suggested by *in vitro* imaging experiments. Scale bar 50 μm.

We did not observe acute responses to GLP1R agonists in any vagal sensory neurons by calcium imaging, whole nerve electrophysiology, or *in vivo* calcium imaging (Figure 3.8),

suggesting a modulatory or developmental role for this receptor in vagal afferents, rather than direct signaling from GLP1R leading to action potential generation.

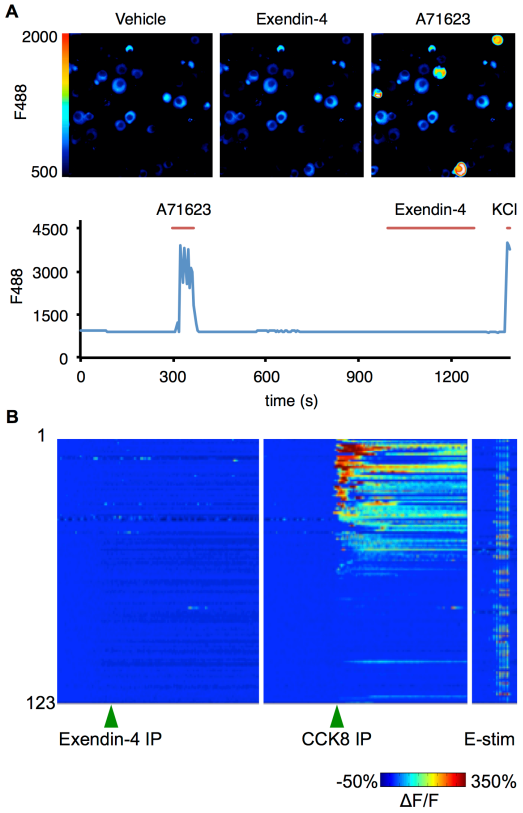

Figure 3.8 The GLP1R agonist exendin-4 does not acutely activate vagal sensory neurons. (A) Calcium responses to agonists for GLP1R (exendin-4, 100 nM) and CCKAR (A71623, 100 nM) were imaged using GCaMP3 in dissociated vagal sensory neurons from *Vglut2-ires-Cre*; *lox-GCaMP3* mice. Top: GCaMP3 fluorescence (color scale) visualized by microscopy, bottom: responses of a single neuron. (B) *In vivo* calcium transients were imaged in vagal ganglia using GCaMP3. Responses in 123 electrical stimulation-activated neurons (E-stim) were measured in response to intraperitoneal (IP) injection of exendin-4 (10 μM) and CCK8 (100 μM)

Finally, to determine the conduction velocities of GLP1R and GPR65 neurons, Rui Chang crossed *Glp1r-ires-Cre*, *Gpr65-ires-Cre*, and *Vglut2-ires-Cre* mice with a Cre-dependent channelrhodopsin allele (*lox-ChR2;* offspring of crosses to *Marker-Cre* mice are subsequently referred to as *Marker-ChR2*). Activating all sensory neurons in *Vglut2-ChR2* mice generated a compound action potential resulting from both A and C fiber currents, as published. Similar experiments in *Gpr65-ChR2* and

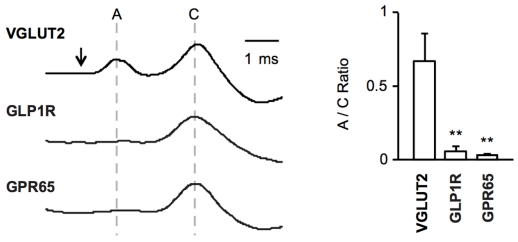

Figure 3.9 Conduction velocities of GLP1R and GPR65 neurons. Compound action potentials after brief optogenetic stimulation (arrow) in *Vglut2-ChR2*, *Glp1r-ChR2*, and *Gpr65-ChR2* mice show A and C fibers (mean ± sem, n=4-5, **p<.01).

Glp1r-ChR2 mice revealed that most GLP1R and GPR65 neurons (>95%, >97%) are slow-conducting C fibers (Figure 3.9).

Discussion

GLP1R and GPR65 mark discrete subsets of vagal sensory neurons with intriguing receptor co-expression profiles (summarized in Figure 3.10). The non-overlapping receptor expression and hormone responses of vagal GPR65 and GLP1R neurons *in vitro* suggest the potential for complementary roles in internal sensation, with GLP1R neurons sensitive to gut peptide hormones and GPR65 neurons sensitive to serotonin. Generation and validation of *Glp1r-ires-Cre* and *Gpr65-ires-Cre* mice provides powerful genetic tools to query the response properties, anatomical projections and physiological roles of these neuron types.

Table 3.4 Summary of GPR65 and GLP1R neuron characteristics

	GPR65	**GLP1R**
Receptor co-expression	Htr3a positive Cckar negative Trpv1 negative	Htr3a partial Cckar positive Trpv1 positive
Conduction velocity	C-fiber	C-fiber

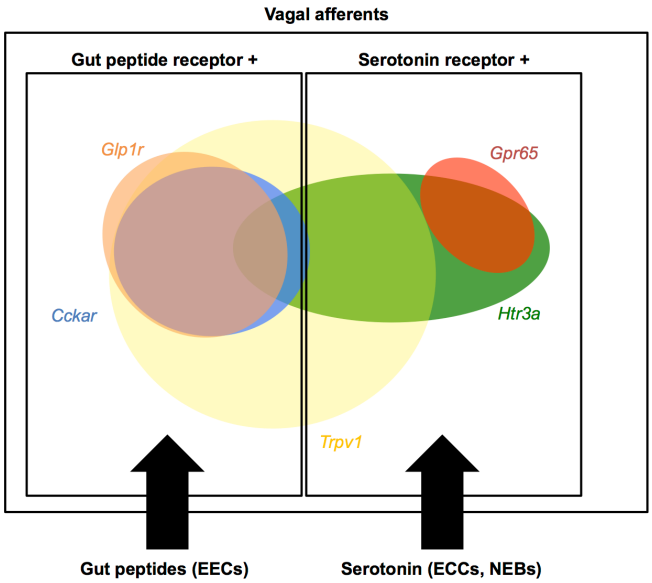

Figure 3.10 Schematic of nodose sensory neuron subtypes determined by *in vitro* calcium imaging and two-color *FISH*.

3.2 Imaging responses of molecularly defined subsets

Introduction

GLP1R and GPR65 mark discrete neuron cohorts that are responsive *in vitro* to gut hormones. We sought to determine whether these two molecularly defined neuron subsets detect specific cues *in vivo*, and which cues those might be.

Methods

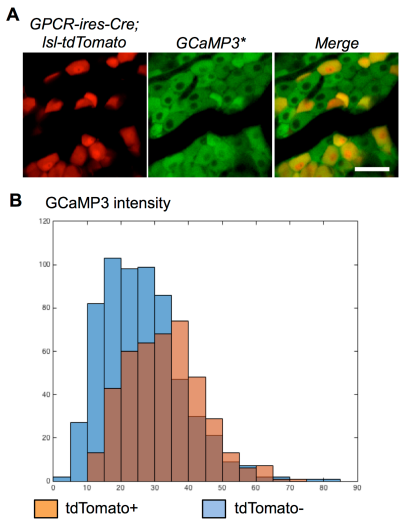

Figure 3.11 Imaging responses in molecularly defined nodose neuron subsets. (A) Representative field of view of tdTomato and GCaMP3* fluorescence in triple-cross animals. Scale bar: 50 μm. (B) Histogram of GCaMP3 fluorescence intensity for tdTomato+ (peach) and tdTomato- (blue) neurons.

To measure the response properties of each neuron type, we developed an *in vivo* nodose ganglion imaging approach involving constitutive expression of the genetically encoded calcium indicator GCaMP3, and the Cre-dependent expression of tdTomato (Figure 3.11 A). We generated two triple knock-in mouse lines: *Glp1r-ires-Cre; lox-tdTomato; Rosa26-GCaMP3* (*Glp1r-GCaMP3**) and *Gpr65-ires-Cre; lox-tdTomato; Rosa26-GCamp3* (*Gpr65-GCaMP3**) mice. Because all sensory neurons express GCaMP3 from a constitutive allele, and targeted neurons were visualized by tdTomato expression, this enables a direct comparison of responses in Cre-positive and Cre-negative neurons.

Imaging, stimulus administration, and analysis were performed as described previously. However, in triple cross animals, the wavelength range collected for GCaMP3 imaging was restricted to prevent bleed-through (standard wavelengths collected: 500-

600nm, triple cross wavelengths collected: 500-540nm). This resulted in baseline GCaMP3 fluorescence intensity measurements that were similar between tdTomato-positive and tdTomato-negative neurons (Figure 3.11 B).

Results

We asked whether vagal GLP1R and GPR65 neurons sensed gastric distension, intestinal nutrients, or lung inflation. Using *Gpr65-GCaMP3** mice, we failed to identify any GPR65 neurons that responded to lung inflation (0/48, 3 mice) and observed only rare GPR65 neurons that responded to gastric distension induced by liquid diet infusion (2.9%, 3/104, 3 mice) or inflation with a gastric balloon (5%, 4/77, 4 mice), or to small intestine distension (9.1%, 3/33, 3 mice). Instead, GPR65 neurons accounted for the majority of neurons responsive to intestinal nutrients (66%, 27/41, 4 mice) (Figure 3.12).

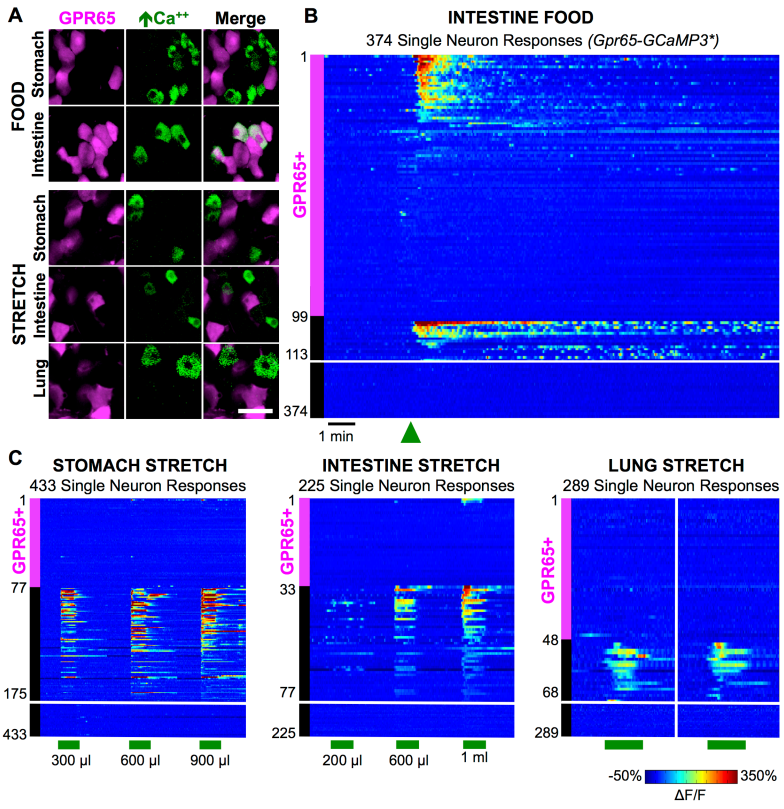

Figure 3.12 GPR65 neurons respond to chemical cues in the intestine. (A) Representative images showing GPR65 neurons and neurons responsive to each of the stimuli listed. Scale bar 50µm. (B, C) Single neuron responses in vagal ganglia of *Gpr65-GCaMP3** mice to intestine food (green arrow), stomach food (green arrows), intestine food (green arrows), and lung inflation (green bars, 15 seconds). Each row indicates GCaMP3 fluorescence intensity changes (ΔF/F, color coded) of one neuron over a 500 second trial (stomach food, intestine food) or two 50-second trials (lung inflation). Magenta and black bars represent tdTomato-positive and tdTomato-negative neurons respectively.

Using *Glp1r-GCaMP3** mice, we observed only rare vagal GLP1R neurons that responded to lung inflation (1%, 2/204, 4 mice), and some that detected intestinal nutrients (9.2%, 18/195, 3 mice). GLP1R neurons accounted for most neurons responsive to gastric distension induced by liquid diet infusion (85%, 39/46, 3 mice), or by inflation of the stomach with nitrogen gas (81%, 46/57, 3 mice). Furthermore, a separate cohort of GLP1R neurons accounted for most neurons responsive to saline-induced intestinal distension (67.7%, 88/130, 2 mice) (Extended Data Fig. 8). Therefore, stomach and intestinal stretch each activated subsets of vagal GLP1R neurons (Figure 3.13).

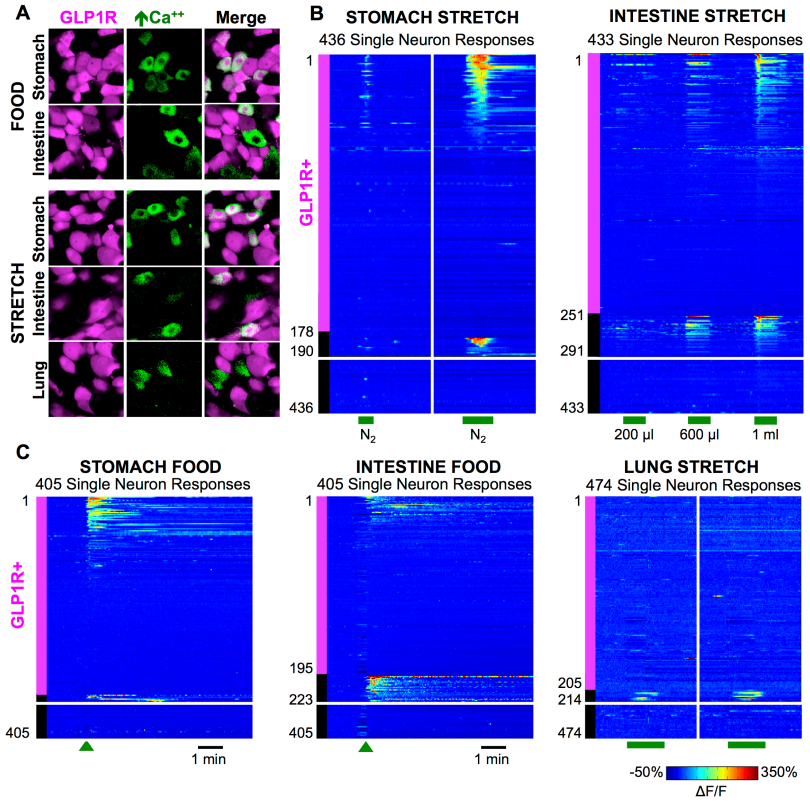

Figure 3.13 GLP1R neurons respond to stomach and intestine stretch. (A) Representative images showing GLP1R neurons, and neurons responsive to each of the stimuli listed. Scale bar 50µm. (B, C) Single neuron responses in vagal ganglia of *Glp1r-GCaMP3** mice to stomach inflation by nitrogen (left 7 seconds, right 15 seconds), , intestine stretch (green bars 30 seconds), stomach food (green arrow), intestine food (green arrows), and lung inflation (green bars, 15 seconds). Each row indicates GCaMP3 fluorescence intensity changes (ΔF/F, color coded) of one neuron over a 500 second trial (stomach food, intestine food) or two 50-second trials (lung inflation). Magenta and black bars represent tdTomato-positive and tdTomato-negative neurons respectively.

Discussion

Taken together, GPR65 neurons account for most vagal chemoreceptors in the proximal small intestine, while GLP1R neurons account for most vagal mechanoreceptors

in the stomach and intestine. Interestingly, GLP1R neurons do not seem to respond to GLP-1. This may be due to 1) insensitivity of the calcium imaging preparation, 2) route of GLP-1 administration in these experiments, or 3) absence of a signaling pathway that directly links GLP-1 to action potential generation. GLP-1 may rather play a modulatory role in these neurons, for example tuning their stretch sensitivity as the fed vs fasted state of the animal changes.

We also observed a number of neurons that responded to intestinal nutrients and gastrointestinal stretch that were not positive for GPR65 or GLP1R, respectively. Generally, these populations could be explained in several ways.

First, perhaps the molecular marks we are using do not capture all of the neurons within a particular class. For example, the GLP1R negative gastrointestinal mechanosensors may belong to a unique mechanosensitive sub-population. For example, IMAs are hypothesized to be mechanosensitive based on their anatomical association with gastrointestinal muscle and sphincter sites. However, whether these terminal types are truly mechanosensitive and the extent to which GLP1R might label them as well are unknown. Identification and use of the receptors involved in sensory transduction itself for these responses would improve concordance between molecular mark and response properties.

Second, the power of an intact *in vivo* imaging preparation also comes with the associated caveat that secondary and tertiary effects of stimulus administration may also activate discrete cohorts of vagal sensory neurons. These responses may be difficult to discriminate. Greater monitoring of multiple physiological parameters during stimulus administration may help to resolve these effects. For example, GPR65-negative intestinal

food responders may detect pancreatic secretion, gall bladder contraction, changes in hepatic metabolism, or induction of peristalsis in different intestinal segments. The GPR65-negative responders tended to exhibit a slightly more delayed and protracted response, and future studies measuring and manipulating specific organ systems may reveal the identity of the GPR65-negative food-responsive cohort.

GPR65 offered the most specific mark; only three GPR65 neurons were responsive to stomach food and three to intestinal stretch. These unexpected double-positive neurons can likely be attributed either to a slight imperfection of the molecular mark, or non-specificity in stimulus delivery. For example, stomach food responders may be intestinal chemosensors that were included in the stomach by imperfect placement of the suture. Intestinal stretch responders may be intestinal chemosensors activated because infusion of saline into the intestine may mimic mucosal stroking, especially for terminals close to the higher-flow saline infusion site. Mucosal stroking is a known stimulus for chemically sensitive intestinal vagal afferents.

GLP1R neurons did account for 44% of all intestinal food responders. This neuron set is best evaluated following results of genetically guided anatomical tracing.

3.3 Anatomical tracing of molecularly defined subsets

Introduction

The response properties of GLP1R and GPR65 neurons suggest they transmit information from the gastrointestinal tract. We sought to define the peripheral terminal

types of these neuron cohorts, and to also map their projection fields within the brainstem. David Strochlic and Ben Umans performed all anatomical studies.

Methods: AAV-guided anatomical mapping

David developed a genetic approach involving adeno-associated viruses (AAVs) to map vagal sensory neuron anatomy[50]. Cre-dependent AAVs encoding a fluorescent reporter (*AAV-flex-tdTomato*) were directly injected into vagal ganglia of knock-in mice, and about four weeks later, labeled fibers were visualized in peripheral tissues and brainstem by whole mount fluorescence and/or immunohistochemistry. AAV infections occurred in ~50% of vagal sensory neurons, without apparent preference for particular neuron classes. Anatomical mapping of all vagal sensory neurons in *Vglut2-ires-Cre* mice yielded bright fluorescent fibers in lung, stomach, and small intestine, as well as axon terminals in the brainstem.

Tissues (lung, duodenum, stomach, brain, ganglia) were collected for fluorescence imaging (unfixed) and immunohistochemistry (fixed). For immunohistochemistry, fixation involved standard protocols for transcardial perfusion with paraformaldhyde, post-dissection fixation and sucrose cryopreservation[223].

Table 3.5 Summary of IHC antibodies

Antibody	Catalog #	Dilution
Chicken-anti-GFP	Abcam, AB_300798,	1:1000
Rabbit-anti-DsRed	Clontech, AB_10013483,	1:1000
Donkey-anti-Chicken-647	Jackson ImmunoResearch, AB_2340379	1:300
Donkey-anti-Chicken-488	Jackson ImmunoResearch, AB_2340375	1:300
Donkey-anti-Rabbit-Cy3	Jackson ImmunoResearch, AB_2307443	1:300
Donkey-anti-Rabbit-647	Jackson ImmunoResearch, AB_2340624	1:300

Innervation of duodenum was quantified in cryosections (12 μm) sampled every millimeter from the pyloric sphincter over a distance of 1 centimeter. Normalized villus innervation was quantified by dividing the number of villi innervated with tdTomato-containing fibers by the number of villi innervated with GFP-containing fibers.

For wholemount analysis of IGLE innervation, enteric neurons were labeled by intraperitoneal injection of Fluorogold (30 mg/kg) and, 3-5 days later the ventral stomach corpus was dissected and the muscular layer was gently isolated and imaged. Stomach IGLEs were identified using standard criteria[102], and the numbers of enteric ganglia innervated were counted. In Figure 3.14, DAPI and Fluorogold fluorescence images were gamma-corrected to enhance visualization of tissue architecture and Sobel edge detection was used to enhance display of tdTomato fibers in low magnification images. Non-linear enhancements were not used prior to quantification.

Images were acquired either by 1) confocal microscopy (Leica SP5 II, maximum projections of confocal stacks) for nodose/jugular ganglia, 2) Olympus VS120 whole slide scanner for flattened whole-mount tissues (lung lobes, intestinal segments, stomach muscular wall), or 3) standard fluorescence microscopy for tissue sections.

Results

AAV-guided anatomical mapping of GPR65 neurons using *Gpr65-ires-Cre* mice revealed extensive innervation of intestinal villi in the duodenum immediately proximal to the pyloric sphincter (Figure 3.14). In contrast, GLP1R neurons surprisingly did not innervate villi in the proximal duodenum. For quantitative analysis, vagal ganglia of *Gpr65-ires-Cre* and *Glp1r-ires-Cre* mice were simultaneously infected with *AAV-flex-tdTomato* and a Cre-independent GFP reporter virus (*AAV-GFP*) for normalization. GPR65 neurons

accounted for most vagal innervation of duodenal villi (57.4 ± 11.9 %, n=6) while GLP1R neurons did not (5.8 ± 2.2 %, n=6). We observed that GLP1R neurons accounted for some fiber tracts confined to intestinal muscle, and whole-mount en-face imaging of the muscular layer revealed GLP1R+ IGLE-type endings in intestinal muscle. Despite being a sparser cohort, vagal GPR65 neurons innervated 10-fold more intestinal villi than vagal GLP1R neurons.

Next, we analyzed innervation of stomach muscle by each vagal afferent type (Figure 3.14). The extent of innervation was quantified by counting the number of enteric ganglia contacted by labeled IGLEs in *Vglut2-ires-Cre*, *Gpr65-ires-Cre,* and *Glp1r-ires-Cre* mice. AAV infections occurred unilaterally in the left ganglion, which innervates the ventral half of the stomach. We counted 101 ± 17 enteric ganglia innervated by labeled IGLEs per ventral stomach in *Vglut2-ires-Cre* mice, 131 ± 38 in *Glp1r-ires-Cre* mice, and only 6 ± 4 in *Gpr65-ires-Cre* mice. GLP1R neurons account for 22-fold more stomach innervation by IGLEs than GPR65 neurons. Thus, GLP1R and GPR65 neurons display strikingly distinct

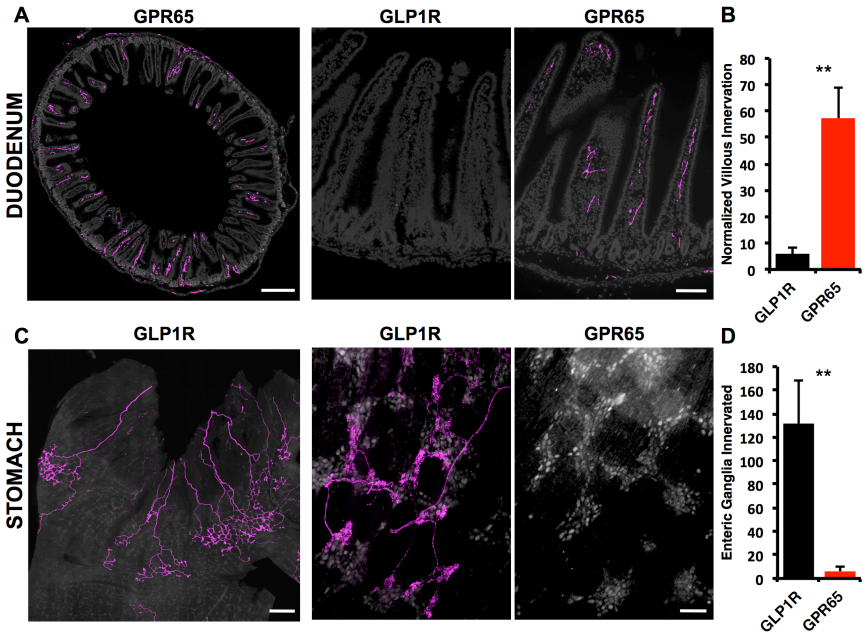

Figure 3.14 Visualizing gut innervation. Vagal sensory neuron projections were mapped by infecting nodose ganglia of *Glp1r-ires-Cre* and *Gpr65-ires-Cre* mice with *AAV-flex-tdTomato.* Terminals were visualized by (A) immunofluorescence of duodenum (cryosections) and (C) stomach corpus (muscle wholemount); stomach enteric neurons were counterstained with Fluorogold (grey). Scale bars: 1 mm (left), 100 μm (right). (B, D) Numbers of gastric enteric ganglia and intestinal villi innervated by vagal sensory neurons were counted and villi counts normalized using a Cre-independent reporter. (mean ± sem, n=6, **p<.01, Student's t-test).

anatomical targets in the periphery, with GPR65 neurons accounting for most vagal innervation of duodenal villi and GLP1R neurons accounting for most vagal IGLEs in stomach muscle.

Next we used AAV mapping to ask whether GPR65 and GLP1R inputs are segregated centrally (Figure 3.15). We simultaneously infected vagal ganglia of *Gpr65-ires-Cre* and *Glp1r-ires-Cre* mice with *AAV-flex-tdTomato* and *AAV-GFP*. GFP signal revealed axons of all types of vagal sensory neurons in the nucleus of the solitary tract (NTS) and area postrema, while tdTomato signal specifically labeled GPR65 and GLP1R axons in each line.

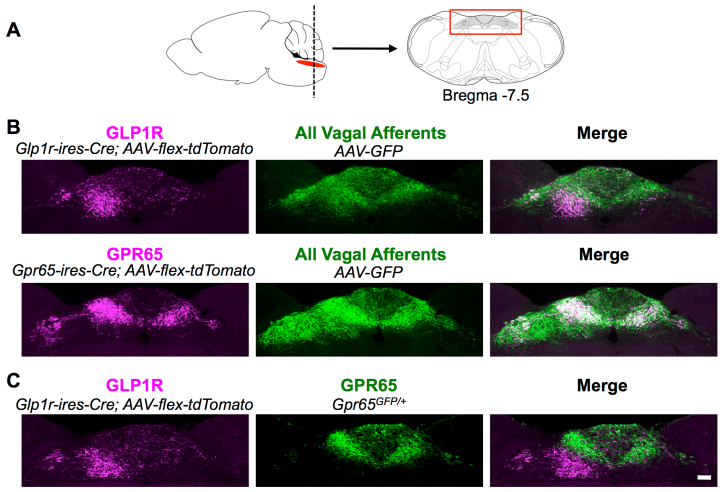

3.15 Visualizing brainstem innervation. (A) Vagal sensory neuron axons were analyzed in a brainstem region (red box) containing the NTS and area postrema. (B) Vagal ganglia of *Glp1r-ires-Cre* and *Gpr65-ires-Cre* mice were infected with *AAV-flex-tdTomato* and *AAV-GFP* for immunofluorescence-based detection of Cre-containing (magenta) and all (green) vagal sensory neuron axons. (C) Vagal ganglia of *Glp1r-ires-Cre; Gpr65$^{GFP/+}$* mice were infected with *AAV-flex-tdTomato* for simultaneous visualization of GLP1R (magenta) and GPR65 (green) axons. Scale bar: 100 μm.

The discrete projection patterns of these two neuron types were also compared in the same mouse. In *Gpr65$^{GFP/+}$* mice, vagal GPR65 fibers can be visualized in the brainstem by anti-GFP immunohistochemistry. Fiber tracts observed in *Gpr65$^{GFP/+}$* mice were similar to fiber tracts visualized using AAVs in *Gpr65-ires-Cre* mice, and expression of GPR65 in central neurons was not observed. Next, we injected vagal ganglia of *Glp1r-ires-Cre*; *Gpr65$^{GFP/+}$* mice with *AAV-flex-tdTomato* to label simultaneously GLP1R neurons

(tdTomato) and GPR65 neurons (GFP). Using this strategy, we found that vagal GLP1R and GPR65 neurons target immediately adjacent but distinct NTS sub-regions (Figure 3.15 C).

GLP1R and GPR65 axons segregate to topographically distinct regions of the posterior NTS (Figure 3.16). Vagal GLP1R neurons predominantly target the medial NTS sub nucleus, a region known to receive input from gastric mechanoreceptors[157,224]. In contrast, GPR65 neurons projected more medially to the NTS commissural zone, just beneath the area postrema. Most GLP1R neuron projections occurred ipsilateral to the infected ganglion, while GPR65 neuron projections occurred bilaterally. Projections of GPR65 and GLP1R neurons were each also distinct from more lateral projections of P2RY1 neurons reported previously.

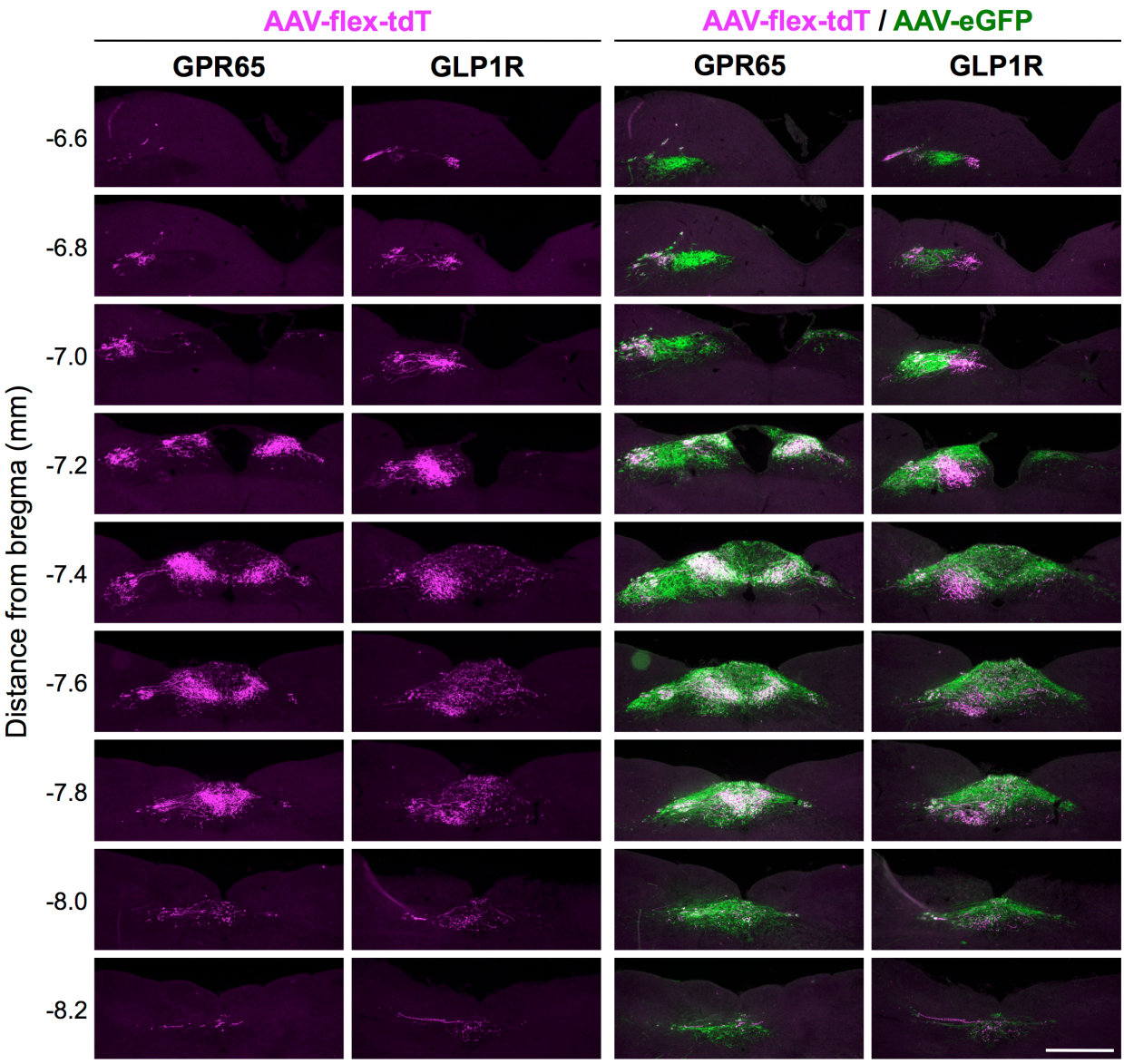

Figure 3.16 Brainstem projections of vagal GLP1R and GPR65 neurons are revealed along the entire anterior-posterior axis. Vagal ganglia of *Gpr65-ires-Cre* and *Glp1-ires-Cre* mice were infected with *AAV-flex-tdTomato* and *AAV-GFP*, and axons visualized in the brainstem by two-color immunofluorescence. A dorsomedial region of each coronal section is depicted, similar to Fig. 5a, scale bar: 500 µm.

Discussion

GLP1R neurons form IGLEs, a peripheral terminal anatomy consistent with their sensitivity to gastrointestinal wall distension. Importantly, GLP1R neurons do not project to intestinal villi, the site of GLP1 release from enteroendocrine cells. Furthermore, we were unable to observe responses to GLP1 agonist administration in vivo. These two lines of evidence support the hypothesis that GLP1R, and perhaps other gut peptide hormone receptors co-expressed on GLP1R neurons, modulate vagal mechanoreceptor sensitivity, but do not alone drive vagal afferent activity.

Importantly, though the imaging experiments show that GLP1R neurons can detect some intestinal chemical cues, given the anatomical specificity observed in tracing studies, the imaging results are more likely to be secondary to the lower specificity of the GLP1R mouse line. Cre recombination, once it has occurred in a cell, is permanent. Therefore *Glp1r-ires-cre, lox-tdTomato* mice may mark neurons that no longer actively express GLP1R. However, AAV viral delivery methods circumvent this confound, because the cre-dependent reporter is only delivered in the adult organism. Therefore, the absence of GLP1R innervation in the small intestine is likely representative of innervation targets of GLP1R-expressing vagal afferents in the adult, while GLP1R neuron responsiveness to chemical cues could be attributed to developmentally driven over-expression of the cre-dependent reporter.

GPR65 neurons, in contrast, densely project to intestinal villi. Because vagal innervation and intestinal food detection is greatest within the proximal few centimeters of the duodenum, vagal mucosal afferents of this class are ideally poised to detect the transit of chemical cues from the stomach into this intestinal segment. Incidentally, the Sphincter

of Oddi, or junction at which pancreatic bicarbonate, pancreatic enzymes, and bile enter the intestine, is located approximated 1.5cm along the intestinal length in the mouse. Therefore, much of GPR65 neuron innervation occurs proximal to the site at which gastric contents would begin to undergo changes induced by intestinal chemical digestion. Vagal sensory neurons cannot discriminate between vastly different chemical cues in the intestinal lumen. Therefore, GPR65 neurons likely are not tuned to the specific chemical features, but would be exquisitely sensitive to the introduction of a broad array of luminal contents introduced by gastric emptying into the small intestine.

The distinct central innervation fields of vagal GLP1R and GPR65 neurons suggest engagement of different higher order neural circuits. GLP1R neurons project primarily to the medial NTS, a region implicated in gastrointestinal function. Intriguingly, the unilateral innervation pattern centrally mirrors the unilateral innervation of the ventral vs. dorsal surface of the stomach. GPR65 neurons project to the commissural NTS and AP, regions implicated in a broad diversity of autonomic processes. Their bilateral projection field is consistent with absence of laterality in innervation of the intestine, and is perhaps an unsurprising feature in a system designed to detect a gross chemical milieu in a single luminal space. While topographic maps in the NTS are imprecise, the striking absence of overlap between these two vagal sensory neuron populations in the brainstem speaks to the existence of a functional map that may span several organ systems (e.g. mechano- vs. chemo- sensation).

3.4 Optogenetic control of gut motility

Introduction

The response properties and anatomical projection patterns of GLP1R and GPR65 neurons indicates unique roles in gastrointestinal physiology. Therefore, we sought to determine the physiological impact of activation of these discrete neuron subsets. Rui Chang, a post doc in the laboratory, performed all optogenetics experiments.

Methods

Studies involving optogenetics, whole nerve electrophysiology to quantify neuron conduction velocity, and physiological measurements of heart rate, gastric pressure, and respiratory rate were as described[50].

Results

We used optogenetic approaches to ask whether vagal GLP1R and GPR65 neurons might regulate gastrointestinal physiology. We crossed *Glp1r-ires-Cre*, *Gpr65-ires-Cre*, *P2ry1-ires-Cre*, and *Vglut2-ires-Cre* mice with a Cre-dependent channelrhodopsin. Activating all vagal sensory neurons in *Vglut2-ChR2* mice caused profound and immediate drops in breathing rate, heart rate, and gastric pressure. Consistent with our prior studies, activating vagal P2RY1 neurons acutely stopped breathing without impacting other physiological parameters analyzed. In contrast, activating vagal GPR65 neurons did not influence heart rate or breathing rate, but instead causing a striking light-induced blockade of gastric contractions. Gastric contractions typically occurred at a frequency of 3.4 ± 0.3 per minute in control *lox-ChR2* mice, and their frequency was not altered by vagus nerve

illumination (3.4 ± 0.6 per minute, 6 mice). In *Gpr65-ChR2* mice, gastric contractions occurred at a similar frequency at rest (3.1 ± 0.3 per minute, 5 mice), but optogenetic activation of GPR65 neurons stopped or reduced gastric contractions during a 1 minute (0 ± 0.0 per minute, 5 mice) and 3 minute (0.6 ± 0.3 per minute, 3 mice) photostimulation period. Activating vagal GLP1R neurons caused a different response characterized by an increase in gastric pressure, and also produced a small but significant change in breathing and heart rate, suggesting that some vagal GLP1R neurons communicate information from organ systems other than the gut. The selective physiological response evoked by GPR65 neuron activation strengthens the conclusion that the vagus nerve consists of several co-fasciculating classes of sensory neurons (so-called 'labeled lines'), each of which conveys a highly specific signal relevant for autonomic physiology.

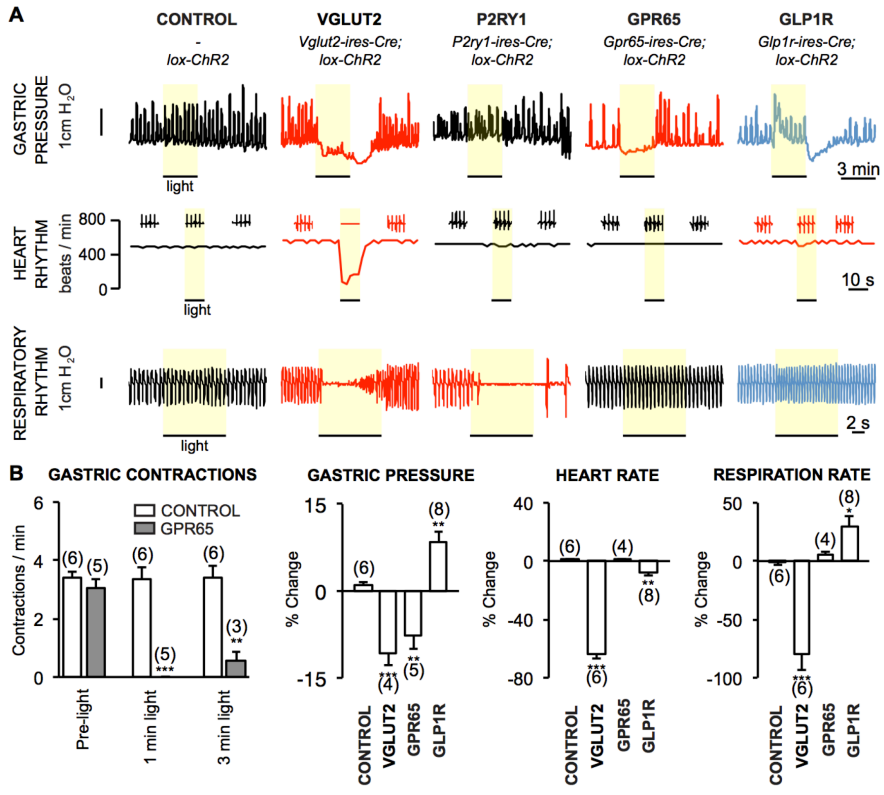

Figure 3.17 Optogenetic control of gut motility. (A) Physiological responses (gastric pressure, heart rate, respiratory rhythm) to optogenetic activation (yellow bar) of vagal sensory neuron subtypes. (B) Quantifying physiological changes to neuron subtype stimulation (mean ± sem, n=3-8, *p<.05, **p<.01, ***p<.001).

Discussion

Activation of GPR65 neurons produced a specific reduction in gastric contractility, consistent with the well-described vagal duodenal-gastric reflexes, and also with reflex responses in mice to introduction of gastrointestinal toxins. Activation of GPR65 neurons resulted in a greater phenotype than activation of all vagal sensory neurons. Therefore, GPR65 neurons are not only sufficient to induce gastric contraction cessation, but also may represent a more pure neuron population responsible for gastric contraction cessation.

GLP1R neuron activation resulted in several physiological changes. The reduced specificity observed with this neuron population may be attributable to several factors. One possibility is that *Glp1r-ires-cre* mice can drive channelrhodopsin expression in neurons no longer expressing high levels of *Glp1r*, a developmental effect that may reduce the specificity of this mouse tool in the adult. Another possibility is that GLP1R neurons may truly encompass several neuron classes, each responsible for a different autonomic role. Third, and most speculatively, perhaps GLP1R neurons do not connect only or primarily with vago-vagal reflex circuits with easily measureable outputs in the anesthetized preparation, but rather connect centrally to mediate other organism responses.

3.5 Conclusions

Internal sensory neurons of the vagus nerve survey the state of several major physiological systems. Within the gastrointestinal tract, sensation of gastric distension and intestinal nutrients are long-appreciated signals that activate vagal afferents and impact physiology and behavior. Here, we genetically define sensory neurons that detect these

cues, and use Cre-based anatomical mapping, *in vivo* imaging, and optogenetics to decipher aspects of gut-to-brain signaling.

One small group of vagal afferents marked by expression of the receptor GPR65 (~230 neurons per ganglion) innervates villi in the proximal small intestine close to the gastro-duodenal junction. GPR65 neurons respond to serotonin, but not other gut hormones such as GLP-1 and cholecystokinin. *In vivo* calcium imaging revealed acute responses of GPR65 neurons to food introduced into the intestinal lumen, providing a direct functional link between sensory neurons with terminal fields in intestinal villi and nutrient detection. Responses of vagal GPR65 neurons to nutrients were rapid and transient, presumably turning off as peristaltic movements removed stimuli from the duodenal bulb. Vagal GPR65 neurons accounted for most but not all nutrient-responsive neurons, indicating at least one other class of nutrient-responsive vagal afferent.

The ability of vagal GPR65 neurons to slow gastric motility suggests a two-pronged response to nutrient-evoked serotonin release in the duodenal bulb. During a meal, food is released through the pyloric sphincter into the duodenal bulb. When a critical level is reached in the duodenal bulb, as detected by a deflection in osmolarity, pH, and/or mechanical brushing, a burst of serotonin is released. Serotonin is a classic signal that promotes gut motility through the enteric nervous system, propelling resident contents distally to sites of enzyme secretion and absorption[225]. Simultaneously, serotonin-responsive GPR65 neurons of the vagus nerve initiate an intestine-brain-stomach circuit that causes a striking feedback blockade of gastric motility, decreasing entry of new content into the duodenal bulb. This dual activity of serotonin should purge the proximal intestine of contents. After the first bolus has migrated, the system re-sets and presumably

re-fills to prepare the next bolus. Based on these findings, we propose an important role for vagal GPR65 neurons in controlling the pulsatile rhythm of food entry into the intestine. Optogenetics enables a specific analysis of vagal chemosensors in the intestine that was not possible with sham feeding, which triggers a complex response involving multiple vagal afferent types but also enteric neurons, spinal neurons, circulating hormones, and direct nutrient effects. Whole nerve stimulations also do not distinguish contributions from villous neurons, gastrointestinal mechanoreceptors, motor neurons, or other fiber types. Future studies are needed to determine the role of GPR65 itself in intestinal homeostasis, as these studies indicate it to be a prime candidate for regulating gastrointestinal physiology.

In rodents, intriguingly, halting gastric contractions can also serve as a defense against ingested toxins. Pica, the ingestion of non-nutritive substances, is thought beneficial in this context because it allows for adsorption of toxins by the ingested substance so that toxins cannot be absorbed as readily by the intestine[201]. GPR65 neurons halt gastric contractions, like illness cues in rodents do, and express the primary target for anti-nausea medications, HTR3A, rendering them likely candidates in peripheral illness circuitry.

Genetically guided anatomical tracing revealed the central representation of nutrient-responsive vagal afferents containing GPR65. Anterograde tracing studies from the intestine using bulk tracing techniques are technically challenging and have not enabled differential analysis of fiber type-specific projection fields, such as those from chemoreceptors and mechanoreceptors. Immediate early gene (IEG) analysis in the NTS suggested a relatively broad topographical domain responsive to intestinal nutrients, and nausea-inducting toxins [226,227]. However, nutrient-evoked IEG induction potentially

includes direct or indirect contributions from multiple vagal afferent types, as well as effects propagating from enteric neurons, spinal neurons, and hormones. Experiments here instead reveal strikingly restricted central projections of vagal GPR65 neurons that are confined to the commissural NTS. This projection field is distinct from that of gastrointestinal mechanoreceptors, and apnea-promoting pulmonary afferents, consistent with a topographical NTS map linked to physiological input. Revealing the spatially confined projections of vagal GPR65 neurons highlights the power of using genetic tools for selective visualization of afferent subtype-specific terminal fields in the brainstem.

Four findings suggest that villous nutrient detection by the vagus nerve occurs primarily through GLP1R-independent mechanisms. Vagal GLP1R sensory neurons 1) do not account for most nutrient-responsive neurons, 2) do not densely innervate intestinal villi, 3) do not respond to GLP1R agonists *in vitro*, and 4) do not respond to GLP1R agonists administered intraperitioneally by *in vivo* ganglion imaging. Instead a cohort of vagal GLP1R neurons forms IGLE terminals in stomach, and accounts for most gastric stretch receptors by *in vivo* imaging. Furthermore, vagal GLP1R neurons project centrally to medial NTS regions that show IEG induction following gastric distension[224]. The same genetically defined neuron type forms IGLEs and senses stomach stretch, supporting the model that IGLEs are mechanosensitive terminals[115] . A second cohort of vagal GLP1R neurons responds to intestinal distention, indicating that vagal GLP1R neurons generally account for several classes of gastrointestinal mechanoreceptors.

These studies add to the list of gut hormone receptors expressed by gastric mechanoreceptors. In some studies, but not all, cholecystokinin was reported to activate the same sensory neurons that detect gastric distension[228,229]. One caveat is that

cholecystokinin exerts profound effects on gastric motility and tone, effects which might secondarily impact stretch sensitivity. Here, analyzing responses of genetically defined gastrointestinal mechanoreceptors in cell culture reveals acute and direct cholecystokinin-evoked calcium transients that are independent of secondary physiological effects. One model is that gut hormones relay convergent state-dependent information about ingested and stored nutrients to modulate the sensitivity of gastric stretch sensors. When nutrients are abundant, sub threshold sensitization of gastric mechanoreceptors would promote satiety at lower distension levels; in contrast, when nutrients are scarce, a larger sized meal would be required for the same sensory neuron response. Here, we reveal that GLP1R is also expressed by mechanoreceptors in stomach, as well as intestine. Unlike CCKAR agonists, GLP1R agonists do not acutely activate vagal afferents, suggesting a modulatory role. Intriguingly, introduction of GLP1R agonists directly into the brainstem can gate NTS responses to stomach distension, and a model was proposed involving GLP1R expression in intrinsic NTS neurons[230]. Our studies raise the possibility that GLP1R agonists instead, or in addition, directly modulate vagal sensory neuron axons in the brainstem to control presynaptic neurotransmitter release. Together, these findings suggest that gut hormones exert multi-tiered control over gastric stretch sensitivity at different processing levels in the same neuron.

Sensory systems use different strategies to encode peripheral information. For example, the olfactory system can generate a myriad of odor perceptions. To achieve this, odors are encoded by combinations of receptors and sensory neuron types in the periphery. Olfactory sensory neuron inputs are subsequently mixed without apparent topography in olfactory cortex. This organization allows individual cortical neurons to

integrate responses from multiple receptors, which is relevant for generating diverse perceptions. In contrast, the gustatory system is more streamlined, with different sensory cells and peripheral neural circuits devoted to perception of sweet, salty, sour, umami, and bitter taste modalities[222]. Our data indicate that the vagus nerve uses a labeled-line coding logic that shares many similarities with gustatory nerves. Individual vagal sensory neurons transmit highly specific information from peripheral organs- such as stomach stretch during feeding and lung inflation during breathing. Furthermore, optogenetic stimulation of vagal GPR65 neurons inhibits gastric contractions without impacting breathing or heart rate, suggesting that individual sensory neurons can not only monitor but also control particular organ systems. The sensory arm of the vagus nerve thus consists of several co-fasciculating labeled lines dedicated for particular sensory modalities. Moreover, the cell bodies of neurons responsive to different pulmonary and gastrointestinal inputs are intermingled within vagal ganglia in a salt-and-pepper manner, suggesting that spatial information from the periphery is largely not apparent at the level of the ganglion.

Genetically identifying neuron subtypes relevant for physiology and behavior is a major goal of the neuroscience field. Recent advances revealed neuron types involved in numerous perceptions and behaviors, such as touch, itch, hunger, and aggression[231-234]. Genetic approaches help paint a comprehensive picture of neuron function that includes gene expression, peripheral anatomy, central anatomy, *in vivo* and *in vitro* responsiveness, and physiological function. Here, we genetically define two discrete classes of gut-to-brain afferents that differentially monitor and control the digestive system, providing a pivotal molecular foundation for exploring the sensory biology and neural circuitry associated with gut-to-brain signaling.

Chapter 4: Future Directions

In vivo imaging and genetic deconstruction of vagal sensory circuits provides a foundation for future investigation. Summarized here are a few of the outstanding questions and means to approach them that arise as a result of this thesis work.

4.1 Vagal afferent information coding

Expansion of the stimulus repertoire

In vivo imaging provides a powerful tool to query vagal afferent neurobiology. However, the current stimulus repertoire presented here covers only ~65% of all vagal afferents, meaning that several stimulus classes remain unexplored using this technique. The ability to survey the full range of vagal afferent receptive fields and stimulus types should be technically possible, and would be exceedingly useful to complete characterization of this sensory subsystem, and to determine the functions of novel molecularly marked neuron sets.

The ability to detect responses to cardiac stimuli such as mechanical forces on and chemical cues within the walls of the heart might allow for identification of molecularly defined neurons responsible for key cardiac reflexes. Furthermore, in the whole-mouse preparation, the vagal survey of cardiac events such as volume overload, or myocardial ischemia could be directly queried, providing information about the sensory autonomic circuits activated by pathological cardiac stressors. To access all cardiac vagal afferents, including those sensitive to individual components of the cardiac cycle would involve use

of improved GCaMP species such as GCaMP6, which affords better signal-to-noise than GCaMP3, and kinetics fast enough to capture action-potential events. In addition, an upgraded microscope system could allow for much faster scan speeds to match the rapid rate of heart beats in the mouse (300+ beats per minute).

In addition, while many vagal afferents in the lung are mechanosensitive, current methods cannot successfully access irritant-only responsive neuron subsets. Pulmonary C-fibers are reported to account for the majority of vagal lung innervation, suggesting that these fibers may compose much of the remaining ~35% of unidentified vagal neurons in the *in vivo* imaging preparation. Several well-established inhalation paradigms for pulmonary irritants are readily interface-able with imaging. One particularly interesting stimulus might be OVA sensitization, a standard mouse model of asthma, particularly given recent finding that vagal afferents are necessary for the development of in airway hyper-reactivity, the defining pathological change in asthma[96].

4.2 Investigation of GLP1R and GPR65 neurons

Response properties

In vivo imaging revealed that the majority of gastric mechanoreceptors are GLP1R neurons, and the majority of intestinal chemosensors are GPR65 neurons. Reciprocally, however, GI mechanosensors account for ~40-50% of GLP1R neurons, and duodenal chemosensors account for ~30% of GPR65 neurons. Therefore, many GLP1R and GPR65 neurons have as-yet undefined receptive fields or response properties.

Some un-accounted for GLP1R neurons may be mechanosensors in distal regions of the gastrointestinal tract. Mechanical distension was spatially restricted in experiments to-date to the stomach and proximal ~11 cm of small intestine. While these regions are most densely innervated by IGLEs, IGLEs can be found throughout the gastrointestinal tract, including the esophagus and distal intestine. It is also possible, given the pleiotropic effects of optogenetic activation of GLP1R neurons, that this subset innervates other distinct organ systems. Future studies expanding the anatomical characterization of distal intestine, esophagus, lung, and heart would shed light on other sites of GLP1R innervation.

Additional anatomical characterization of GPR65 neurons has already been initiated. Ben Umans, a graduate student in the lab, has found that while GPR65 neurons do not innervate the gastric muscle, they do form afferent terminals in the gastric mucosa (Figure 4.1). This is a shocking finding given that not a single stomach stimulus activated any GPR65 neurons by *in vivo* imaging, including liquid diet and several iterations of mechanical distension. The presence of fibers here, and the absence of mechanically-evoked responses in GPR65 neurons indicates that mechanically insensitive vagal fibers do innervate the stomach, and that not all gastric information transmitted by the vagus is necessarily mechanical. One possibility is that these GPR65 gastric fibers are the stretch-insensitive cohort described by Iggo in 1957, that responds selectively to changes in gastric pH[121].

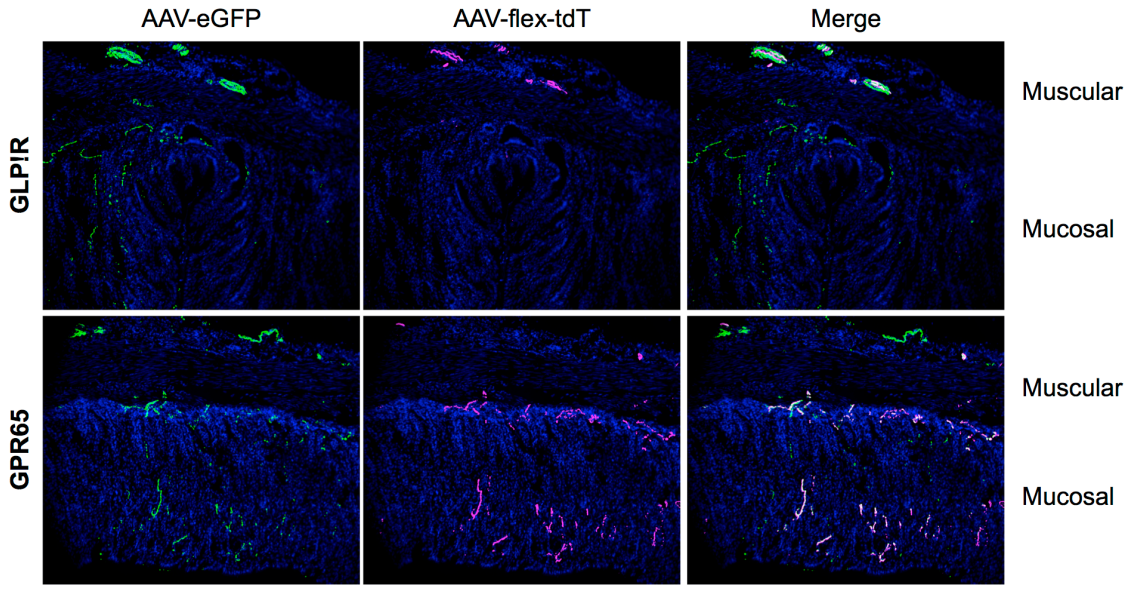

Figure 4.1 GPR65 neurons project to the gastric mucosa. Stomach sections from *Glp1r-ires-cre* and *Gpr65-ires-cre* mice injected with Cre-independent AAV-eGFP and Cre-dependent AAV-tdTomato.

Finally, it would be of great physiological interest to determine the cues to which these neuron cohorts are responsive in the awake and behaving mouse. Infection of vagal sensory neurons with cre-recombinase dependent GCaMP6 AAV vectors would afford labeling of genetically defined vagal afferents, whose population activity could be recorded using fiber optic insertion into the nodose ganglion, or into neuron projection fields in the brainstem. Studies of similar design have provided fundamental insights in feeding-circuitry in the hypothalamus[235-237].

Molecular mechanisms of cue detection

The receptors used in this work to mark neuron subsets are likely not the receptors involved in detection of intestinal luminal cues, nor of gastrointestinal stretch. However, molecular marks of the relevant neuron populations provide a powerful tool for molecular target discovery.

GPR65 neurons respond to luminal intestine cues, express the serotonin receptor *Htr3a*, and respond *in vitro* to serotonin and *Htr3a*-specific agonists. Given the extensive evidence that serotonin plays a key role in transmission of gastrointestinal cues to vagal afferents, that *Htr3a* is the relevant receptor for GPR65 neurons presents itself as a natural hypothesis. To investigate this finding, nodose neuron specific knockdown of *Htr3a* can be achieved using viral vector delivery of *shRNA* or *siRNA* targeting *Htr3a*, and imaging performed to determine if loss of *Htr3a* results in loss of GPR65 neuron activation by intestinal cues. A current post doc in the lab, Nikhil Sharma, is taking on this project.

Because GLP1R marks gastrointestinal mechanosensors, these neurons can now be sorted and sequenced. Transcriptional analysis comparing GLP1R positive versus GLP1R negative versus GPR65 neurons could generate an intriguing list of targets selectively enriched in GLP1R neurons, and therefore putative modulators of mechanosensation, or potentially the mechanosensitive element itself (assuming vagal sensory neurons are the primary mechanosensor [117]). Validation of targets could be achieved by assaying mechanosensitivity either in *in vitro* or *in vivo* in the context of target knockdown.

Roles of neuron subsets in the awake-behaving animal

Do gastrointestinal mechanosensors mediate nausea and satiety? What role does specific activation of duodenal chemosensors play in organism feeding or illness behaviors? Genetic tools allow for specific activation and ablation of molecularly defined neuron subsets. Therefore, use of *Gpr65-ires-cre* and *Glp1r-ires-cre* mice may resolve long-standing

questions about how vagal afferent information from the gastrointestinal tract drives animal behavior.

To investigate these questions would require a means by which GPR65 and GLP1R nodose sensory neurons could be specifically activated or ablated in the awake, behaving mouse. Activation could be achieved using channelrhodopsin, with light delivery to the vagus nerve configured so as to be compatible with awake studies. This is a surgically technically challenging task. Therefore, Designer Receptors Exclusively Activated by Designer Drugs (DREADDs) provide an intriguing non-surgical alternative. DREADDs were generated by mutating GPCRs to lose their endogenous ligand affinity, and instead gain affinity to a synthetic ligand. Expression of DREADDs in desired neuron targets and systemic administration of the synthetic ligand, either by intraperitoneal injection or by provision in the drinking water, can allow for activation or inhibition of the neuron cohort in question in the intact mouse.

Specific targeting of DREADDs to the cell cohort of interest can be achieved using intersectional genetics[238]. Intersectional genetics reporter alleles restrict reporter expression to cells that express both a Cre recombinase and a Flp recombinase. This is a critically important feature because *Gpr65* and *Glp1r* are both expressed in extra-nodose sites: *Gpr65* is expressed in resident immune cells throughout every tissue surveyed in *Gpr65-ires-cre; lox-tdTomato* animals, while *Glp1r* is expressed in many central nervous system neurons, pancreatic islet beta cells, and other non-specific sites. Therefore, a triple cross using a vagal complex specific Flp line (e.g. *Phox2b-Flp*), and a nodose-specific cre line (egg *Gpr65-ires-cre*), can enable restricted expression of DREADDs only in GPR65 nodose

neurons. Changes in body weight, feeding behavior, conditioned taste aversion, and pica could then all be measured in triple-cross animals with and without injection of the synthetic DREADD ligand to determine the effects of activating and silencing this neuron population on mouse behavior. Furthermore, the synthetic ligand dose could be modulated to vary the strength of activation of these circuits, to directly test if low activation might yield satiety-like phenotypes, while high activation reveals nausea-like behaviors, or whether these two behavioral modes are rather mediated by independent neuron subsets.

4.3 Exploration of additional vagal sensory neuron subsets

GPR65 and GLP1R have been illustrative markers for deconstruction of vagal sensory circuits. However, division of the vagus nerve by GPCR expression is far from the only molecular classification scheme available. Transcription factors, other sensory receptor classes, and peptides may all serve as useful alternative subset marks.

The serotonin receptor Htr3 is an intriguing molecular target in the vagus because it is the site of action for most anti-emetic agents used to treat acute chemotherapy-induced nausea[239].. By our counts using two-color *in situ* and *in vitro* calcium imaging, GPR65 neurons only cover approximately 25% of all *Htr3a*-expressing vagal sensory neurons, leaving a large cohort of serotonin-sensitive vagal sensory neurons to be explored. Intriguingly, Htr3 receptors are pentamers, potentially composed of a mix of up to five unique (*Htr3a*-*e*) subunits. Htr3a homomers have a single-channel conductance below the resolution of recording techniques. However, addition of Htr3b subunits increases Htr3 conductance by at least 16-fold, suggesting the heteromeric channels are truly responsible for Htr3 signaling[240]. Polymorphisms in Htr3b and Htr3a associate with human likelihood

to develop post-operative nausea and vomiting and disorders[241-243]. Furthermore, *Htr3b* is preferentially expressed in the peripheral versus central nervous system, and within the nodose Htr3b is expressed in a small subset of Htr3a+ vagal sensory neurons[191]. Understanding the relationship of *Htr3b* and *Gpr65* expression in the nodose would be intriguing. If these two neuron cohorts overlapped, this might support the notion that signaling occurs though Htr3 receptors in GPR65 neurons. However, if these populations do not overlap, perhaps Htr3b can serve to further sub-divide vagal Htr3-expressing populations.

Given the mechanosensitive roles of many vagal sensory neurons, the response profiles of nodose neurons expressing the known mammalian mechanosensor Piezo2 would be of great interest. Piezo2 is expressed in a small nodose neuron subset, and *in vivo* calcium imaging could address whether Piezo2 neurons respond to physiologically relevant stretch stimuli. Both *Piezo2* knockout and *Piezo2-ires-cre* lines are commercially available.

In summary, molecular deconstruction of the vagus sensory system offers a plethora of intriguing experimental approaches that can span several sensory modalities and internal physiologies. Much work remains to explore vagal sensory neurobiology in the molecular/genetic age.

Addendum: Response properties of other vagal sensory neuron subsets

P2RY1

Imaging the nodose ganglion

Introduction

Prior work in the laboratory identified neurons expressing the GPCR *P2ry1* as critically involved in the regulation of breathing. P2RY1 neurons densely innervate the lung, and form specialized candelabra endings around neuroepithelial bodies. Activation of P2RY1 neurons using optogenetic techniques results in complete apnea, with no effect on other autonomic physiologies such as gastric contractions and heart rate. Furthermore, P2RY1 neurons are capsaicin insensitive A-fibers. All of these features strongly supported the hypothesis that P2RY1 neurons would be slowly adapting stretch receptors in the lung responsible for mediating the Hering-Breuer reflex. Using the imaging technique, we could directly test this hypothesis.

Methods

Imaging and lung stretch stimulus delivery were as described, but using triple-cross *P2ry1-ires-cre*, *lox-tdTomato*, *GCaMP3** mice.

Results

Lung stretch responsive neurons were not P2RY1 neurons, and P2RY1 neurons were not responsive to lung stretch (Figure A1).

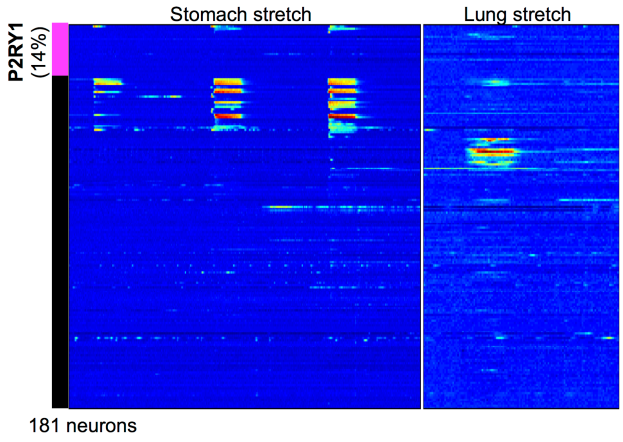

Figure A1. P2RY1 neurons do not respond to lung stretch by *in vivo* imaging.

Discussion

P2RY1 neurons in the nodose ganglion do not detect lung inflation. We can therefore conclude: 1) P2RY1 neurons in the nodose are likely responsible for detection of a different type of sensory stimulus. 2) Lung stretch responsive neurons in the nodose belong to a P2RY1-negative neuron subset. However, these conclusions are not necessarily incompatible with a role for jugular P2RY1 neurons in the detection of lung stretch. Jugular neurons are labeled with AAV infection, and their fibers of passage would be activated by optogenetic approaches used in Chang, 2015. However, jugular neurons rarely populate the imaging field of view using the current imaging approach, so their response properties might be missed.

Imaging the Jugular Ganglion

Introduction

The cell bodies of the sensory neurons of the vagus reside in the superior, neural-crest-derived jugular ganglion, as well as the inferior, placode-derived nodose ganglion. These ganglia are of unique embryologic origin, and also contain neurons with different sensory and neurochemical properties. While ~75% of jugular sensory fibers project to the surface of the ear via the auricular branch[6], one of the branches severed during this imaging preparation, the remaining 25% project through the vagus nerve trunk. A subset of jugular ganglion neurons respond to mechanical forces in an isolated guinea pig lung preparation, and can be visualized by retrograde labeling from lung and airways. Furthermore, the distribution of innervation, fiber type composition, and neurochemical properties of jugular and nodose neurons innervating the respiratory system differ [244], supporting the hypothesis that nodose and jugular P2RY1 neurons may be distinct. Therefore, we sought to access jugular ganglia via imaging as well.

Methods

Methods were as described for the imaging preparation, but with surgical modifications to expose the jugular ganglion. During ganglion exposure, carotid branches extending laterally from the carotid trunk superior to the ganglion surgical field were tied to minimize bleeding. Overlying musculature was gently transected, cauterized and reflected. The bones overlying the ear were gently broken and removed, and gentle tension was used to widen and open the jugular foramen. The jugular ganglion is situated within

the foramen itself, so additional access allowed for nerve trunk transection further superiorly within the foramen structure.

Results

Surgical preparation for jugular imaging resulted in a high mortality rate. 8/10 (80%) of animals died during surgery, most within ~15 minutes of opening of the jugular foramen, likely secondary to hemorrhage from highly vascularized bony tissues, or potentially to exposure of the delicate brainstem. One animal died within 5 minutes of the initiation of imaging, likely for the same reasons.

In the single surviving animal, two cell body clusters were visually apparent by wide-field fluorescence (Figure A2). However, confocal microscopy of the superior-most neuron set revealed only a limited imaging field (Figure A2, inset). None of these neurons were responsive to electrical stimulation of the nerve trunk, either because their branches do not pass through the main nerve trunk, or because of damage to the axons during ganglion isolation.

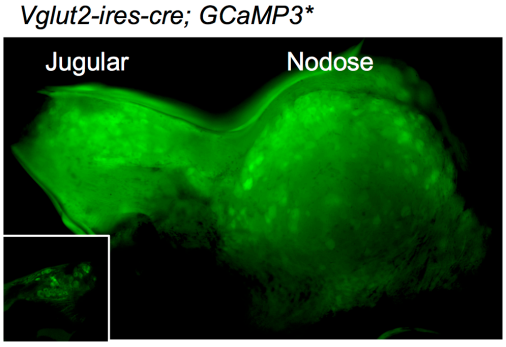

Figure A2. Attempts at imaging the superior jugular ganglion *in vivo*.

Discussion

The technical difficulties of jugular ganglion isolation prevented collection of data concerning response properties of jugular ganglion neurons.

NPY2R

Summary

The gut peptide PYY, like CCK and GLP-1, is synthesized and released by chemosensory cells within the epithelial lining of the gut, and has been implicated in vagal modulation of feeding behavior[146]. As noted in Chapter 3, NPY2R is expressed in a subset of vagal afferents, many of which also express CCKAR and GLP1R. However, NPY2R is also expressed in many CCKAR and GLP1R negative neurons, raising intriguing questions about what additional cues this neuron subtype might detect. Rui Chang generated an *Npy2r-ires-cre* mouse line to investigate this population. However, the mouse line appears to drive much broader expression of cre-dependent reporters (~60% of the nodose neurons) than suggested by *Npy2r* expression examined using two-color FISH (~30% of nodose neurons). Triple-cross animals were generated and imaged, though interpretation of this data is limited given that such a large proportion of nodose ganglion neurons are tdTomato positive.

Results

NPY2R partially covered stomach-stretch –responsive neurons. In addition, every neuron responsive to intestinal perfusion was positive for tdTomato, suggesting that a

subset of *Npy2r-ires-Cre; lox-tdTomato* positive neurons do play an important role in intestinal chemosensation (Figure A3). Greater confidence that these are truly NPY2R neurons in the adult may be achieved by combining AAV delivery of cre-dependent reporters to bypass potential developmental effects driving NPY2R expression so broadly within the ganglion. Pilot work using injections of AAV vectors containing *lox-tdTomato* in *Glp1r-ires-cre* mice indicates that imaging and viral infection may be compatible if imaging is performed within 1-1.5 weeks of virus injection.

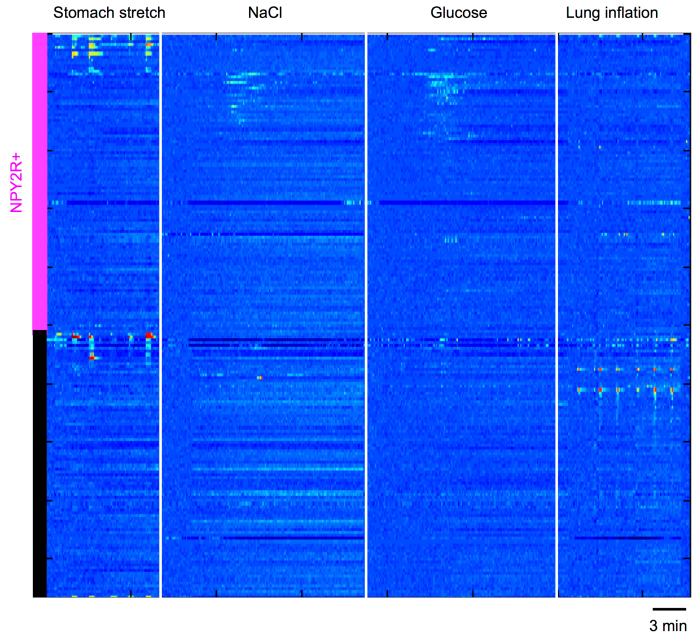

Figure A3. NPY2R neurons encompass all intestinal perfusion responsive neurons by *in vivo* imaging.

MC4R

Summary

The melanocortin-4 receptor (MC4R) plays a key role in a broad array of systems, including the regulation of feeding behavior[245]. Using an MC4R-GFP mouse, prior groups have shown that subsets of both vagal sensory and motor neurons express GFP in this

line.[246] Furthermore, circumstantial evidence suggested that MC4R-positive afferents may project to the intestinal wall and intestinal villi[247]. Brad Lowell's group had recently generated an *MC4R-2a-cre* line, and generously provided animals so that we could test the response properties of MC4R vagal sensory neurons.

Results

MC4R neurons using this line accounted for less than 6% of all viable, imaged neurons. Furthermore, none of these neurons responded to perfusion of intestinal cues, stomach stretch, or carbon dioxide administration in the lung (Figure A4). Future experiments examining if these neurons are responsive to intestinal food injection or other untested stimuli would be of great interest. Currently, the response properties of this very small neuron subset remains a mystery.

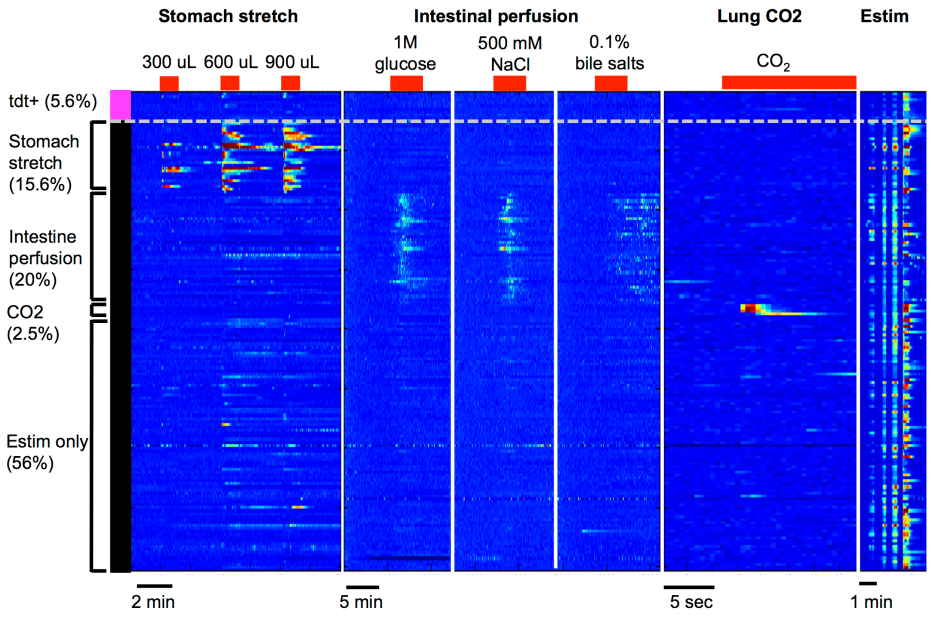

Figure A4. MC4R neurons do not respond to stomach stretch, intestinal perfusion or pulmonary CO_2 by *in vivo* imaging.

Bibliography

1. Foley, J. O. & DuBois, F. S. Quantitative studies of the vagus nerve in the cat. I. The ratio of sensory to motor fibers. *Journal of Comparative Neurology* **67,** 49–67 (1937).

2. Narayanan, C. H. & Narayanan, Y. Neural crest and placodal contributions in the development of the glossopharyngeal-vagal complex in the chick. *Anat. Rec.* **196,** 71–82 (1980).

3. Baker, C. V. H. & Bronner-Fraser, M. Vertebrate Cranial Placodes I. Embryonic Induction. *Developmental Biology* **232,** 1–61 (2001).

4. Takano-Maruyama, M., Chen, Y. & Gaufo, G. O. Differential contribution of Neurog1and Neurog2on the formation of cranial ganglia along the anterior-posterior axis. *Dev. Dyn.* **241,** 229–241 (2011).

5. D'Autreaux, F., Coppola, E., Hirsch, M. R., Birchmeier, C. & Brunet, J. F. Homeoprotein Phox2b commands a somatic-to-visceral switch in cranial sensory pathways. *Proceedings of the National Academy of Sciences* **108,** 20018–20023 (2011).

6. DuBois, F. S. & Foley, J. O. Quantitative studies of the vagus nerve in the cat. II. The ratio of jugular to nodose fibers. *J. Comp. Neurol.* **67,** 69–87 (1937).

7. Berthoud, H. R. & Neuhuber, W. L. Functional and chemical anatomy of the afferent vagal system. *Auton Neurosci* **85,** 1–17 (2000).

8. Sawchenko, P. E. Central connections of the sensory and motor nuclei of the vagus nerve. *J. Auton. Nerv. Syst.* **9,** 13–26 (1983).

9. Saper, C. B. The central autonomic nervous system: conscious visceral perception and autonomic pattern generation. *Annu. Rev. Neurosci.* **25,** 433–469 (2002).

10. Contreras, R. J., Beckstead, R. M. & Norgren, R. The central projections of the trigeminal, facial, glossopharyngeal and vagus nerves: an autoradiographic study in the rat. *J. Auton. Nerv. Syst.* **6,** 303–322 (1982).

11. TORVIK, A. Afferent connections to the sensory trigeminal nuclei, the nucleus of the solitary tract and adjacent structures; an experimental study in the rat. *J. Comp. Neurol.* **106,** 51–141 (1956).

12. Kalia, M. & Sullivan, J. M. Brainstem projections of sensory and motor components of the vagus nerve in the rat. *J. Comp. Neurol.* **211,** 248–265 (1982).

13. Sawchenko, P. E. & Swanson, L. W. Central noradrenergic pathways for the integration of hypothalamic neuroendocrine and autonomic responses. *Science* **214,** 685–687 (1981).

14. Bailey, T. W., Hermes, S. M., Andresen, M. C. & Aicher, S. A. Cranial Visceral Afferent Pathways through the Nucleus of the Solitary Tract to Caudal Ventrolateral Medulla or Paraventricular Hypothalamus: Target-Specific Synaptic Reliability and Convergence Patterns. *Journal of Neuroscience* **26,** 11893–11902 (2006).

15. Strain, S. M., Gwyn, D. G., Rutherford, J. G. & Losier, B. J. Direct vagal input to neurons in the area postrema which project to the parabrachial nucleus: an electron microscopic-HRP study in the cat. *Brain Res. Bull.* **24,** 457–463 (1990).

16. Norgren, R. Projections from the nucleus of the solitary tract in the rat. *Neuroscience* **3,** 207–218 (1978).

17. Rinaman, L., Card, J. P., Schwaber, J. S. & Miselis, R. R. Ultrastructural demonstration of a gastric monosynaptic vagal circuit in the nucleus of the solitary tract in rat. *Journal of Neuroscience* **9,** 1985–1996 (1989).

18. Blinder, K. J. *et al.* Ultrastructural circuitry of cardiorespiratory reflexes: there is a monosynaptic path between the nucleus of the solitary tract and vagal preganglionic motoneurons controlling atrioventricular conduction in the cat. *Brain Research* **785,** 143–157 (1998).

19. Coleridge, J. C., Hemingway, A., Holmes, R. L. & Linden, R. J. The location of atrial receptors in the dog: a physiological and histological study. *J. Physiol. (Lond.)* **136,** 174–197 (1957).

20. Cheng, Z., Powley, T. L., Schwaber, J. S. & Doyle, F. J. A laser confocal microscopic study of vagal afferent innervation of rat aortic arch: chemoreceptors as well as baroreceptors. *J. Auton. Nerv. Syst.* **67,** 1–14 (1997).

21. Miller, M. R. & Kasahara, M. Studies On The Nerve Endings In The Heart. *Am. J. Anat.* **115,** 217–233 (1964).

22. Coleridge, H. M., Coleridge, J. C. & Kidd, C. Cardiac Receptors In The Dog, With Particular Reference To Two Types Of Afferent Ending In The Ventricular Wall. *J. Physiol. (Lond.)* **174,** 323–339 (1964).

23. Paintal, A. S. A Study Of Ventricular Pressure Receptors And Their Role In The Bezold Reflex. *Quarterly Journal Of Experimental Physiology And Cognate Medical Sciences* **40,** 348–363 (1955).

24. Cheng, Z., Powley, T. L., Schwaber, J. S. & Doyle, F. J. Vagal afferent innervation of the

atria of the rat heart reconstructed with confocal microscopy. *J. Comp. Neurol.* **381,** 1–17 (1997).

25. Krauhs, J. M. Structure of rat aortic baroreceptors and their relationship to connective tissue. *J. Neurocytol.* **8,** 401–414 (1979).

26. Paintal, A. S. A study of right and left atrial receptors. *J. Physiol. (Lond.)* **120,** 596–610 (1953).

27. Thorén, P. N. Characteristics of left ventricular receptors with nonmedullated vagal afferents in cats. *Circulation Research* **40,** 415–421 (1977).

28. Armour, J. A. Myocardial ischaemia and the cardiac nervous system. *Cardiovasc. Res.* **41,** 41–54 (1999).

29. Kaufman, M. P., Baker, D. G., Coleridge, H. M. & Coleridge, J. C. Stimulation by bradykinin of afferent vagal C-fibers with chemosensitive endings in the heart and aorta of the dog. *Circulation Research* **46,** 476–484 (1980).

30. Benson, C. J., Eckert, S. P. & McCleskey, E. W. Acid-evoked currents in cardiac sensory neurons: A possible mediator of myocardial ischemic sensation. *Circulation Research* **84,** 921–928 (1999).

31. Thames, M. D. & Minisi, A. J. Reflex responses to myocardial ischemia and reperfusion. Role of prostaglandins. *Circulation* **80,** 1878–1885 (1989).

32. Ustinova, E. E. & Schultz, H. D. Activation of cardiac vagal afferents in ischemia and reperfusion. Prostaglandins versus oxygen-derived free radicals. *Circulation Research* **74,** 904–911 (1994).

33. Coleridge, H. M. & Coleridge, J. C. Cardiovascular afferents involved in regulation of peripheral vessels. *Annu. Rev. Physiol.* **42,** 413–427 (1980).

34. Brown, A. M. Mechanoreceptors In Or Near The Coronary Arteries. *J. Physiol. (Lond.)* **177,** 203–214 (1965).

35. Coleridge, H. M., Coleridge, J. C. & Schultz, H. D. Characteristics of C fibre baroreceptors in the carotid sinus of dogs. *J. Physiol. (Lond.)* **394,** 291–313 (1987).

36. Coleridge, H. M. *Et al.* Impulses in Slowly Conducting Vagal Fibers from Afferent Endings in the Veins, Atria, and Arteries of Dogs and Cats. *Circulation Research* **33,** 87–97 (1973).

37. Coleridge, H. M., Coleridge, J. C., Poore, E. R., Roberts, A. M. & Schultz, H. D. Aortic wall properties and baroreceptor behaviour at normal arterial pressure and in acute hypertensive resetting in dogs. *J. Physiol. (Lond.)* **350,** 309–326 (1984).

38. Coleridge, H. M., Coleridge, J. C., Kaufman, M. P. & DANGEL, A. Operational sensitivity and acute resetting of aortic baroreceptors in dogs. *Circulation Research* **48,** 676–684 (1981).

39. Sullivan, M. J. *et al.* Non Voltage-Gated Ca2+ Influx Through Mechanosensitive Ion Channels in Aortic Baroreceptor Neurons. *Circulation Research* **80,** 861–867 (1997).

40. Bainbridge, F. A. The influence of venous filling upon the rate of the heart. *J. Physiol. (Lond.)* **50,** 65–84 (1915).

41. Paintal, A. S. A STUDY OF VENTRICULAR PRESSURE RECEPTORS AND THEIR ROLE IN THE BEZOLD REFLEX. *Quarterly Journal of Experimental Physiology and Cognate Medical Sciences* **40,** 348–363 (1955).

42. DAWES, G. S. & Widdicombe, J. G. The afferent pathway of the Bezold reflex: the left vagal branches in dogs. *Br J Pharmacol Chemother* **8,** 395–398 (1953).

43. Paintal, A. S. Vagal sensory receptors and their reflex effects. *Physiol. Rev.* **53,** 159–227 (1973).

44. Widdicombe, J. Airway receptors. *Respiration Physiology* **125,** 3–15 (2001).

45. Yamamoto, Y., Hosono, I., Atoji, Y. & Suzuki, Y. Morphological study of the vagal afferent nerve endings in the laryngeal mucosa of the dog. *Ann. Anat.* **179,** 65–73 (1997).

46. Baluk, P., Nadel, J. A. & McDonald, D. M. Substance P-immunoreactive sensory axons in the rat respiratory tract: A quantitative study of their distribution and role in neurogenic inflammation. *Journal of Comparative Neurology* **319,** 586–598 (1992).

47. Sweazey, R. D., Edwards, C. A. & Kapp, B. M. Fine structure of taste buds located on the lamb epiglottis. *Anat. Rec.* **238,** 517–527 (1994).

48. Desaki, J., Kawakita, S. & Yamagata, T. Existence of a muscle spindle on the posterior cricoarytenoid muscle of the guinea pig. *J Electron Microsc (Tokyo)* **46,** 257–261 (1997).

49. Yamamoto, Y., Atoji, Y. & Suzuki, Y. Calretinin immunoreactive nerve endings in the trachea and bronchi of the rat. *J. Vet. Med. Sci.* **61,** 267–269 (1999).

50. Chang, R. B., Strochlic, D. E., Williams, E. K., Umans, B. D. & Liberles, S. D. Vagal Sensory Neuron Subtypes that Differentially Control Breathing. *Cell* **161,** 622–633 (2015).

51. Adriaensen, D. *et al.* Pulmonary intraepithelial vagal nodose afferent nerve terminals are confined to neuroepithelial bodies: an anterograde tracing and confocal microscopy study in adult rats. *Cell Tissue Res* **293,** 395–405 (1998).

52. Brouns, I. *et al.* Neurochemical pattern of the complex innervation of neuroepithelial bodies in mouse lungs. *Histochem Cell Biol* **131,** 55–74 (2008).

53. Tsubone, H., Sant'Ambrogio, G., Anderson, J. W. & Orani, G. P. Laryngeal afferent activity and reflexes in the guinea pig. *Respiration Physiology* **86,** 215–231 (1991).

54. Lee, B. P., Sant'Ambrogio, G. & Sant'Ambrogio, F. B. Afferent innervation and receptors of the canine extrathoracic trachea. *Respiration Physiology* **90,** 55–65 (1992).

55. Sant'Ambrogio, G. Information arising from the tracheobronchial tree of mammals. *Physiol. Rev.* **62,** 531–569 (1982).

56. Mathew, O. P., Sant'Ambrogio, G., Fisher, J. T. & Sant'Ambrogio, F. B. Laryngeal pressure receptors. *Respiration Physiology* **57,** 113–122 (1984).

57. Adrian, E. D. Afferent impulses in the vagus and their effect on respiration. *J. Physiol. (Lond.)* **79,** 332–358 (1933).

58. Bartlett, D., Sant'Ambrogio, G. & Wise, J. C. Transduction properties of tracheal stretch receptors. *J. Physiol. (Lond.)* **258,** 421–432 (1976).

59. Boushey, H. A., Richardson, P. S., Widdicombe, J. G. & Wise, J. C. M. The response of laryngeal afferent fibres to mechanical and chemical stimuli. *J. Physiol. (Lond.)* **240,** 153–175 (1974).

60. Schelegle, E. S. & Green, J. F. An overview of the anatomy and physiology of slowly adapting pulmonary stretch receptors. *Respiration Physiology* **125,** 17–31 (2001).

61. Yu, J. & Zhang, J. A single pulmonary mechano-sensory unit possesses multiple encoders in rabbits. *Neuroscience Letters* **362,** 171–175 (2004).

62. Yu, J., Wang, Y. F. & Zhang, J. W. Structure of slowly adapting pulmonary stretch receptors in the lung periphery. *J. Appl. Physiol.* **95,** 385–393 (2003).

63. Bartlett, D. & Sant'Ambrogio, G. Effects of local and systemic hypercapnia on the discharge of stretch receptors in the airways of the dog. *Respiration Physiology* **26,** 91–99 (1976).

64. Sheldon, M. I. & Green, J. F. Evidence for pulmonary CO2 chemosensitivity: effects on ventilation. *J Appl Physiol Respir Environ Exerc Physiol* **52,** 1192–1197 (1982).

65. Matsumoto, S., Takahashi, T., Tanimoto, T., Saiki, C. & Takeda, M. Effects of potassium channel blockers on CO2-induced slowly adapting pulmonary stretch receptor inhibition. *The Journal of Pharmacology and Experimental Therapeutics* **290,** 974–979 (1999).

66. Knowlton, G. C. & Larrabee, M. G. A unitary analysis of pulmonary volume receptors. *Am. J. Physiol.* **147,** 100–114 (1946).

67. Pack, A. I. & DeLaney, R. G. Response of pulmonary rapidly adapting receptors during lung inflation. *J Appl Physiol Respir Environ Exerc Physiol* **55,** 955–963 (1983).

68. Sant'Ambrogio, G. & Widdicombe, J. Reflexes from airway rapidly adapting receptors. *Respiration Physiology* **125,** 33–45 (2001).

69. Widdicombe, J. G. Receptors in the trachea and bronchi of the cat. *J. Physiol. (Lond.)* **123,** 71–104 (1954).

70. Yu, J. Spectrum of myelinated pulmonary afferents. *AJP: Regulatory, Integrative and Comparative Physiology* **279,** R2142–8 (2000).

71. Pisarri, T. E., Jonzon, A., Coleridge, H. M. & Coleridge, J. C. Vagal afferent and reflex responses to changes in surface osmolarity in lower airways of dogs. *J. Appl. Physiol.* **73,** 2305–2313 (1992).

72. Lai, C. J. & Kou, Y. R. Stimulation of pulmonary rapidly adapting receptors by inhaled wood smoke in rats. *J. Physiol. (Lond.)* **508 (Pt 2),** 597–607 (1998).

73. Mills, J. E., Sellick, H. & Widdicombe, J. G. Activity of lung irritant receptors in pulmonary microembolism, anaphylaxis and drug-induced bronchoconstrictions. *J. Physiol. (Lond.)* **203,** 337–357 (1969).

74. Sellick, H. & Widdicombe, J. G. Stimulation of lung irritant receptors by cigarette smoke, carbon dust, and histamine aerosol. *J. Appl. Physiol.* **31,** 15–19 (1971).

75. Mortola, J., Sant'Ambrogio, G. & Clement, M. G. Localization of irritant receptors in the airways of the dog. *Respiration Physiology* **24,** 107–114 (1975).

76. Sant'Ambrogio, G., Remmers, J. E., de Groot, W. J., Callas, G. & Mortola, J. P. Localization of rapidly adapting receptors in the trachea and main stem bronchus of the dog. *Respiration Physiology* **33,** 359–366 (1978).

77. Coleridge, J. C., Coleridge, H. M., Schelegle, E. S. & Green, J. F. Acute inhalation of ozone stimulates bronchial C-fibers and rapidly adapting receptors in dogs. *J. Appl. Physiol.* **74,** 2345–2352 (1993).

78. Roberts, A. M., Bhattacharya, J., Schultz, H. D., COLERIDGE, H. M. & COLERIDGE, J. C. Stimulation of pulmonary vagal afferent C-fibers by lung edema in dogs. *Circulation Research* **58,** 512–522 (1986).

79. Paintal, A. S. Some recent advances in studies on J receptors. *Adv. Exp. Med. Biol.* **381,** 15–25 (1995).

80. Paintal, A. S. Mechanism of stimulation of type J pulmonary receptors. *J. Physiol. (Lond.)* **203,** 511–532 (1969).

81. Ho, C. Y., Gu, Q., Lin, Y. S. & Lee, L. Y. Sensitivity of vagal afferent endings to chemical irritants in the rat lung. *Respiration Physiology* **127,** 113–124 (2001).

82. Sant'Ambrogio, F. B., Anderson, J. W. & Sant'Ambrogio, G. Menthol in the upper airway depresses ventilation in newborn dogs. *Respiration Physiology* **89,** 299–307 (1992).

83. Sant'Ambrogio, G., Mathew, O. P. & Sant'Ambrogio, F. B. Characteristics of laryngeal cold receptors. *Respiration Physiology* **71,** 287–297 (1988).

84. Nishijima, K., Tsubone, H. & Atoji, Y. Contribution of free nerve endings in the laryngeal epithelium to CO2 reception in rats. *Autonomic Neuroscience* **110,** 81–88 (2004).

85. Anderson, J. W., Sant'Ambrogio, F. B., Orani, G. P., Sant'Ambrogio, G. & Mathew, O. P. Carbon dioxide-responsive laryngeal receptors in the dog. *Respiration Physiology* **82,** 217–226 (1990).

86. Sant'Ambrogio, G., Tsubone, H. & Sant'Ambrogio, F. B. Sensory information from the upper airway: role in the control of breathing. *Respiration Physiology* **102,** 1–16 (1995).

87. Widdicombe, J. Reflexes from the lungs and airways: historical perspective. *J. Appl. Physiol.* **101,** 628–634 (2006).

88. Ravi, K. Effect of carbon dioxide on the activity of slowly and rapidly adapting pulmonary stretch receptors in cats. *J. Auton. Nerv. Syst.* **12,** 267–277 (1985).

89. Green, J. F., Schertel, E. R., COLERIDGE, H. M. & COLERIDGE, J. C. Effect of pulmonary arterial PCO2 on slowly adapting pulmonary stretch receptors. *J. Appl. Physiol.* **60,** 2048–2055 (1986).

90. Yu, J. *et al.* Pulmonary rapidly adapting receptors reflexly increase airway secretion in dogs. *J. Appl. Physiol.* **67,** 682–687 (1989).

91. Widdicombe, J. G. Afferent receptors in the airways and cough. *Respiration*

Physiology **114,** 5–15 (1998).

92. Widdicombe, J. G. & Sellick, H. Vagal deflation and inflation reflexes mediated by lung irritant receptors. *Quarterly Journal of Experimental Physiology and Cognate Medical Sciences* **55,** 153–163 (1970).

93. Schultz, H. D. *et al.* Pulmonary C-fibers reflexly increase secretion by tracheal submucosal glands in dogs. *J. Appl. Physiol.* **58,** 907–910 (1985).

94. Coleridge, J. C. G. & Coleridge, H. M. In *Reviews of Physiology, Biochemistry and Pharmacology, Volume 99* **99,** 1–110 (Springer Berlin Heidelberg, 1984).

95. Lee, L. Y. & Pisarri, T. E. Afferent properties and reflex functions of bronchopulmonary C-fibers. *Respiration Physiology* **125,** 47–65 (2001).

96. Trankner, D., Hahne, N., Sugino, K., Hoon, M. A. & Zuker, C. Population of sensory neurons essential for asthmatic hyperreactivity of inflamed airways. *Proceedings of the National Academy of Sciences* **111,** 11515–11520 (2014).

97. Agostoni, E., Chinnock, J. E., De Daly, M. B. & Murray, J. G. Functional and histological studies of the vagus nerve and its branches to the heart, lungs and abdominal viscera in the cat. *J. Physiol. (Lond.)* **135,** 182–205 (1957).

98. Powley, T. L., Spaulding, R. A. & Haglof, S. A. Vagal afferent innervation of the proximal gastrointestinal tract mucosa: Chemoreceptor and mechanoreceptor architecture. *J. Comp. Neurol.* **519,** 644–660 (2011).

99. Brookes, S. J. H., Spencer, N. J., Costa, M. & Zagorodnyuk, V. P. Extrinsic primary afferent signalling in the gut. *Nat Rev Gastroenterol Hepatol* **10,** 286–296 (2013).

100. Rinaman, L. & Miselis, R. R. The organization of vagal innervation of rat pancreas using cholera toxin-horseradish peroxidase conjugate. *J. Auton. Nerv. Syst.* **21,** 109–125 (1987).

101. Neuhuber, W. L. Vagal afferent fibers almost exclusively innervate islets in the rat pancreas as demonstrated by anterograde tracing. *J. Auton. Nerv. Syst.* **29,** 13–18 (1989).

102. Wang, F. B. & Powley, T. L. Topographic inventories of vagal afferents in gastrointestinal muscle. *J. Comp. Neurol.* **421,** 302–324 (2000).

103. Powley, T. L. *et al.* Ultrastructural evidence for communication between intramuscular vagal mechanoreceptors and interstitial cells of Cajal in the rat fundus. *Neurogastroenterology & Motility* **20,** 69–79 (2008).

104. Berthoud, H. R. & Powley, T. L. Vagal afferent innervation of the rat fundic stomach:

morphological characterization of the gastric tension receptor. *J. Comp. Neurol.* **319,** 261–276 (1992).

105. Berthoud, H. R., Patterson, L. M., Neumann, F. & Neuhuber, W. L. Distribution and structure of vagal afferent intraganglionic laminar endings (IGLEs) in the rat gastrointestinal tract. *Anatomy and Embryology* **195,** 183–191 (1997).

106. fox, E. A., phillips, R. J., Martinson, F. A., Baronowsky, E. A. & Powley, T. L. Vagal afferent innervation of smooth muscle in the stomach and duodenum of the mouse: morphology and topography. *J. Comp. Neurol.* **428,** 558–576 (2000).

107. Neuhuber, W. L. Sensory vagal innervation of the rat esophagus and cardia: a light and electron microscopic anterograde tracing study. *J. Auton. Nerv. Syst.* **20,** 243–255 (1987).

108. NONIDEZ, J. F. Afferent nerve endings in the ganglia of the intermuscular plexus of the dog's oesophagus. *J. Comp. Neurol.* **85,** 177–189 (1946).

109. Berthoud, H.-R., Kressel, M., Raybould, H. & Neuhuber, W. Vagal sensors in the rat duodenal mucosa: distribution and structure as revealed by in vivo DiI-tracing. *Anatomy and Embryology* **191,** (1995).

110. Berthoud, H. R., Kressel, M. & Neuhuber, W. L. An anterograde tracing study of the vagal innervation of rat liver, portal vein and biliary system. *Anatomy and Embryology* **186,** 431–442 (1992).

111. Iggo, A. Tension receptors in the stomach and the urinary bladder. *J. Physiol. (Lond.)* **128,** 593–607 (1955).

112. Paintal, A. S. A study of gastric stretch receptors; their role in the peripheral mechanism of satiation of hunger and thirst. *J. Physiol. (Lond.)* **126,** 255–270 (1954).

113. Iggo, A. Gastro‐Intestinal Tension Receptors With Unmyelinated Afferent Fibres In The Vagus Of The Cat. *Quarterly Journal of Experimental Physiology and Cognate Medical Sciences* **42,** 130–143 (1957).

114. Grundy, D. Ainsley Iggo's early recordings from C fibre vagal afferents supplying the gut. *Exp Physiol* **93,** 1170–1173 (2008).

115. Zagorodnyuk, V. P., Chen, B. N. & Brookes, S. J. Intraganglionic laminar endings are mechano-transduction sites of vagal tension receptors in the guinea-pig stomach. *J. Physiol. (Lond.)* **534,** 255–268 (2001).

116. Zagorodnyuk, V. P. & Brookes, S. J. Transduction sites of vagal mechanoreceptors in

the guinea pig esophagus. *Journal of Neuroscience* **20,** 6249–6255 (2000).

117. Zagorodnyuk, V. P., Chen, B. N., Costa, M. & Brookes, S. J. H. Mechanotransduction by intraganglionic laminar endings of vagal tension receptors in the guinea-pig oesophagus. *J. Physiol. (Lond.)* **553,** 575–587 (2004).

118. Horn, C. C., Murat, C., Rosazza, M. & Still, L. Effects of gastric distension and infusion of umami and bitter taste stimuli on vagal afferent activity. *Brain Research* **1419,** 53–60 (2011).

119. Powley, T. L. & Phillips, R. J. Gastric satiation is volumetric, intestinal satiation is nutritive. *Physiology & Behavior* **82,** 69–74 (2004).

120. phillips, R. J. & Powley, T. L. Gastric volume rather than nutrient content inhibits food intake. *Am. J. Physiol.* **271,** R766–9 (1996).

121. Iggo, A. Gastric mucosal chemoreceptors with vagal afferent fibres in the cat. *Quarterly Journal of Experimental Physiology and Cognate Medical Sciences* **42,** 398–409 (1957).

122. Page, A. J., Martin, C. M. & Blackshaw, L. A. Vagal mechanoreceptors and chemoreceptors in mouse stomach and esophagus. *Journal of Neurophysiology* **87,** 2095–2103 (2002).

123. Blackshaw, L. A. & Grundy, D. Effects of 5-hydroxytryptamine on discharge of vagal mucosal afferent fibres from the upper gastrointestinal tract of the ferret. *J. Auton. Nerv. Syst.* **45,** 41–50 (1993).

124. Clarke, G. D. & Davison, J. S. Mucosal Receptors In The Gastric Antrum And Small Intestine Of The Rat With Afferent Fibres In The Cervical Vagus. *Journal of Phyiology* 1–13 (1978).

125. Cottrell, D. F. & Iggo, A. Mucosal Enteroceptors With Vagal Afferent Fibres In The Proximal Duodenum Of Sheep. *Journal of Phyiology* 1–26 (1984).

126. Davison, J. S. Response Of Single Vagal Afferent Fibres To Mechanical And Chemical Stimulation Of The Gastric And Duodenal Mucosa In Cats. *Quarterly Journal of Experimental Physiology* 1–12 (2016).

127. Berthoud, H.-R. The vagus nerve, food intake and obesity. *Regulatory Peptides* **149,** 15–25 (2008).

128. Randich, A. *et al.* Responses of celiac and cervical vagal afferents to infusions of lipids in the jejunum or ileum of the rat. *AJP: Regulatory, Integrative and Comparative Physiology* **278,** R34–43 (2000).

129. Mei, N. Vagal glucoreceptors in the small intestine of the cat. *J. Physiol. (Lond.)* **282,**

485–506 (1978).

130. Jeanningros, R. Vagal unitary responses to intestinal amino acid infusions in the anesthetized cat: A putative signal for protein induced satiety. *Physiology & Behavior* **28,** 9–21 (1982).

131. Ewart, W. R. & Wingate, D. L. Central representation of arrival of nutrient in the duodenum. *Am. J. Physiol.* **246,** G750–6 (1984).

132. Zhu, J. X., Zhu, X. Y., Owyang, C. & Li, Y. Intestinal serotonin acts as a paracrine substance to mediate vagal signal transmission evoked by luminal factors in the rat. *J. Physiol. (Lond.)* **530,** 431–442 (2001).

133. Mei, N. & Garnier, L. Osmosensitive vagal receptors in the small intestine of the cat. *J. Auton. Nerv. Syst.* **16,** 159–170 (1986).

134. Blackshaw, L. A. & Grundy, D. Effects of cholecystokinin (CCK-8) on two classes of gastroduodenal vagal afferent fibre. *J. Auton. Nerv. Syst.* **31,** 191–201 (1990).

135. Blackshaw, L. A. & Grundy, D. Effects of cholecystokinin (CCK-8) on two classes of gastroduodenal vagal afferent fibre. *J. Auton. Nerv. Syst.* **31,** 1–11 (1990).

136. Zittel, T. T., Rothenhöfer, I., Meyer, J. H. & Raybould, H. E. Small intestinal capsaicin-sensitive afferents mediate feedback inhibition of gastric emptying in rats. *Am. J. Physiol.* **267,** G1142–5 (1994).

137. Tamura, C. S. & Ritter, R. C. Intestinal capsaicin transiently attenuates suppression of sham feeding by oleate. *Am. J. Physiol.* **267,** R561–8 (1994).

138. Nakabayashi, H., Nishizawa, M., Nakagawa, A., Takeda, R. & Niijima, A. Vagal hepatopancreatic reflex effect evoked by intraportal appearance of tGLP-1. *Am. J. Physiol.* **271,** E808–13 (1996).

139. Vahl, T. P. *et al.* Glucagon-Like Peptide-1 (GLP-1) Receptors Expressed on Nerve Terminals in the Portal Vein Mediate the Effects of Endogenous GLP-1 on Glucose Tolerance in Rats. *Endocrinology* **148,** 4965–4973 (2007).

140. Horn, C. C. & Friedman, M. I. 2,5-Anhydro-D-mannitol induces Fos-like immunoreactivity in hindbrain and forebrain: relationship to eating behavior. *Brain Research* **779,** 17–25 (1998).

141. Lutz, T. A., Niijima, A. & Scharrer, E. Intraportal infusion of 2,5-anhydro-D-mannitol increases afferent activity in the common hepatic vagus branch. *J. Auton. Nerv. Syst.* **61,** 204–208 (1996).

142. Ripken, D. *et al.* Cholecystokinin regulates satiation independently of the abdominal

vagal nerve in a pig model of total subdiaphragmatic vagotomy. *Physiology & Behavior* **139,** 167–176 (2015).

143. Zhang, J. & Ritter, R. C. Circulating GLP-1 and CCK-8 reduce food intake by capsaicin-insensitive, nonvagal mechanisms. *AJP: Regulatory, Integrative and Comparative Physiology* **302,** R264–R273 (2012).

144. Reidelberger, R. D., Hernandez, J., Fritzsch, B. & Hulce, M. Abdominal vagal mediation of the satiety effects of CCK in rats. *AJP: Regulatory, Integrative and Comparative Physiology* **286,** R1005–12 (2004).

145. Smith, G. P., Jerome, C., Cushin, B. J., Eterno, R. & Simansky, K. J. Abdominal vagotomy blocks the satiety effect of cholecystokinin in the rat. *Science* **213,** 1036–1037 (1981).

146. Reidelberger, R., Haver, A., Anders, K. & Apenteng, B. Role of capsaicin-sensitive peripheral sensory neurons in anorexic responses to intravenous infusions of cholecystokinin, peptide YY-(3-36), and glucagon-like peptide-1 in rats. *AJP: Endocrinology and Metabolism* **307,** E619–E629 (2014).

147. Schwartz, G. J., Berkow, G., McHugh, P. R. & Moran, T. H. Gastric branch vagotomy blocks nutrient and cholecystokinin-induced suppression of gastric emptying. *Am. J. Physiol.* **264,** R630–7 (1993).

148. Cox, J. E. & Randich, A. CCK-8 activates hepatic vagal C-fiber afferents. *Brain Research* **776,** 189–194 (1997).

149. Davison, J. S. & Clarke, G. D. Mechanical properties and sensitivity to CCK of vagal gastric slowly adapting mechanoreceptors. *Am. J. Physiol.* **255,** G55–61 (1988).

150. Eastwood, C., Maubach, K., Kirkup, A. J. & Grundy, D. The role of endogenous cholecystokinin in the sensory transduction of luminal nutrient signals in the rat jejunum. *Neuroscience Letters* **254,** 145–148 (1998).

151. Peters, J. H., Simasko, S. M. & Ritter, R. C. Modulation of vagal afferent excitation and reduction of food intake by leptin and cholecystokinin. *Physiology & Behavior* **89,** 477–485 (2006).

152. Kurosawa, M. *et al.* Response of the gastric vagal afferent activity to cholecystokinin in rats lacking type A cholecystokinin receptors. *J. Auton. Nerv. Syst.* **75,** 51–59 (1999).

153. Raybould, H. E. & Lloyd, K. C. Integration of postprandial function in the proximal gastrointestinal tract. Role of CCK and sensory pathways. *Ann NY Acad Sci* **713,** 143–156 (1994).

154. Lal, S., Kirkup, A. J., Brunsden, A. M., Thompson, D. G. & Grundy, D. Vagal afferent responses to fatty acids of different chain length in the rat. *AJP: Gastrointestinal and Liver Physiology* **281,** G907–15 (2001).

155. Hölzer, H. H., Turkelson, C. M., Solomon, T. E. & Raybould, H. E. Intestinal lipid inhibits gastric emptying via CCK and a vagal capsaicin-sensitive afferent pathway in rats. *Am. J. Physiol.* **267,** G625–9 (1994).

156. Patterson, L. M., Zheng, H. & Berthoud, H.-R. Vagal afferents innervating the gastrointestinal tract and CCKA-receptor immunoreactivity. *Anat. Rec.* **266,** 10–20 (2001).

157. Huo, L., Maeng, L., Bjørbæk, C. & Grill, H. J. Leptin and the Control of Food Intake: Neurons in the Nucleus of the Solitary Tract Are Activated by Both Gastric Distension and Leptin. *Endocrinology* **148,** 2189–2197 (2007).

158. Hayes, M. R., Kanoski, S. E., Alhadeff, A. L. & Grill, H. J. Comparative Effects of the Long-Acting GLP-1 Receptor Ligands, Liraglutide and Exendin-4, on Food Intake and Body Weight Suppression in Rats. *Obesity* **19,** 1342–1349 (2011).

159. Hayes, M. R. *et al.* The common hepatic branch of the vagus is not required to mediate the glycemic and food intake suppressive effects of glucagon-like-peptide-1. *AJP: Regulatory, Integrative and Comparative Physiology* **301,** R1479–R1485 (2011).

160. Abbott, C. R. *et al.* The inhibitory effects of peripheral administration of peptide YY3–36 and glucagon-like peptide-1 on food intake are attenuated by ablation of the vagal–brainstem–hypothalamic pathway. *Brain Research* **1044,** 127–131 (2005).

161. Kanoski, S. E., Fortin, S. M., Arnold, M., Grill, H. J. & Hayes, M. R. Peripheral and Central GLP-1 Receptor Populations Mediate the Anorectic Effects of Peripherally Administered GLP-1 Receptor Agonists, Liraglutide and Exendin-4. *Endocrinology* **152,** 3103–3112 (2011).

162. Labouesse, M. A. *et al.* Vagal Afferents Mediate Early Satiation and Prevent Flavour Avoidance Learning in Response to Intraperitoneally Infused Exendin-4. *J Neuroendocrinol* **24,** 1505–1516 (2012).

163. Plamboeck, A. *et al.* The effect of exogenous GLP-1 on food intake is lost in male truncally vagotomized subjects with pyloroplasty. *AJP: Gastrointestinal and Liver Physiology* **304,** G1117–G1127 (2013).

164. Jang, H.-J. *et al.* Gut-expressed gustducin and taste receptors regulate secretion of glucagon-like peptide-1. *Proceedings of the National Academy of Sciences* **104,** 15069–15074 (2007).

165. Bucinskaite, V. *et al.* Receptor-mediated activation of gastric vagal afferents by glucagon-like peptide-1 in the rat. *Neurogastroenterology & Motility* **21,** 978–e78 (2009).

166. Sclafani, A., Glass, D. S., Margolskee, R. F. & Glendinning, J. I. Gut T1R3 sweet taste receptors do not mediate sucrose-conditioned flavor preferences in mice. *AJP: Regulatory, Integrative and Comparative Physiology* **299,** R1643–R1650 (2010).

167. Sclafani, A. & Lucas, F. Abdominal vagotomy does not block carbohydrate-conditioned flavor preferences in rats. *Physiology & Behavior* **60,** 447–453 (1996).

168. Sisley, S. *et al.* Neuronal GLP1R mediates liraglutide's anorectic but not glucose-lowering effect. *J Clin Invest* **124,** 2456–2463 (2014).

169. Mellitzer, G. *et al.* Loss of enteroendocrine cells in mice alters lipid absorption and glucose homeostasis and impairs postnatal survival. *J Clin Invest* **120,** 1708–1721 (2010).

170. Gribble, F. M. & Reimann, F. Enteroendocrine Cells: Chemosensors in the Intestinal Epithelium. *Annu. Rev. Physiol.* **78,** 277–299 (2016).

171. Psichas, A., Reimann, F. & Gribble, F. M. Gut chemosensing mechanisms. *J Clin Invest* **125,** 908–917 (2015).

172. Burdyga, G. *et al.* Cholecystokinin Regulates Expression of Y2 Receptors in Vagal Afferent Neurons Serving the Stomach. *Journal of Neuroscience* **28,** 11583–11592 (2008).

173. Kentish, S. *et al.* Diet-induced adaptation of vagal afferent function. *J. Physiol. (Lond.)* **590,** 209–221 (2011).

174. De Lartigue, G. *et al.* Cocaine- and Amphetamine-Regulated Transcript Mediates the Actions of Cholecystokinin on Rat Vagal Afferent Neurons. *Gastroenterology* **138,** 1479–1490 (2010).

175. Kentish, S. J. *et al.* Gastric vagal afferent modulation by leptin is influenced by food intake status. *J. Physiol. (Lond.)* **591,** 1921–1934 (2013).

176. Babic, T., Troy, A. E., Fortna, S. R. & Browning, K. N. Glucose-dependent trafficking of 5-HT3 receptors in rat gastrointestinal vagal afferent neurons. *Neurogastroenterology & Motility* **24,** e476–e488 (2012).

177. Braun, T., Voland, P., Kunz, L., Prinz, C. & Gratzl, M. Enterochromaffin Cells of the Human Gut: Sensors for Spices and Odorants. *Gastroenterology* **132,** 1890–1901 (2007).

178. Hagbom, M. *et al.* Rotavirus Stimulates Release of Serotonin (5-HT) from Human Enterochromaffin Cells and Activates Brain Structures Involved in Nausea and Vomiting. *PLoS Pathog* **7,** e1002115–10 (2011).

179. Nozawa, K. *et al.* TRPA1 regulates gastrointestinal motility through serotonin release from enterochromaffin cells. *Proc. Natl. Acad. Sci. U.S.A.* **106,** 3408–3413 (2009).

180. Liu, Q. *et al.* Discovery and Characterization of Novel Tryptophan Hydroxylase Inhibitors That Selectively Inhibit Serotonin Synthesis in the Gastrointestinal Tract. *The Journal of Pharmacology and Experimental Therapeutics* **325,** 47–55 (2008).

181. De Jonghe, B. C. & Horn, C. C. Chemotherapy-induced pica and anorexia are reduced by common hepatic branch vagotomy in the rat. *AJP: Regulatory, Integrative and Comparative Physiology* **294,** R756–R765 (2008).

182. Horn, C. C. Measuring the nausea-to-emesis continuum in non-human animals: refocusing on gastrointestinal vagal signaling. *Exp Brain Res* **232,** 2471–2481 (2014).

183. Yamamoto, K., Matsunaga, S., Matsui, M., Takeda, N. & Yamatodani, A. Pica in mice as a new model for the study of emesis. *Methods and Findings in Experimental and Clinical Pharmacology* **24,** 135 (2002).

184. Takeda, N., Hasegawa, S., Morita, M. & Matsunaga, T. Pica in rats is analogous to emesis: an animal model in emesis research. *Pharmacol. Biochem. Behav.* **45,** 817–821 (1993).

185. Fukui, H., Yamamoto, M., Sasaki, S. & Sato, S. Involvement of 5-HT3 receptors and vagal afferents in copper sulfate- and cisplatin-induced emesis in monkeys. *European Journal of Pharmacology* **249,** 13–18 (1993).

186. Kamato, T. *et al.* Mechanisms of cisplatin- and m-chlorophenylbiguanide-induced emesis in ferrets. *European Journal of Pharmacology* **238,** 369–376 (1993).

187. Cubeddu, L. X., Hoffmann, I. S., Fuenmayor, N. T. & Finn, A. L. Efficacy of ondansetron (GR 38032F) and the role of serotonin in cisplatin-induced nausea and vomiting. *N. Engl. J. Med.* **322,** 810–816 (1990).

188. Jones, A. L. *et al.* Comparison of dexamethasone and ondansetron in the prophylaxis of emesis induced by moderately emetogenic chemotherapy. *Lancet* **338,** 483–487 (1991).

189. Manocha, M. & Khan, W. I. Serotonin and GI Disorders: An Update on Clinical and Experimental Studies. *Clin Trans Gastroenterol* **3,** e13–6 (2012).

190. Italian Group for Antiemetic Research. Dexamethasone, granisetron, or both for the prevention of nausea and vomiting during chemotherapy for cancer. *N. Engl. J. Med.* **332,** 1–5 (1995).

191. Morales, M. & Wang, S.-D. Differential composition of 5-hydroxytryptamine3 receptors synthesized in the rat CNS and peripheral nervous system. *J. Neurosci.* **22,** 6732–6741 (2002).

192. Hillsley, K. & Grundy, D. Serotonin and cholecystokinin activate different populations of rat mesenteric vagal afferents. *Neuroscience Letters* **255,** 63–66 (1998).

193. Dockray, G. J. Luminal Sensing In The Gut: An Overview. *journal of physiology and pharmacology* **54,** 9–17 (2003).

194. Davis, J. D. & Smith, G. P. Learning to sham feed: behavioral adjustments to loss of physiological postingestional stimuli. *Am. J. Physiol.* **259,** R1228–35 (1990).

195. Takahashi, T. & Owyang, C. Characterization of vagal pathways mediating gastric accommodation reflex in rats. *J. Physiol. (Lond.)* **504,** 479–488 (1997).

196. Walls, E. K., phillips, R. J., Wang, F. B., Holst, M. C. & Powley, T. L. Suppression of meal size by intestinal nutrients is eliminated by celiac vagal deafferentation. *Am. J. Physiol.* **269,** R1410–9 (1995).

197. Yox, D. P., Stokesberry, H. & Ritter, R. C. Vagotomy attenuates suppression of sham feeding induced by intestinal nutrients. *Am. J. Physiol.* **260,** R503–8 (1991).

198. Sclafani, A., Ackroff, K. & Schwartz, G. J. Selective effects of vagal deafferentation and celiac-superior mesenteric ganglionectomy on the reinforcing and satiating action of intestinal nutrients. *Physiology & Behavior* **78,** 285–294 (2003).

199. Kanoski, S. E., Rupprecht, L. E., Fortin, S. M., De Jonghe, B. C. & Hayes, M. R. The role of nausea in food intake and body weight suppression by peripheral GLP-1 receptor agonists, exendin-4 and liraglutide. *Neuropharmacology* **62,** 1916–1927 (2012).

200. van Boxel, O. S., Linde, ter, J. J. M., Siersema, P. D. & Smout, A. J. P. M. Role of Chemical Stimulation of the Duodenum in Dyspeptic Symptom Generation. *Am J Gastroenterol* **105,** 803–811 (2010).

201. De Jonghe, B. C., Lawler, M. P., Horn, C. C. & Tordoff, M. G. Pica as an adaptive response: Kaolin consumption helps rats recover from chemotherapy-induced illness. *Physiology & Behavior* **97,** 87–90 (2009).

202. Feinle, C., Grundy, D. & Read, N. W. Effects of duodenal nutrients on sensory and

motor responses of the human stomach to distension. *Am. J. Physiol.* **273,** G721–6 (1997).

203. Zariwala, H. A. *et al.* A Cre-dependent GCaMP3 reporter mouse for neuronal imaging in vivo. *J. Neurosci.* **32,** 3131–3141 (2012).

204. Kokrashvili, Z., Mosinger, B. & Margolskee, R. F. Taste signaling elements expressed in gut enteroendocrine cells regulate nutrient-responsive secretion of gut hormones. *American Journal of Clinical Nutrition* **90,** 822S–825S (2009).

205. Tizzano, M., Cristofoletti, M., Sbarbati, A. & Finger, T. E. Expression of taste receptors in solitary chemosensory cells of rodent airways. *BMC Pulm Med* **11,** 3 (2011).

206. Andrews, P. L. R. & Horn, C. C. Signals for nausea and emesis: Implications for models of upper gastrointestinal diseases. *Autonomic Neuroscience* **125,** 100–115 (2006).

207. Riley, T. P., Neal-McKinney, J. M., Buelow, D. R., Konkel, M. E. & Simasko, S. M. Capsaicin-sensitive vagal afferent neurons contribute to the detection of pathogenic bacterial colonization in the gut. *Journal of Neuroimmunology* **257,** 36–45 (2013).

208. Ek, M., Kurosawa, M., Lundeberg, T. & Ericsson, A. Activation of vagal afferents after intravenous injection of interleukin-1beta: role of endogenous prostaglandins. *Journal of Neuroscience* **18,** 9471–9479 (1998).

209. Gaykema, R. P. A. *et al.* Bacterial Endotoxin Induces Fos Immunoreactivity in Primary Afferent Neurons of the Vagus Nerve. *Neuroimmunomodulation* **5,** 234–240 (1998).

210. Goehler, L. E., Gaykema, R. P., Hammack, S. E., Maier, S. F. & Watkins, L. R. Interleukin-1 induces c-Fos immunoreactivity in primary afferent neurons of the vagus nerve. *Brain Research* **804,** 306–310 (1998).

211. Niijima, A. The afferent discharges from sensors for interleukin 1 beta in the hepatoportal system in the anesthetized rat. *J. Auton. Nerv. Syst.* **61,** 287–291 (1996).

212. Rosas-Ballina, M. *et al.* Acetylcholine-Synthesizing T Cells Relay Neural Signals in a Vagus Nerve Circuit. *Science* **334,** 98–101 (2011).

213. Rosas-Ballina, M. & Tracey, K. J. The Neurology of the Immune System: Neural Reflexes Regulate Immunity. *Neuron* **64,** 28–32 (2009).

214. Olofsson, P. S. *et al.* α7 nicotinic acetylcholine receptor (α7nAChR) expression in bone marrow-derived non-T cells is required for the inflammatory reflex. *Mol. Med.*

18, 539–543 (2012).

215. Rosas-Ballina, M. *et al.* Splenic nerve is required for cholinergic antiinflammatory pathway control of TNF in endotoxemia. *Proc. Natl. Acad. Sci. U.S.A.* **105,** 11008–11013 (2008).

216. Pavlov, V. A. & Tracey, K. J. Controlling inflammation: the cholinergic anti-inflammatory pathway. *Biochem. Soc. Trans.* **34,** 1037–1040 (2006).

217. Bonaz, B., Picq, C., Sinniger, V., Mayol, J. F. & Clarençon, D. Vagus nerve stimulation: from epilepsy to the cholinergic anti-inflammatory pathway. *Neurogastroenterology & Motility* **25,** 208–221 (2013).

218. Yano, J. M. *et al.* Indigenous Bacteria from the Gut Microbiota Regulate Host Serotonin Biosynthesis. *Cell* **161,** 264–276 (2015).

219. Kaiser, P., Diard, M., Stecher, B. & Hardt, W.-D. The streptomycin mouse model for Salmonella diarrhea: functional analysis of the microbiota, the pathogen's virulence factors, and the host's mucosal immune response. *Immunological Reviews* **245,** 56–83 (2012).

220. Broz, P., Ohlson, M. B. & Monack, D. M. Innate immune response to Salmonella typhimurium, a model enteric pathogen. *Gut Microbes* **3,** 62–70 (2014).

221. Horn, C. C., Richardson, E. J., Andrews, P. L. R. & Friedman, M. I. Differential effects on gastrointestinal and hepatic vagal afferent fibers in the rat by the anti-cancer agent cisplatin. *Autonomic Neuroscience* **115,** 74–81 (2004).

222. Barretto, R. P. J. *et al.* The neural representation of taste quality at the periphery. *Nature* **517,** 373–376 (2014).

223. Ferrero, D. M. *et al.* A juvenile mouse pheromone inhibits sexual behaviour through the vomeronasal system. *Nature* **502,** 368–371 (2013).

224. Willing, A. E. & Berthoud, H. R. Gastric distension-induced c-fos expression in catecholaminergic neurons of rat dorsal vagal complex. *Am. J. Physiol.* **272,** R59–67 (1997).

225. Bertrand, P. P. & Bertrand, R. L. Serotonin release and uptake in the gastrointestinal tract. *Autonomic Neuroscience* **153,** 47–57 (2010).

226. Phifer, C. B. & Berthoud, H. R. Duodenal nutrient infusions differentially affect sham feeding and Fos expression in rat brain stem. *Am. J. Physiol.* **274,** R1725–33 (1998).

227. Horn, C. C., Ciucci, M. & Chaudhury, A. Brain Fos expression during 48 h after cisplatin treatment: Neural pathways for acute and delayed visceral sickness.

Autonomic Neuroscience **132,** 44–51 (2007).

228. Schwartz, G. J., McHugh, P. R. & Moran, T. H. Gastric loads and cholecystokinin synergistically stimulate rat gastric vagal afferents. *Am. J. Physiol.* **265,** R872–6 (1993).

229. Schwartz, G. J., McHugh, P. R. & Moran, T. H. Integration of vagal afferent responses to gastric loads and cholecystokinin in rats. *Am. J. Physiol.* **261,** R64–9 (1991).

230. Hayes, M. R., Bradley, L. & Grill, H. J. Endogenous Hindbrain Glucagon-Like Peptide-1 Receptor Activation Contributes to the Control of Food Intake by Mediating Gastric Satiation Signaling. *Endocrinology* **150,** 2654–2659 (2009).

231. Aponte, Y., Atasoy, D. & Sternson, S. M. AGRP neurons are sufficient to orchestrate feeding behavior rapidly and without training. *Nat Neurosci* **14,** 351–355 (2011).

232. Bai, L. *et al.* Genetic Identification of an Expansive Mechanoreceptor Sensitive to Skin Stroking. *Cell* **163,** 1783–1795 (2015).

233. Han, L. *et al.* A subpopulation of nociceptors specifically linked to itch. *Nat Neurosci* **16,** 174–182 (2012).

234. Lee, H. *et al.* Scalable control of mounting and attack by Esr1+ neurons in the ventromedial hypothalamus. *Nature* **509,** 627–632 (2014).

235. Mandelblat-Cerf, Y. *et al.* Arcuate hypothalamic AgRP and putative POMC neurons show opposite changes in spiking across multiple timescales. *Elife* **4,** 351 (2015).

236. Chen, Y., Lin, Y.-C., Kuo, T.-W. & Knight, Z. A. Sensory Detection of Food Rapidly Modulates Arcuate Feeding Circuits. *Cell* **160,** 829–841 (2015).

237. Betley, J. N. *et al.* Neurons for hunger and thirst transmit a negative-valence teaching signal. *Nature* **521,** 180–185 (2015).

238. Ray, R. S. *et al.* Impaired Respiratory and Body Temperature Control Upon Acute Serotonergic Neuron Inhibition. *Science* **333,** 637–642 (2011).

239. Horn, C. C., Wallisch, W. J., Homanics, G. E. & Williams, J. P. Pathophysiological and neurochemical mechanisms of postoperative nausea and vomiting. *European Journal of Pharmacology* **722,** 55–66 (2014).

240. Barnes, N. M., Hales, T. G., Lummis, S. C. R. & Peters, J. A. The 5-HT3 receptor – the relationship between structure and function. *Neuropharmacology* **56,** 273–284 (2009).

241. Rueffert, H. *et al.* Do Variations in the 5-HT3A and 5-HT3B Serotonin Receptor

Genes (HTR3A and HTR3B) Influence the Occurrence of Postoperative Vomiting? *Anesthesia & Analgesia* **109,** 1442–1447 (2009).

242. Hammer, C. *et al.* Functional variants of the serotonin receptor type 3A and B gene are associated with eating disorders. *Pharmacogenetics and Genomics* **19,** 790–799 (2009).

243. Ma, X.-X., Chen, Q.-X., Wu, S.-J., Hu, Y. & Fang, X.-M. Polymorphisms of the HTR3B gene are associated with post-surgery emesis in a Chinese Han population. *J Clin Pharm Ther* **38,** 150–155 (2013).

244. Undem, B. J. *et al.* Subtypes of vagal afferent C-fibres in guinea-pig lungs. *J. Physiol. (Lond.)* **556,** 905–917 (2004).

245. Cone, R. D. Studies on the Physiological Functions of the Melanocortin System. *Endocrine Reviews* **27,** 736–749 (2006).

246. Gautron, L., Lee, C. E., Lee, S. & Elmquist, J. K. Melanocortin-4 receptor expression in different classes of spinal and vagal primary afferent neurons in the mouse. *J. Comp. Neurol.* **520,** 3933–3948 (2012).

247. Gautron, L. *et al.* Melanocortin-4 receptor expression in a vago-vagal circuitry involved in postprandial functions. *J. Comp. Neurol.* **518,** 6–24 (2010).